DEGREE PROJECT IN ENERGY AND ENVIRONMENT,
SECOND CYCLE, 30 CREDITS
STOCKHOLM, SWEDEN 2021

CO2 Refrigeration with Integrated Ejectors

Modelling and Field Data Analysis of Two Ice Rinks and Two Supermarket Systems

SIMON FEHLING

KTH ROYAL INSTITUTE OF TECHNOLOGY
SCHOOL OF INDUSTRIAL ENGINEERING AND MANAGEMENT

KTH Industrial Engineering and Management

Master of Science Thesis

Department of Energy Technology

KTH 2020

CO2 Refrigeration with Integrated Ejectors

Modelling and Field Data Analysis of Two Ice Rinks and Two Supermarket Refrigeration Systems

TRITA: TRITA-ITM-EX 2021:444

Simon Fehling

Approved	Examiner	Supervisors
2020-07-02	Samer Sawalha	Samer Sawalha Sotiris Thanasoulas
	Industrial Supervisor	Contact person
	Jörgen Rogstam	

Abstract

With the increasing importance of CO_2 as natural refrigerant with low Global Warming Potential (GWP) ejectors have been used in a number of recent installations to recover expansion work at the high operating pressures of these systems. In colder climates, this is particularly seen in combination with heat recovery due to the high compressor discharge pressures.
This work analyses the field measurement data of two ice rink refrigeration systems with integrated vapor ejectors and two supermarket refrigeration systems with integrated liquid ejectors, all located in northern Europe. The aim is to evaluate the interaction of the ejector with the refrigeration system in practical applications. A theoretical model of the ejector systems is developed and evaluated in parallel as a reference for the analysed system installations.
The model of the analysed vapor ejector system shows an increasing efficiency improvement potential by the ejector for higher gas cooler outlet temperatures, while the liquid ejector system model indicates higher efficiency improvement potential at relatively lower gas cooler outlet temperatures and pressures.
From the vapor ejector field data evaluation, this is confirmed with additional findings of low ejector work recovery efficiencies at low gas cooler outlet temperatures. Furthermore, problems in the ejector operation are found for too low evaporation temperatures in one of the systems. In addition, an unstable ejector control at certain operating conditions is linked to a decreasing ejector performance. While the ejector is found not to provide any significant savings in one of the systems mainly due to low evaporation temperatures, the other ice rink system is found to achieve total energy savings of 7 % from the ejector.
For the liquid ejector field data evaluation, the ejectors are found to work as expected for the purpose of removing liquid from the low-pressure receiver. However, overfed evaporation conditions are only found temporarily for most cabinets in the analysed systems, with remaining high average superheat values. Low required air supply temperatures in the cabinets and the dimensioning of the expansion valves at the evaporator inlet are identified as possible limitations for a further decrease of the superheat and increase of the evaporation temperature.

Keywords: Vapor Ejector, Liquid Ejector, Field Data Evaluation, Modelling, Refrigeration, CO2, Ice Rink, Supermarket, Heat Recovery

Sammanfattning

Med den ökande betydelsen av CO2 som naturligt köldmedium med låg global uppvärmningspotential (GWP) har ejektorer använts i ett antal nya installationer för att återvinna expansionsarbete vid de höga drifttrycken i dessa system. I kallare klimat är detta särskilt vanligt i kombination med värmeåtervinning på grund av de höga utloppstrycken i kompressorerna.
I detta arbete analyseras fältmätdata från två kylsystem för isbanor med integrerade ångejektorer och två kylsystem för livsmedelsbutiker med integrerade vätskeejektorer. Samtliga system finns i norra Europa. Syftet med studien är att utvärdera ejektorns samverkan med kylsystemet i praktiska tillämpningar. En teoretisk modell av ejektorsystemen utvecklas och utvärderas parallellt som referens för de analyserade systeminstallationerna.
Modellen för det analyserade ångejektorsystemet visar att potentialen för effektivitetsförbättring genom ejektorn ökar vid högre utloppstemperaturer för gaskylare, medan modellen för systemet med vätskeutkastare visar att potentialen för effektivitetsförbättring ökar vid relativt lägre utloppstemperaturer och tryck för gaskylare.
Detta bekräftas i utvärderingen av fältdata från ångejektorsystemen som vid låga utloppstemperaturer i gaskylaren samtidigt ger låg effektivitet för ejektorn. Dessutom noteras problem med ejektorns funktion vid för låga förångningstemperaturer i ett av systemen. En instabil styrning av ejektorn vid vissa driftsförhållanden leder vidare till en minskad ejektoreffektivitet. Medan ejektorn inte ger några betydande besparingar i det ena systemet, främst på grund av låga avdunstningstemperaturer, har en total energibesparing på 7 % från ejektorn hittats i den andra isbanan.
När det gäller utvärderingen av fältdata för vätskeejektorer konstateras att ejektorerna fungerar som förväntat för att avlägsna vätska från vätskeavskiljaren. För de flesta kyldiskar i de analyserade systemen syns dock bara kortvarigt flödad tillstånd i förångrarna, och i övrigt en kvarvarande hög genomsnittlig överhettning. Låg erforderlig tilluftstemperatur i kyldiskarna och dimensioneringen av expansionsventilerna vid förångarens inlopp identifieras som möjliga begränsningar för en ytterligare minskning av överhettningen och en ökning av förångningstemperaturen.

Nyckelord: Ångejektor, Vätskeejektor, Fältmätdata, Modellering, Kylteknik, CO2, Isbana, Livsmedelsbutik, Värmeåtervinning

Acknowledgements

I would like to express my gratitude to Samer Sawalha, my supervisor at the division of Applied Thermodynamics and Refrigeration at KTH Royal Institute of Technology for the guidance, supportive feedback and fruitful discussions about my findings, as well as for the possibility to present part of my results to the research framework on supermarket refrigeration at KTH.
I also would like to thank Sotiris Thanasoulas from the division of Applied Thermodynamics and Refrigeration for his support in the data acquisition process and the helpful feedback during project meetings.

Furthermore, I want to express my gratitude to Jörgen Rogstam of EKA Energi & Kylanalys AB for initiating this interesting thesis project and for supporting my work by providing important feedback from a experienced practical refrigeration perspective during our regular meetings.
I would also like to thank Juris Pomerancevs of EKA Baltic for the contact with the Mogilev State University of Food Technologies in Belarus and his support in presenting my thesis work at the conference on Engineering and Technology of Food Production there.
Thank you also to the other team members of EKA for their support with technical questions and their interest in the topic and my work.

Contents

List of Figures

List of Abbreviations

Notation	Description
CFD	Computational Fluid Dynamics
COP	Coefficient of Performance
HPrec	High Pressure Receiver
HPV	High Pressure Expansion Valve
IHX	Internal Heat Exchanger
LEJ	Liquid Ejector System
LEJ-A	LEJ System "A" for Field Data Evaluation
LEJ-B	LEJ System "B" for Field Data Evaluation
LPrec	Low Pressure Receiver
LT	Low Temperature
MC	Main Compressor
MT	Medium Temperature
PC	Parallel Compressor
REF	Reference System without ejector
VEJ	Vapor Ejector System without parallel compression
VEJ-A	VEJ System "A" for Field Data Evaluation
VEJ-B	VEJ System "B" for Field Data Evaluation
VPC	Vapor Ejector System with parallel compression and HPV

List of Symbols

Symbol	Unit	Description
COP_1	–	Heating COP of the analysed system
$COP_{1,\mathrm{ref}}$	–	Heating COP of the reference system
COP_2	–	Cooling COP of the analysed system
$COP_{2,\mathrm{ref}}$	–	Cooling COP of the reference system
$h_{\mathrm{disc,mixed}}$	$^{\mathrm{kJ}}/_{\mathrm{kg}}$	Enthalpy of the mixed discharge flow of MC and PC
$h_{\mathrm{ej,e}}$	$^{\mathrm{kJ}}/_{\mathrm{kg}}$	Ejector entrainment enthalpy
$h_{\mathrm{ej,e,exp,is}}$	$^{\mathrm{kJ}}/_{\mathrm{kg}}$	Enthalpy of entrainment flow after theoretical isentropic expansion
$h_{\mathrm{ej,out}}$	$^{\mathrm{kJ}}/_{\mathrm{kg}}$	Ejector outlet enthalpy
$h_{\mathrm{ej,s}}$	$^{\mathrm{kJ}}/_{\mathrm{kg}}$	Ejector suction enthalpy
$h_{\mathrm{ej,s,comp,is}}$	$^{\mathrm{kJ}}/_{\mathrm{kg}}$	Enthalpy of suction flow after theoretical isentropic compression
$h_{\mathrm{MC,disc}}$	$^{\mathrm{kJ}}/_{\mathrm{kg}}$	MC discharge enthalpy
$h_{\mathrm{PC,disc}}$	$^{\mathrm{kJ}}/_{\mathrm{kg}}$	PC discharge enthalpy
$h_{\mathrm{rec,mixed}}$	$^{\mathrm{kJ}}/_{\mathrm{kg}}$	Receiver enthalpy after mixing
$Incr_{\mathrm{COP2}}$	–	Relative increase in cooling COP
$Incr_{\mathrm{Q1}}$	–	Relative increase in heating capacity
$\dot{m}_{\mathrm{comp}}$	$^{\mathrm{kg}}/_{\mathrm{s}}$	Compressor mass flow
$\dot{m}_{\mathrm{ej,e}}$	$^{\mathrm{kg}}/_{\mathrm{s}}$	Ejector entrainment mass flow
$\dot{m}_{\mathrm{ej,out}}$	$^{\mathrm{kg}}/_{\mathrm{s}}$	Ejector outlet mass flow
$\dot{m}_{\mathrm{ej,s}}$	$^{\mathrm{kg}}/_{\mathrm{s}}$	Ejector suction mass flow
$\dot{m}_{\mathrm{evap}}$	$^{\mathrm{kg}}/_{\mathrm{s}}$	Evaporator mass flow
$\dot{m}_{\mathrm{fg}}$	$^{\mathrm{kg}}/_{\mathrm{s}}$	Mass flow in flash gas bypass
$\dot{m}_{\mathrm{gc}}$	$^{\mathrm{kg}}/_{\mathrm{s}}$	Gas cooler mass flow
$m_{\mathrm{gc,rel}}$	–	Gas cooler mass flow relative to the evaporator mass flow
$\dot{m}_{\mathrm{HPV}}$	$^{\mathrm{kg}}/_{\mathrm{s}}$	Mass flow through HPV
$\dot{m}_{\mathrm{MC}}$	$^{\mathrm{kg}}/_{\mathrm{s}}$	MC mass flow
$\dot{m}_{\mathrm{PC}}$	$^{\mathrm{kg}}/_{\mathrm{s}}$	PC mass flow

Symbol	Unit	Description
P_{comp}	kW	Compressor power input
$P_{\text{comp,ref}}$	kW	Compressor power input in the REF system
$p_{\text{comp,suc}}$	bar(a)	Compressor suction pressure
p_{disc}	bar(a)	Compressor discharge pressure and ejector entrainment pressure
$p_{\text{ej,e}}$	bar(a)	Ejector entrainment pressure measured after gas cooler, in case of separate measurement in VEJ-B
$p_{\text{ej,out}}$	bar(a)	Ejector outlet pressure
$p_{\text{ej,s}}$	bar(a)	Ejector suction pressure
p_{evap}	bar(a)	Evaporating pressure
p_{rec}	bar(a)	Receiver pressure
P_{tot}	kW	Measured total power input to the refrigeration system (used in the field data evaluation if the compressor power was not available)
Q_1	–	Heating capacity of the analysed system
$Q_{1,\text{ref}}$	–	Heating capacity of the reference system
Q_2	–	Cooling capacity of the analysed system
$Rel_{\text{ej/rec}}$	–	Ratio of ejector mass flow to total receiver mass flow
$s_{\text{ej,e}}$	$^{\text{kJ}}/_{\text{kgK}}$	Ejector entrainment entropy
$s_{\text{ej,s}}$	$^{\text{kJ}}/_{\text{kgK}}$	Ejector suction entropy
$T_{\text{air,in}}$	°C	Evaporator air inlet temperature
$T_{\text{air,out}}$	°C	Evaporator air outlet temperature
T_{amb}	°C	Ambient temperature
$T_{\text{comp,disc}}$	°C	Compressor discharge temperature
$T_{\text{comp,suc}}$	°C	Compressor suction temperature
$T_{\text{ej,e}}$	°C	Ejector entrainment temperature
$T_{\text{ej,s}}$	°C	Ejector suction temperature
T_{evap}	°C	Evaporating temperature
$T_{\text{evap,out}}$	°C	Evaporator CO2 outlet temperature
$T_{\text{gc,out}}$	°C	Gas cooler outlet temperature
$T_{\text{HR,out}}$	°C	Heat recovery outlet temperature
W_{r}	kW	Recovered work by the ejector, for assumed isentropic compression in the ejector
$W_{\text{r,max}}$	kW	Maximum recoverable work by the ejector, for isentropic expansion in the ejector
$x_{\text{ej,out}}$	–	Ejector outlet vapor quality

Symbol	Unit	Description
x_{fg}	$-$	Vapor quality at the outlet of the flash gas valve
x_{HPrec}	$-$	Vapor quality in high pressure receiver after mixing ejector and HPV mass flows
x_{LPrec}	$-$	Vapor quality in the LPrec after mixing of mass flows of flooded evaporator outlet and flash gas bypass
Δh_{comp}	$^{\mathrm{kJ}}/_{\mathrm{kg}}$	Compressor enthalpy difference
$\Delta h_{\mathrm{r,max}}$	$^{\mathrm{kJ}}/_{\mathrm{kg}}$	Available isentropic enthalpy difference for the the maximum recoverable work by the ejector
Δp_{lift}	bar(a)	Ejector pressure lift
$\Delta T_{\mathrm{SH,evap}}$	K	Superheat in the evaporator (internal)
$\eta_{\mathrm{comp,is}}$	$-$	Isentropic compressor efficiency
η_{ej}	$-$	Ejector efficiency
η_{elm}	$-$	Efficiency of the electrical motor driving the compressor
ω	$-$	Ejector mass entrainment ratio
τ	$-$	Ejector pressure ratio

1 Introduction and Background

The use of carbon dioxide (CO2) in refrigeration applications has gained increasing importance in recent years. Statistics indicate that the number of refrigeration systems worldwide with CO2 as refrigerant have increased by a factor of more than 5 between 2015 and 2020 to more than 35 000 installations [1]. This trend is expected to continue due to environmental advantages of CO2 as natural refrigerant with very low Global Warming Potential (GWP) compared to most synthetic refrigerants, as well as the possibility for energy efficient solutions particularly in combination with heat recovery.

The high pressures in refrigeration systems with CO2 make it particularly interesting to recover expansion work [2]. In this context, ejectors are a relatively new component which potentially offers a cost-effective option [3] for energy efficiency improvements by recovering expansion work to achieve higher suction pressures. While ejectors were previously seen mainly as an option to improve the system performance of CO2 refrigeration systems in warm climates, they have also recently been implemented in systems in colder climates, particularly in combination with heat recovery due to the increased high-side pressures, as seen in the analysed systems in this study.

Two main principles of efficiency improvements by the ejector in vapor compression refrigeration systems are currently available and analysed in this study: The vapor ejector directly lifts the pressure of refrigerant at the evaporator outlet to an intermediate pressure level. In contrast, the liquid ejector is used similar to a liquid pump to remove liquid from the evaporator outlet, by this means enabling overfed conditions in the evaporator which in turn facilitate higher evaporation pressures for the same cooling effect. In both cases, energy savings are achieved by increasing the compressor suction pressure and thus reducing the required compressor pressure ratio.

While theoretical evaluations indicate significant energy savings by the ejectors, challenges are found to occur in actual field installations with ejectors. In particular, in one of the analysed ice rink systems the heat recovery was turned off in the previous hockey season to achieve proper ejector operation. To avoid the need for such steps in the future, reasons for the observed insufficient ejector performance are analysed as part of this study.

The focus in this context is on the operation and work recovery efficiency of the ejector under varying conditions, in particular with respect to the heat recovery. For the particular case of liquid ejectors, the implementation of overfed conditions for a large number of evaporators in refrigeration cabinets is analysed.

1.1 Objective

Based on the findings from previous research work on ejectors, the objective of this project is to analyse the available field measurement data from ice rinks and supermarkets and evaluate the performance of the ejector as well as its effect on the overall system performance. This includes a particular focus on the interaction of the ejector and the heat recovery systems as well as an overall analysis of the control mechanisms.
In parallel to the field measurement data evaluation, an analytical model of the ejector is developed based on previous research on ejectors, with the aim to predict the benefits of the different ejector types for the system performance under different conditions.
The field measurement data will then be compared to the modelling results to understand the system performance in comparison to theoretical expectations and develop possible improvements for the analysed systems and future system installations with ejectors.

1.2 Field Measurement Data

The field measurement data which are evaluated for this project come from four CO2 refrigeration systems, two ice rink refrigeration systems with vapor ejectors (VEJ) and two supermarket refrigeration systems with liquid ejectors (LEJ). All four systems are located in Scandinavia and include heat recovery on the high-pressure side.

For the two ice rink systems, field data is provided by EKA Energi & Kylanalys AB.
System VEJ-A, shown in figure 3.1, is a direct expansion (DX) system located in the northern part of Sweden, with a capacity of 320 kW at $-10\,°C$ evaporation temperature. The capacities for heat recovery in the system are 95 kW at the high temperature level ($40 - 70\,°C$) and 195 kW at the medium temperature level ($25 - 40\,°C$).
System VEJ-B, shown in figure 3.2, is an indirect system located in southern Norway, using ammonia-water as secondary refrigerant. The system is designed for a capacity of 650 kW at $-15\,°C$ evaporation temperature. The capacities for heat recovery in the system are 160 kW at the high temperature level ($60 - 75\,°C$) and 320 kW at the medium temperature level ($30 - 50\,°C$).
System VEJ-A uses three, system VEJ-B four needle-controlled ejectors [4] in parallel. In both systems, the heat recovery uses two separate heat exchangers for high and medium temperature heat recovery, followed by a gas cooler which can be bypassed. In addition, System VEJ-A includes heat exchange with a borehole, enabling additional subcooling after the gas cooler or alternatively additional evaporation if more heat is needed in the heat recovery.

The data for the supermarket systems is obtained from a cooperation by the division of Applied Thermodynamics and Refrigeration at KTH. Both supermarket systems are located in the greater Stockholm area.
System LEJ-A provides refrigeration at low and medium temperature levels, while system LEJ-B has a third high temperature refrigeration level for air conditioning. In both cases, the analysis focuses on the refrigeration at medium temperature level shown in figure 3.4, as the liquid ejectors are only installed at this temperature level.

1.3 Scope and Limitations

This work generally focuses on vapor and liquid ejectors integrated in vapor compression refrigeration systems. An alternative refrigeration system design with ejectors are so-called ejector refrigeration systems, in which the ejector fully replaces the compressor, using a separate high-temperature generator to entrain refrigerant in the ejector. The ejector refrigeration system is however not analysed in this work.
The focus of the VEJ system data evaluation is on the interaction of the ejector with the surrounding parameters of the refrigeration system, particularly with the heat recovery. As the system conditions are changing rapidly, the system data are evaluated with a sample time of one minute. This makes it necessary to select certain representative time periods for the evaluation due to the large amount of data.
For the LEJ system data evaluation, the focus is in contrast on the analysis of the conditions in the evaporators and the liquid handling by the ejectors. This is due to the fact that the ejector performance and interaction with the other system parameters is found to have only a minor impact on the system performance, while the relevant system performance improvement is actually achieved indirectly by enabling overfed evaporation conditions.
The limited available field data measurements require a number of assumptions and parameter estimations during the system evaluation. A major source of uncertainty is the determination of the compressor and evaporator mass flow in the analysed VEJ systems, as the mass flows are not directly measured but calculated from the compressor power and enthalpy difference. For this purpose, the assumption of an efficiency of the compressor motor is necessary. System VEJ-A requires in addition an estimation of the compressor power input from the total refrigeration system power input. A further uncertainty is added to the estimation of the evaporator mass flow rate, which is calculated assuming stationary conditions without changes in the receiver liquid levels. The impact of these uncertainties is limited by comparing to a theoretical reference system during the evaluation for which the same assumptions are taken.

2 Literature Review

2.1 Ejector Working Principle

The general working principle of an ejector is illustrated in figure 2.1. A fluid (refrigerant) stream with high pressure is accelerated in a converting throat before it leaves the entrainment (or "motive") nozzle with supersonic velocity. This high-velocity stream creates low pressure at the suction inlet, enabling the low-pressure fluid from the suction inlet to be pulled into the ejector where the two fluid streams are mixed, exchanging mass, momentum and energy. Subsequently, the mixed fluid flow of high velocity is slowed down in the diverting diffusion section of the ejector. In this way, the kinetic energy of the high-velocity stream is converted back into a pressure increase, resulting in an intermediate pressure level at the ejector outlet. In total, this allows to increase the pressure of a low-pressure fluid stream with the help of another high-pressure fluid stream, allowing to recover work from the high pressure fluid stream [5].

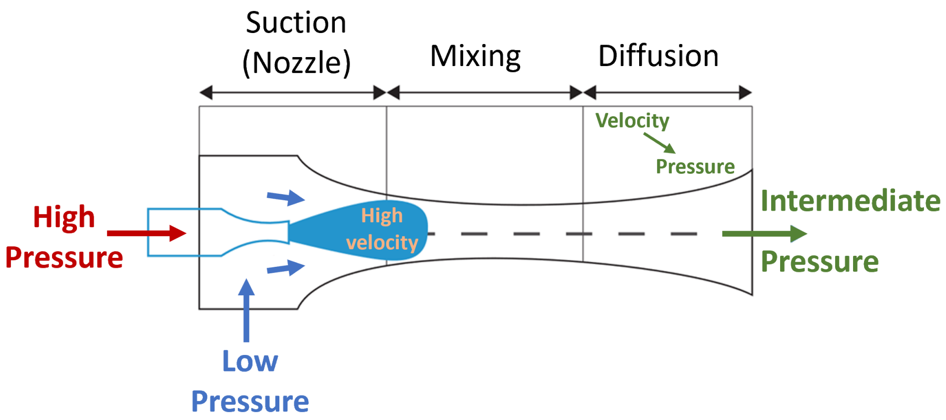

Figure 2.1: Working principle of the ejector (adapted from [1])

2.1.1 Ejector Key Parameters

Based on the described working principle of the ejector, a number of key parameters can be defined for the ejector and its performance.
The mass entrainment ratio describes the ratio of the mass flow at the suction inlet of the ejector $\dot{m}_{\mathrm{ej,s}}$ relative to the mass flow at the entrainment inlet of the ejector $\dot{m}_{\mathrm{ej,e}}$ as shown in equation 2.1.

It is thus a measure for how much low-pressure mass flow can be entrained (i.e. its pressure can be increased by the ejector) per amount of high-pressure mass flow [5].

$$\omega = \frac{\dot{m}_{\mathrm{ej,s}}}{\dot{m}_{\mathrm{ej,e}}} \tag{2.1}$$

A second key parameter is the ejector pressure lift Δp_{lift}, indicating the pressure difference by which the fluid/refrigerant at the suction side is lifted, as described in equation 2.2 [5].

$$\Delta p_{\mathrm{lift}} = p_{\mathrm{ej,out}} - p_{\mathrm{ej,s}} \tag{2.2}$$

The ejector inlet and outlet conditions as well as mass entrainment ratio ω and pressure lift Δp_{lift} are visualized for a vapor ejector cycle in figure 2.2.

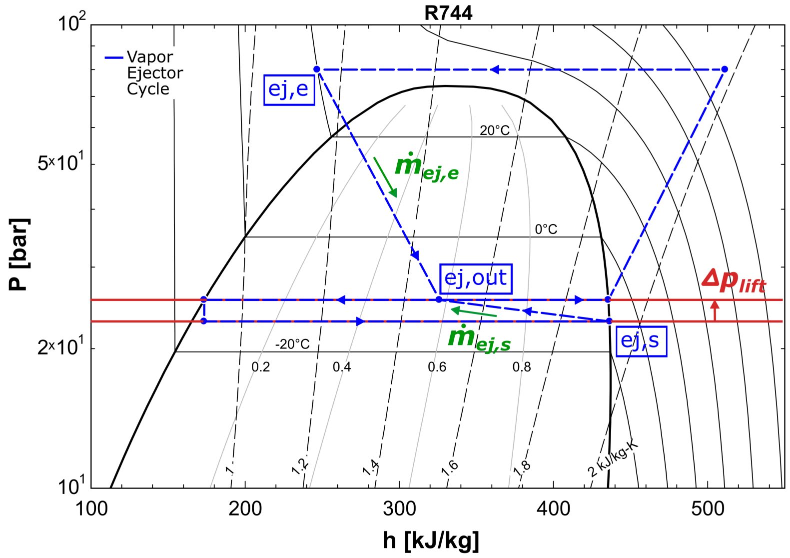

Figure 2.2: Visualization of ejector conditions, ω and Δp_{lift}

As an alternative to the ejector pressure lift Δp_{lift}, some studies use the ejector pressure ratio τ to express the increase in pressure of the suction mass flow, as defined in equation 2.3 [5].

$$\tau = \frac{p_{\mathrm{ej,out}}}{p_{\mathrm{ej,s}}} \tag{2.3}$$

For the ejector refrigeration cycles described in this work, the ejector suction pressure $p_{\mathrm{ej,s}}$ is equal to the evaporation pressure p_{evap} and the ejector outlet pressure $p_{\mathrm{ej,out}}$ is equal to the receiver pressure p_{rec} in the high-pressure receiver (HPrec), i.e. the pressure lift also describes the pressure difference between receiver and evaporator.
The actual work recovery effect of the ejector is achieved by lifting a certain low-pressure mass flow by a certain pressure lift. Both ω and Δp_{lift} thus only describe one part of the ejector effect. Several studies therefore use an ejector efficiency as an overall performance indicator of the ejector. Various definitions based on different concepts are possible as described in [2], the most commonly

used being the one by Elbel and Hrnjak [6], which will also be used in the further evaluations in this work. This ejector efficiency is a work recovery efficiency, describing the ratio of the recovered work W_r by the ejector to the theoretically recoverable work $W_{r,max}$ [5].
The maximum recoverable work $W_{r,max}$ in the ejector under ideal conditions is the work resulting from an isentropic expansion process between the ejector entrainment inlet and the ejector outlet. $W_{r,max}$ is thus calculated as shown in equation 2.4 as product of the entrainment mass flow $\dot{m}_{ej,e}$ and the isentropic enthalpy difference between ejector entrainment inlet and outlet [6].

$$W_{r,max} = \dot{m}_{ej,e} \cdot \left(h_{ej,e} - h_{ej,e,exp,is}\right) \tag{2.4}$$

The resulting recovered work W_r can be described as a compression process of $\dot{m}_{ej,s}$ between the suction and outlet pressure of the ejector. To achieve a conservative estimation of the ejector performance, the minimum work required for this process is used in the description of the ejector efficiency, which is the case of isentropic compression between the ejector suction conditions and the outlet pressure, as shown in equation 2.5 [6].

$$W_r = \dot{m}_{ej,s} \cdot \left(h_{ej,s,comp,is} - h_{ej,s}\right) \tag{2.5}$$

Using equation 2.1 in combination with the two previous equations, the ejector work recovery efficiency η_{ej} is then described by equation 2.6.

$$\eta_{ej} = \frac{W_r}{W_{r,max}} = \omega \cdot \frac{h_{ej,s,comp,is} - h_{ej,s}}{h_{ej,e} - h_{ej,e,exp,is}} \tag{2.6}$$

As described, the respective isentropic enthalpies are the enthalpy after isentropic expansion from the entrainment conditions to the ejector outlet pressure $h_{ej,e,exp,is} = h(s_{ej,e}, p_{ej,out})$, and the enthalpy after isentropic compression from the suction conditions to the ejector outlet pressure $h_{ej,s,comp,is} = h(s_{ej,s}, p_{ej,out})$ [6][7], as visualized in figure 2.3.

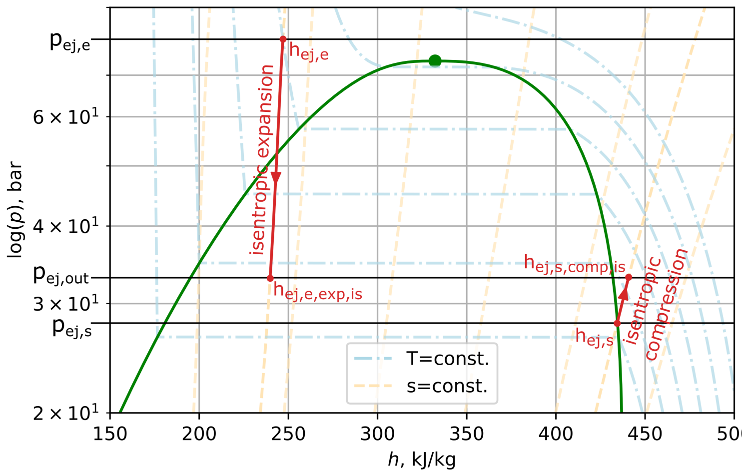

Figure 2.3: Visualization of the processes used in the definition of η_{ej}, based on [6]

With respect to the ejector efficiency, Ringstad et al. [5] underline the particular relevance of ejectors in refrigeration systems with CO2 as refrigerant compared to the use of ejectors with other refrigerants. The study states ejector efficiencies of 0.2 – 0.4 for CO2 systems compared to ejector efficiencies below 0.2 for systems using R404A or R134a as refrigerant, due to the lower operating pressures and thus lower work recovery potential in cycles with these refrigerants [5][8].

2.2 Integration of Ejectors in Refrigeration Systems

The ejectors used in vapor compression refrigeration systems can be mainly classified into two types depending on the physical state of the fluid at the low-pressure suction inlet of the compressor:

- **Vapor (also "Gas" or "Two-Phase") Ejectors** directly lift the pressure of gaseous refrigerant from the evaporator outlet to a higher pressure level.
- **Liquid Ejectors** are used similarly to a pump, moving liquid from the evaporator outlet back to a higher pressure level before the evaporator inlet. This is one option to enable the use of **overfed evaporation**.

In addition to state conditions of pure vapor or pure liquid at the ejector suction inlet, two-phase conditions at the ejector suction inlet are a possible third option, however with little literature available on according ejectors to this date. This third ejector option with two-phase conditions at the suction inlet is not to be confused with the above mentioned vapor ejector which is also named "two-phase ejector" in some sources due to the two-phase conditions at its outlet [9][10].
The high-pressure entrainment inlet of the ejector is in all cases connected to the condenser or gas cooler outlet, if the ejector is integrated in a vapor compression refrigeration system as in this work.

2.2.1 Vapor Ejectors

The entrainment inlet of the vapor ejector is connected to the gas cooler outlet, possibly after an internal heat exchanger (IHX). The suction inlet is connected to the evaporator outlet, while the outlet is connected to an HPrec.
Two different basic system designs with integrated vapor ejectors are mainly found in literature and shown in figures 2.4 and 2.5.
In the system design shown in figure 2.4, the vapor ejector is fully replacing the HPV and used to lift the pressure of the entire evaporation mass flow $\dot{m}_{\mathrm{evap}}$ to the receiver pressure p_{rec}. Thus, no parallel compression is used in this cycle, but the main compressor is directly connected to the receiver instead of the evaporator outlet in this setup. This system configuration is marked as vapor ejector system "VEJ" here and is the system type used in the analysed real vapor ejector systems in this report.
In the VEJ cycle, the mass entrainment ratio ω is in fact the ratio of the evaporator mass flow $\dot{m}_{\mathrm{evap}}$ to the compressor mass flow $\dot{m}_{\mathrm{comp}}$, as the ejector suction inlet is connected to the evaporator outlet and the ejector entrainment inlet to the gas cooler outlet. With the entire evaporator mass

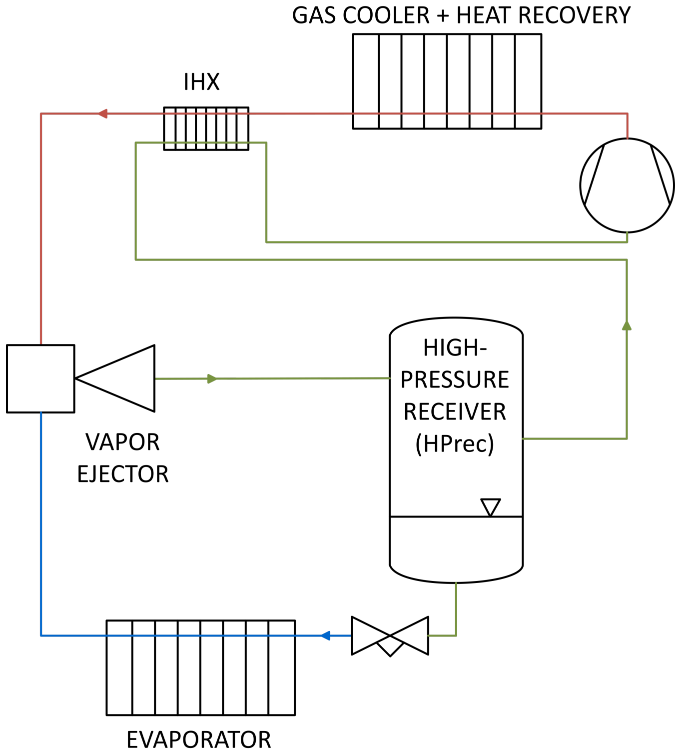

Figure 2.4: Vapor ejector system without parallel compression (VEJ)

flow flowing through the ejector, a higher mass entrainment ratio ω and subsequently a smaller pressure lift is generally found in these systems. The used vapor ejectors are therefore termed as "low pressure" ejectors in some sources.
Furthermore, the ejector replaces the HPV in its role for the control of the discharge pressure p_{disc} in this system [11].

The vapor ejector system with parallel compression "VPC" as shown in figure 2.5 is an alternative refrigeration cycle using vapor ejectors. In comparison to the VEJ system, the suction inlet of the main compressor (MC) in the VPC system is still connected to the evaporator outlet, while the parallel compressor (PC) in the VPC system is replacing the MC of the VEJ system, allowing for two different compression options. In addition, a HPV parallel to the vapor ejector can be alternatively used for expansion, enabling a control of p_{disc} without involvement of the ejector as described in section 2.2.3. If parallel compression is used as in the VPC system, not the entire evaporator mass flow is entrained in the ejector, thus the mass entrainment ratio ω is generally lower in such systems [9]. Furthermore, it is noteworthy that the mass flow through the parallel compressors is increased in the VPC system in comparison to a usage of the parallel compressors only to compress the flash gas from the receiver. As a consequence, the performance of the parallel compressors becomes more relevant when using the VPC system, which should be considered in the choice of components [12].
Regarding the practical implementation of the two different vapor ejector systems, Doerffel et al. [13] states that the VEJ system is less challenging to balance compared to the VPC system due

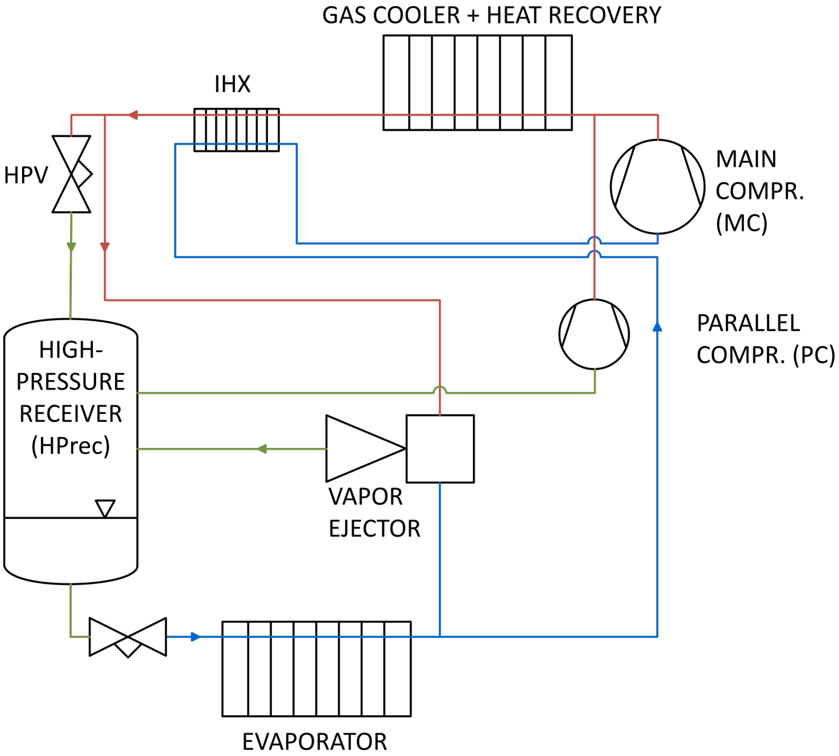

Figure 2.5: Vapor ejector system with parallel compression and HPV (VPC)

to the smaller number of actuators in the VEJ system. At the same time, the study mentions a more difficult start-up process for the VEJ system, as an initial pressure difference between p_{evap} and p_{rec} needs to be created, for example by using pumps. Concerning cost-effectiveness, Gullo et al. [12] states a higher cost effectiveness of the implementation of vapor ejectors compared to the implementation of parallel compressors in a one-stage vapor compression system.

Effect of System Parameters on Ejector Performance

For fixed conditions at the ejector entrainment and suction inlet, the ejector efficiency η_{ej} is only related to the pressure lift Δp_{lift} and the entrainment ratio ω, as can be concluded from equation 2.6. Thus, for a fixed ejector efficiency at fixed entrainment and suction conditions, there is generally a trade-off between ω and Δp_{lift}, i.e. for a higher Δp_{lift}, ω is decreased and vice versa.
The ejector efficiency of a fixed ejector design is in turn found to be depending on the entrainment and suction inlet parameters. A number of studies analysed the performance of ejectors with fixed geometries, commonly finding specific optimum operating conditions [14][15]. In particular, Lucas and Koehler [14] state that the ejector efficiency reaches a maximum for a certain entrainment pressure p_{disc}. This p_{disc} for maximum ejector efficiency is lower for lower evaporation temperatures T_{evap} as well as for lower entrainment temperatures $T_{\mathrm{ej,e}}$. Furthermore, lower evaporation temperatures T_{evap} are also found to decrease the ejector efficiency η_{ej} in the study. Conversely, a

lower entrainment temperature $T_{\mathrm{ej,e}}$ is found to increase the ejector efficiency η_{ej}, an effect which is stronger for lower evaporation temperatures T_{evap}.
Even the experimental data by Banasiak et al. [9], obtained from a VPC system with multi-ejector comprising three parallel vapor ejectors with increasing size, show a maximum ejector efficiency depending on the entrainment pressure. The study finds that this maximum ejector efficiency occurs at increasingly higher pressure lifts Δp_{lift} for higher entrainment enthalpy $h_{\mathrm{ej,e}}$. The ejector efficiencies in this study are found to be $0.22 - 0.34$.
Banasiak et al. [9] also find that the ejector efficiency of the multi-ejector is generally decreasing with higher entrainment mass flow $\dot{m}_{\mathrm{ej,e}}$. In fact, the study results indicate the best ejector efficiency when only the smallest of the three ejectors in the multi-ejector is used, while the efficiency is lowest during the usage of all three ejectors.
The analysis by Lawrence and Elbel [11] of a needle-controlled ejector and a high-pressure control by a parallel HPV to the ejector shows improved ejector efficiencies for off-design conditions for both control cases compared to an ejector with a fixed geometry. The study indicates a small difference of up to 1.5 % higher COP for the needle control compared to the control with a parallel HPV in off-design conditions. Despite the general control improvements, the study also finds a decrease in ejector performance for off-design conditions, particularly for increasing entrainment pressures p_{disc}. For the needle-controlled ejector, the study indicates a drop in ejector efficiency η_{ej} by more than 10 percentage points from about 0.25 to below 0.15 for an increase in p_{disc} by 6 bar from 82 bar(a) to 88 bar(a) at $T_{\mathrm{gc,out}} = 30\,°\mathrm{C}$. The decrease in ejector efficiency appears to decrease for higher $T_{\mathrm{gc,out}}$ at higher pressure levels.
Regarding the combination of ejector and IHX, Lucas and Koehler [14] find for the studied ejector with fixed geometry that the ejector efficiency is increasing with increasing internal heat exchange, reaching an ejector efficiency of up to 0.17 with IHX compared to a maximum of 0.14 without IHX.

Efficiency Improvements

Gullo et al. [12] analyse various studies on the efficiency improvements by ejectors, stating improvements of 7 – 26 % by the implementation of ejectors in a CO2 refrigeration system. For the implementation of ejectors in combination with heat recovery in CO2 refrigeration systems, the study states energy savings of up to 30 % compared to conventional systems using R404A as refrigerant [12][16].
The majority of the studies indicate differences in the system performance depending on the climate conditions, however with generally similar trends. A comprehensive study by Hafner et al. [16] on the performance in different climate conditions finds improvements of the COP_2 between 10 % at 15 °C and 20 % at 45 °C ambient temperature for an ejector efficiency of 20 %, using a steady-state simulation of multi-ejectors in a VPC arrangement. The same study finds 20 – 30 % increase in cooling COP during winter for transient models based on typical heating and cooling demands in Europe. For summer, an increase in cooling COP of 17 % for Athens, 16 % for Frankfurt and 5 % for Trondheim are found with the multi-ejector in comparison to a standard CO2 refrigeration system without ejector [16].
For needle-controlled "modulating ejectors" (named "EMJ" by the manufacturer), an experimental

study for temperature profiles of Madrid, Athens and Riyadh shows reductions in energy consumption between 5 % and 21 % for $T_{\mathrm{gc,out}} = 24 - 39\,°\mathrm{C}$ with increasing improvements for higher temperatures, in comparison to a standard CO2 configuration without ejectors [17]. The ejectors are found to allow higher reductions in energy consumption compared to parallel compression with only 0 – 8 % improvement for the same conditions in this study. The annual energy savings from the ejectors are found to be between 3.6 % and 12 % in this study.
A recent study by Doerffel et al. [13] experimentally compares the effect of the VEJ and the VPC cycle, however for both cases with an optional parallel HPV. The study finds energy savings of about 20 % at $T_{\mathrm{gc,out}} = 20\,°\mathrm{C}$ for both ejector system cases, compared to a reference CO2 system without ejectors and without parallel compression. When comparing the Carnot efficiency of the systems for higher temperatures, the efficiency of the VPC system design with high-pressure ejectors is decreasing less compared to the low-pressure ejectors in the VEJ system design. Nevertheless, the efficiency improvement in comparison to the reference system case is increasing in both cases for higher temperatures.

In total, a relatively wide range of ejector efficiencies and performance increases is found in the analysed studies, likely due to the strong dependence of the ejector performance on the geometrical design [5], the generally varying testing approach and setup as well as the different control approaches in the studies. The cited results give however a general picture of the range of the expected ejector performance and system efficiency improvements.

2.2.2 Liquid Ejectors

The entrainment inlet of the liquid ejector is connected to the gas cooler outlet as in the vapor ejector cycles. The suction inlet is connected to the liquid outlet an LPrec after the evaporator, while the outlet is connected to an HPrec, from where the liquid is then again entering the evaporator.
Figure 2.6 shows a system layout with liquid ejectors, as it is used in the analysed LEJ systems of this report. In contrast to the vapor ejector systems, it can be seen that the compressor suction inlet remains at the evaporator pressure level in the LEJ system. Instead of a direct pressure lift as in the vapor ejector case, the liquid ejector indirectly allows for higher suction pressures by enabling overfed evaporation.
As illustrated in figure 2.7, overfed evaporation means that the internal superheat in the evaporator is removed. This allows for a more narrow temperature profile in the evaporator with higher evaporation temperature and pressure at equal air temperatures. As the suction pressure is equal to the evaporation pressure in the LEJ system, this increases the suction pressure, reducing the compressor power. At the same time, overfed evaporation comes with a small amount of remaining liquid refrigerant at the evaporator outlet, which is collected in the low-pressure liquid receiver (LPrec) and then requires the liquid ejector to pump it back into the HPrec. Due to the indirect effect of the liquid ejector mainly as enabler for overfed evaporation, the ejector performance does not have a direct impact on the pressure lift achieved in the LEJ system. Instead, the overfed evaporation and thus the heat transfer in the evaporator plays an important role in the achievable evaporation temperature increase.

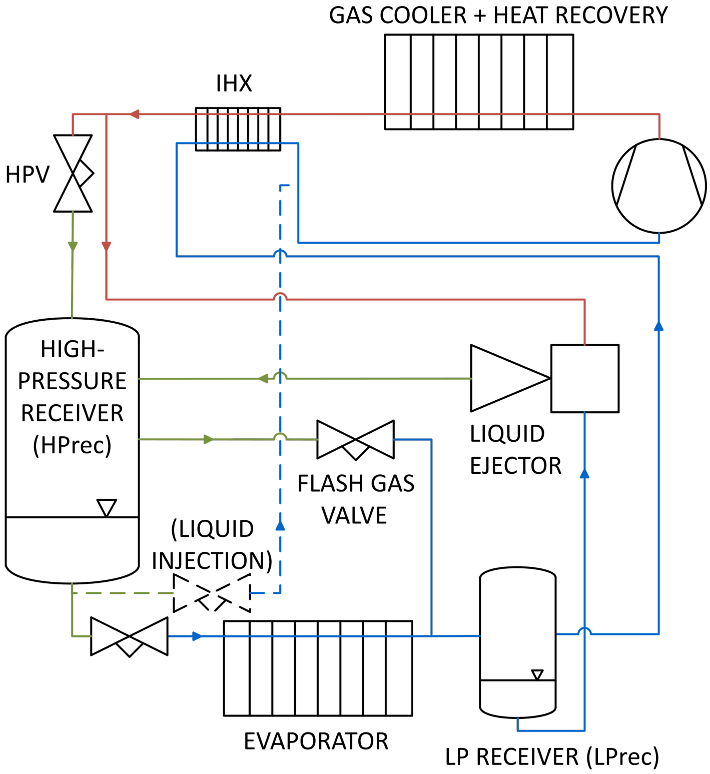

Figure 2.6: Liquid ejector system (LEJ)

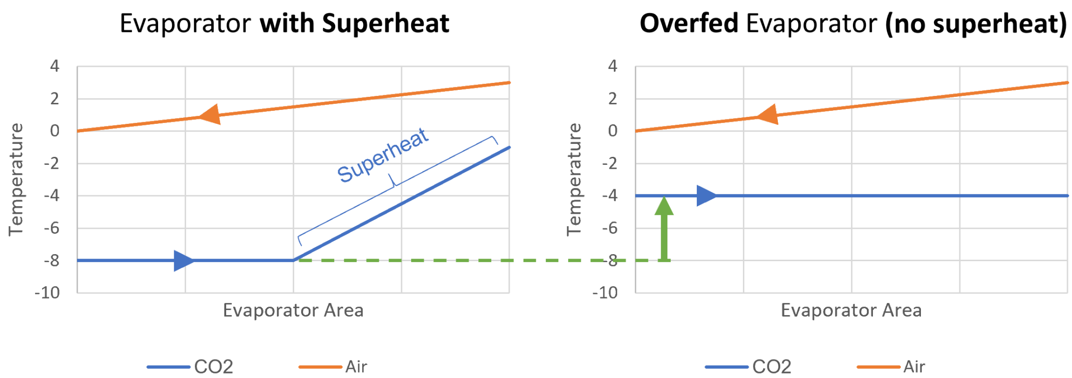

Figure 2.7: Effect of overfed evaporation

Based on a model of a typical 5 kW refrigeration cabinet which cools the air from 8 to 3 K, Karampour and Sawalha [18] find that the change from a system operation mode with 10 K superheat at −8 °C evaporation temperature causes an increase of the evaporation temperature of 3.7 K if overfed conditions (0 K superheat) are used [18]. The study suggests that the use of overfed evaporators can improve the system efficiency by 9 – 10 % [18] in comparison to dry expansion in a parallel compression system.
An experimental study by Minetto et al. [19] finds a reduction of 13 % in compressor power con-

sumption for a system with overfed evaporators compared to a system with dry expansion in a subcritical cycle without parallel compression at $T_{\text{amb}} = 16\,^{\circ}\text{C}$, and $0\,^{\circ}\text{C}$ air temperature in the evaporator. In this study, $\Delta T_{\text{SH,evap}} = 6\,\text{K}$ superheat is used in the dry expansion case. The overfed evaporator case in comparison shows a 2 K higher evaporation temperature, while the air temperature of the cooled space is 0.4 K lower compared to the reference case. The study also finds that the air temperature in the cooled space is more stable with higher evaporation temperatures, as this allows a better adaption to required capacities [19]. The evaluation of the experimental setup in the study indicates a vapor quality of 0.96 at the outlet of the overfed evaporator. However, nearly all liquid at the evaporator outlet is found to be evaporated in the internal heat exchanger after the evaporator [19].

In their comprehensive review of ejector developments, Gullo et al. [20] emphasize the comparatively small impact of ambient temperature changes on the performance improvement in the LEJ cycle by overfed evaporation compared to the more significant impact of changing ambient conditions on the achieved improvements by the ejector in the vapor ejector cycle. The study states 15 % annual energy savings for a liquid ejector with 8 % ejector efficiency compared to only 5 % energy savings on an annual basis for a vapor ejector system using a multi-ejector system with a peak ejector efficiency of 30 %.

For evaporation on two temperature levels as commonly used e.g. in supermarket refrigeration systems, ejectors are mainly installed to lift the pressure from the medium temperature evaporator to the receiver pressure. If the ejector is used to lift the entire mass flow, i.e. all medium-temperature compressors use the receiver pressure rather than the evaporation pressure, it should be considered that the discharge pressure of the low-temperature compressors (which in this case is equal to the receiver pressure) increases with increasing ejector pressure lift Δp_{lift}. The subsequent higher pressure ratio for the low-temperature compressors thus increases the power consumption of these compressors.
As the low-temperature cooling demand is typically significantly lower than the medium-temperature cooling demand, this effect only plays a minor role, with the reduction in energy consumption of the medium-temperature compressors by the ejector outweighing the higher power consumption of the low-temperature compressors. However, the higher the share of the low-temperature cooling demand compared to the medium-temperature cooling demand becomes, the more relevant this effect becomes [16].
In parallel compression systems in contrast, the low-temperature compressor discharge side can be connected to the suction side of main compressors on the medium-temperature levels, rather than to the parallel compressor suction side, thus avoiding the higher discharge pressure for the low-temperature compressors.
A similar effect as described above is also caused by the use of liquid ejectors, as they lift the evaporation pressure for the medium-temperature evaporators.

2.2.3 Ejector Control

In order to adapt the vapor ejector to different capacities in the refrigeration systems, different control strategies are applied. If the ejector fully replaces the HPV as in the VEJ system, the ejector

plays furthermore a key role in the control of the high-side pressure p_{disc} [11]. This is the case for the two analysed vapor ejector systems.
The simplest ejector design has a fixed geometry without any option to control the ejector. This can be an effective solution if the system has no significant deviations from the conditions for which the ejector is designed. However, for changes in capacity with a speed-controlled compressor, the discharge pressure p_{disc} is depending on the capacity in this case and cannot be controlled independently due to the fixed mass flow through the ejector [11]. For off-design operating conditions, the ejector should therefore be controlled by adapting the entrainment mass flow $\dot{m}_{ej,e}$ through the ejector [21].
Two types of capacity control in the vapor ejector are currently mainly used for this purpose and shown in Figure 2.8a and 2.8b [22][5]:

- The **needle-controlled ejector** uses a conical needle which can be moved in and out of the nozzle throat of the ejector to adapt the flow area and thus the entrainment mass flow.
- The **multi-ejector module**, also termed as "parallel ejectors" in some sources, consists of a number of parallel ejectors with different sizes but fixed geometries, which can be individually switched on and off using valves at the entrainment inlets. Multi-ejectors commonly use sizes in "binary" steps, i.e. size ratios of 1:2:4:8, where the nozzle throat area of the largest ejector is eight times the one of the smallest. By combining the ejectors in different ways, i.e. switching them individually on and off, a broad range of operating conditions can be covered in small steps.

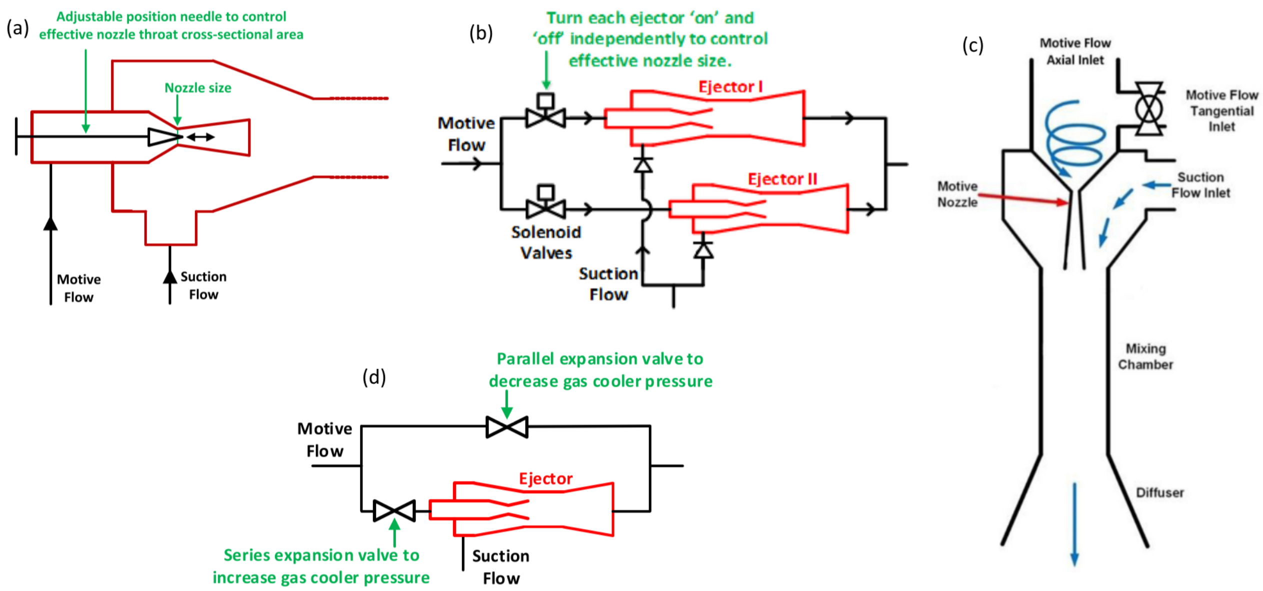

Figure 2.8: Ejector capacity and high-pressure control mechanisms [11][23]

The analysed field installations in this work use a combination of these two control strategies, with three to four needle-controlled ejectors of different size used in parallel. This combined ejector control approach has not yet been analysed in previous research papers to the knowledge of the author.

Smolka et al. [22] compare the two control strategies in a combined CFD and experimental study, finding that the needle-controlled ejectors achieve slightly higher improvements during operating conditions for high capacities with low reduction of the throat area, i.e. minor insertion of the needle into the throat. However, a significant decrease in efficiency is found for higher reductions of the throat area, likely due to increasing pressure losses. In addition, the study finds that the proper positioning of the needle for optimal performance is difficult to determine.
In addition to the mentioned control options, further ejector control mechanisms are subject to research to address the control challenges of current systems [24]. In particular, the so-called vortex ejector shown in figure 2.8c uses part of the entrainment mass flow to create an adjustable swirl before the ejector nozzle, which allows to regulate the entrainment mass flow and thus the capacity of a single ejector without moving parts [25]. Furthermore, a control by pulse-width modulation (PWM) has recently been suggested, using PWM to control the opening and closing of a valve at the entrainment inlet of a fixed-geometry ejector to achieve the required gas cooler mass flow as time-averaged value. This enables a fixed entrainment mass flow at the ejector itself during the time periods when the valve is open [24].
In general, an increase in control instabilities from the implementation of ejectors is found in [26]. In particular, He [21] finds based on Lucas and Koehler [14] that the refrigeration system with ejectors is more sensitive to the high-side pressure p_{disc} than the system without ejectors. This means that a faster decrease in performance for off-design conditions is found in ejector systems compared to systems without ejectors, which can even cause performance decreases under certain off-design operating conditions.
As an alternative to the control of p_{disc} with the ejector, a parallel HPV can be installed in parallel to the ejector [11] as shown in the VPC cycle (figure 2.5) and in figure 2.8d. This potentially reduces however the amount entrainment mass flow and thus of recoverable work while adding the requirement of an additional component to the system.

For liquid ejectors, the ejector control is significantly simpler, as generally only a small amount of the gas cooler refrigerant mass flow is used in the ejector. In both analysed field installations, three parallel liquid ejectors of increasing size are used and switched either on or off by a valve at the high-pressure inlet, depending on the liquid level in the LPrec. For the individual ejectors, a certain liquid level threshold is set above which the ejector starts operating. Furthermore, a minimum valve opening time of e.g. ten seconds is used to avoid unstable operation.

2.3 Key Design Findings

Ringstad et al. [5] state that the mechanical design plays a key role for the performance particularly of vapor ejectors. As this is of particular interest especially for the vapor ejector, a range of studies have been performed to analyse the effect of various geometrical ejector designs numerically and experimentally, with research continuing on the matter [27][21][28][29]. As the geometrical ejector design is not part of this work, this section focuses on few key findings on the effect of internal ejector geometries with direct relation to the ejector operation in relation to the system parameters affecting the ejector.

In general, the ejector nozzle design must be suitable for the entrainment pressure p_{disc} and outlet pressure p_{rec} of the ejector in order to reach critical operating conditions in the ejector. Critical conditions in this context do not refer to the CO2 pressure but to the flow conditions in the nozzle, where only an operation at or above critical flow conditions allows stable operation [21]. In sonic conditions, operation at or above the critical flow conditions cause the entrainment mass flow of a single fixed-geometry ejector to be independent of the evaporation conditions, as choked flow occurs [14][2]. Subcritical flow conditions cause in contrast a rapid decrease in ejector efficiency with strongly decreasing mass entrainment ratio [21].
In this context, Lucas and Koehler [14] find that there is an optimum ratio between motive nozzle area and mixing area, for highest ejector efficiency depending on the high-side pressure p_{disc} for fixed T_{evap} and $T_{\mathrm{gc,out}}$. He et al. [21] state that a decreasing nozzle area moves the critical point to lower entrainment pressures p_{disc} while increasing the mass entrainment ratio in the critical range. With regard to the evaporation temperature, Lucas and Koehler [14] suggest that the decreasing η_{ej} at lower T_{evap} described in section 2.2.1 is possibly caused by increasing frictional pressure losses from an increased fluid velocity due to the lower density in the mixing chamber. Based on these findings, they suggest that an ejector design with a higher mixing chamber diameter but a shorter mixing chamber length can improve η_{ej} at lower T_{evap}. Regarding the presented field data results in this report, this might allow for a better ejector efficiency in the analysed systems at low evaporation temperatures, particularly in system VEJ-B.
Regarding the diffuser, the study states maximum ejector efficiencies at $5\,^{\circ}$ diffuser angle [14].
Furthermore, an experimentally validated CFD study on the effect of the ambient temperature on the ejector performance shows a decrease in mass entrainment ratio of $8-13\,\%$ for non-adiabatic ejector walls compared to adiabatic ejector walls [30], showing the relevance of insulation at the ejector.

2.4 Ejector Analysis and Modelling Approaches

The presented literature results from the previous sections are based on a range of different experimental and modelling approaches.
A large majority of the ejector models are numerical models, mainly addressing geometrical design aspects of ejectors. For a more detailed review of these numerical models, the reader may refer to the overview given by Ringstad et al. [5].
A few recent studies use advanced exergy analyses to evaluate the exergy destruction to identify options for improvement, however not with a particular focus on the ejectors but on a general system level of ejector refrigeration systems.
Experimental ejector studies are used for the validation of modelling results and the evaluation of the actual ejector performance under varying operating conditions. A limited amount of field data measurements exists, though mostly for warmer climates and almost exclusively for multi-ejectors.
Few publications on analytical analysis ejector system models exist to the author's knowledge. Among these, Biner [31] develops an analytical ejector model for a specific ejector design, with the entrainment mass flow based on the ejector geometry.

Furthermore, an analytical model for the ejector performance of a multi-ejector in a VPC system is developed by Gullo et al. [12], based on the findings of [32] and [33]. A similar approach based on experimental data is taken by Banasiak et al. [9], also for a multi-ejector in a VPC system. Due to the system design with parallel compression, both models show relatively low mass entrainment ratios ω and high pressure lifts Δp_{lift}, as expected based on the system description in section 2.2.1.

2.5 Sustainability

From a sustainability perspective, ejectors generally offer an effective and cost-competitive option to achieve a more sustainable utilization of energy in refrigeration systems [3]. This corresponds to the Sustainable Development Goal 7, especially target 7.3 on energy efficiency improvements.
As the use of ejectors particularly benefits the use of CO2 as refrigerant due to its high operating pressures with high work recovery potential compared to other refrigerants [2], it also generally facilitates a more wide-spread use of CO2 as natural refrigerant with low Global Warming Potential (GWP) compared to synthetic refrigerants with typically significantly higher GWP. This is especially the case for countries with warmer climates, where the low performance of CO2 systems has generally been a challenge [34].
Beyond the energy efficiency improvements, a number of studies analyses CO2 refrigeration systems with ejectors from a broader sustainability perspective. In addition to the commonly used performance indicators of refrigeration systems regarding efficiency, these studies focus on indicators incorporating a broader system perspective of ejector systems, in particular the Total Equivalent Warming Impact (TEWI) [35], which incorporates the effect of direct and indirect emissions, and the Life Cycle Climate Performance (LCCP), which in addition considers even embodied emissions in the system [34]. Both mentioned studies indicate significant reductions under various climate conditions in the respective total calculated emissions for the CO2 refrigeration system with ejectors in comparison to conventional refrigeration systems using synthetic refrigerants [35][34].

3 Methodology

The methodological approach of this work comprises two main parts; the analysis of the field measurement data and the development and evaluation of a theoretical ejector system model. Both parts are carried out for vapor and for liquid ejectors, followed by a general comparison of the theoretical findings between VEJ and LEJ system.
The ability of the vapor ejector to improve the system performance depends on two factors:

- The amount of available work to recover, which is the case of isentropic expansion in the maximum case, described by $W_{r,max}$
- The ejector's performance in the recovery of this work, described by the ejector efficiency η_{ej}

The theoretical model is used to analyse the aspect of the theoretically recoverable work for a fixed ejector efficiency. With the field data evaluation, the theoretical model findings are verified while simultaneously allowing to evaluate the dependencies of the ejector efficiency when it deviates from the assumed efficiency in the model.
In a similar way, the liquid ejector is modelled theoretically to analyse the improvement potential by the ejector for different conditions, while the field data evaluation in the liquid ejector case is mainly focusing on the overfed evaporation conditions and the resulting ejector operation.

3.1 Field Data Evaluation

For the field data evaluation, measurement data is obtained from the data logging platform of the respective systems and synchronized for a sampling period of 1 minute, i.e. a mean value for each minute forms the base of the data evaluation.

3.1.1 VEJ System Evaluation

The layouts of the two evaluated ice rink VEJ systems are shown in figures 3.1 and 3.2. In both figures, the relevant state points for the evaluation are indicated with the subscripts used in the respective parameters. As mentioned in section 1, the main difference between the systems is the direct expansion in system VEJ-A while system VEJ-B uses an indirect evaporator. Furthermore, the borehole setup in system VEJ-A allows to provide additional subcooling or evaporation to the system.

The focus of the evaluation for these systems is on the interaction of the vapor ejector with the surrounding system parameters. For this purpose, the system data are used to calculate the previously

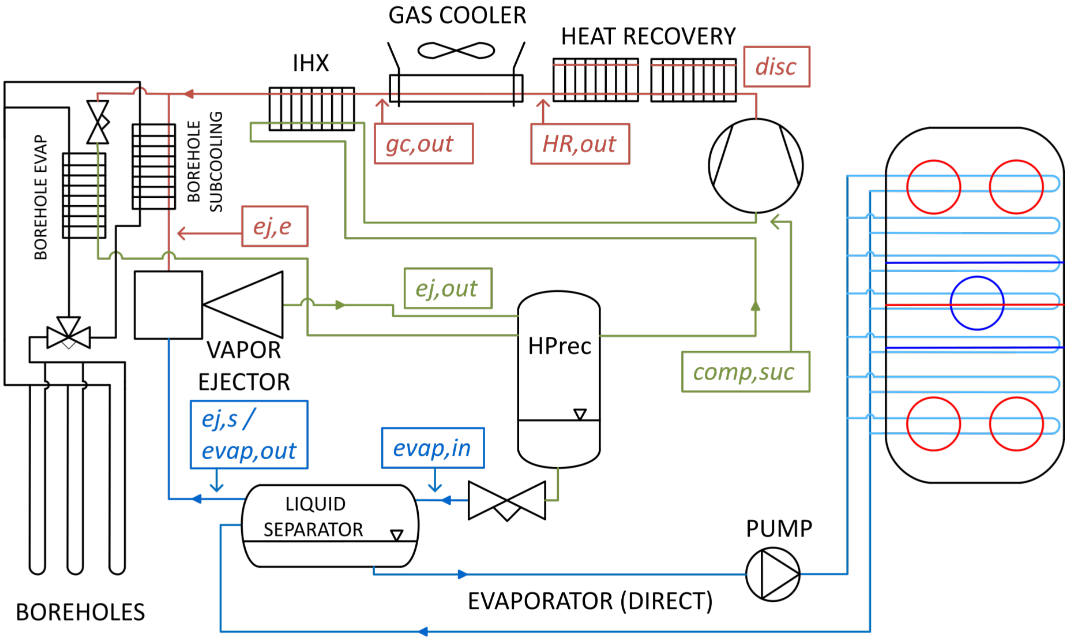

Figure 3.1: System layout VEJ-A with indicated parameter subscripts

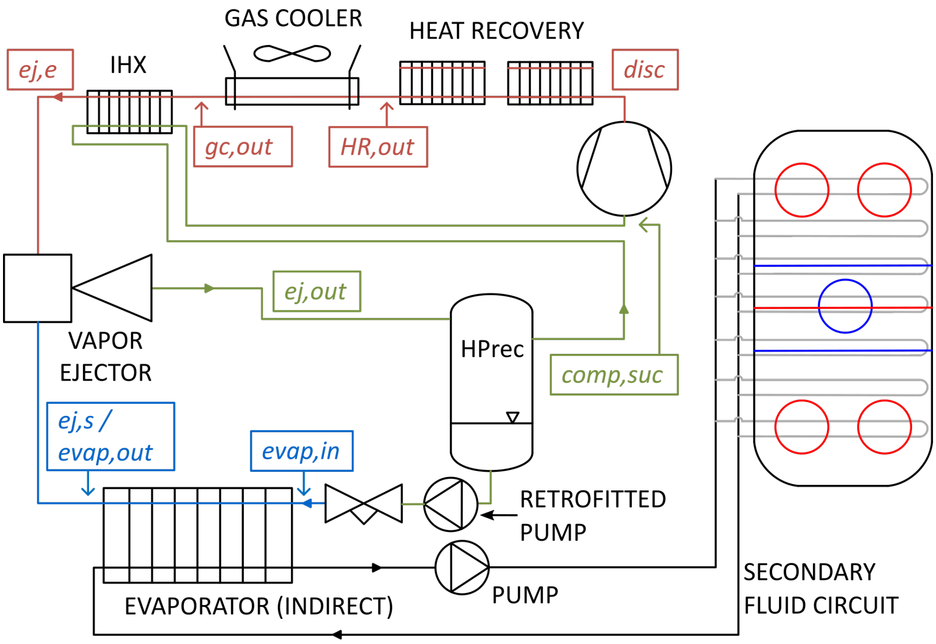

Figure 3.2: System layout VEJ-B with indicated parameter subscripts

introduced ejector parameters as well as the performance improvement relative to a theoretical REF system without ejectors operating under the same conditions. The effect of the surrounding parameters on these performance indicators is then analysed.
The relevant surrounding parameters are considered with reference to the theoretical description

by Banasiak et al. [9] of 5 independent parameters which determine the ejector performance. The determining independent parameters in the focus of this study are the temperature and pressure at the ejector entrainment inlet ($T_{\mathrm{ej,e}}$, $p_{\mathrm{ej,e}}/p_{\mathrm{disc}}$) and the suction inlet ($T_{\mathrm{ej,s}}$, $p_{\mathrm{ej,s}}$), as well as the compressor and evaporator mass flow ($\dot{m}_{\mathrm{comp}}$, $\dot{m}_{\mathrm{evap}}$) which form the mass entrainment ratio ω as the fifth independent parameter. Alternatively to ω the pressure lift Δp_{lift} could be defined as the fifth independent parameter, causing a specific ω as result. In the case of the VEJ system, ω is determined by the four previously mentioned temperatures and pressures due to the system design as explained in the corresponding modelling section, which reduces the number of theoretically independent parameters to four.
From a practical perspective, the actual mass flows $\dot{m}_{\mathrm{comp}}$ and $\dot{m}_{\mathrm{evap}}$ are expected to play a role as they need to fit the ejector design capacity. In addition, for the case of the here analysed needle-controlled ejectors, the actual ejector opening degrees and control naturally have an impact on the ejector operation.
The effect of these primary impact parameters is also considered in the general context of the system operation.

For the analysis, the obtained field data is shown in the system drawings in figures 3.1, 3.2. The evaluated refrigeration cycle for the VEJ is also visualised in a log(p)-h chart in figure 3.3 for example conditions, together with the calculated corresponding REF cycle.

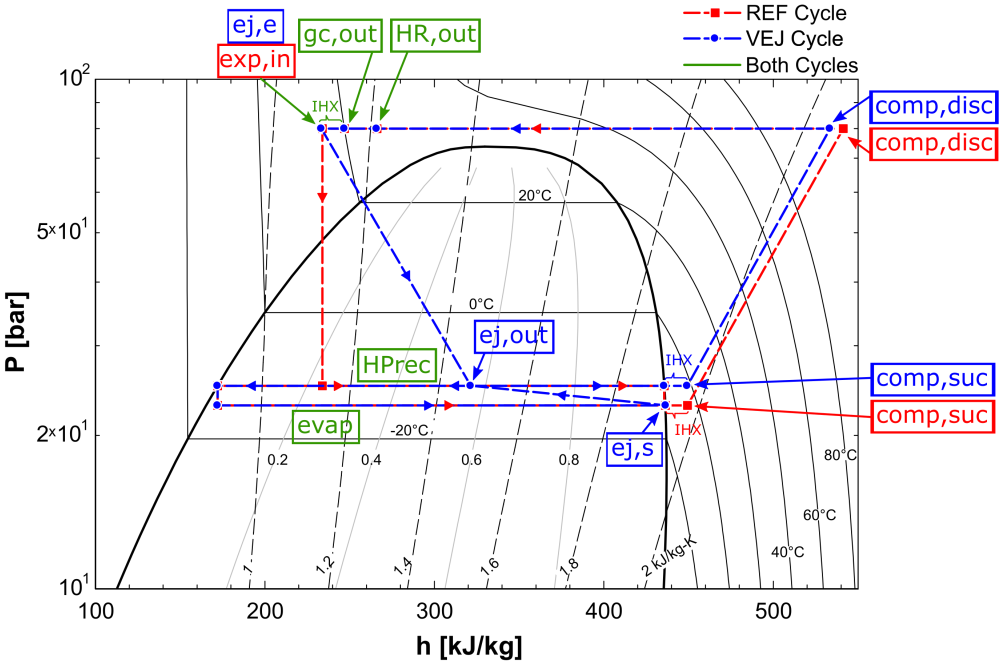

Figure 3.3: Visualization of the used field data of the VEJ systems, together with the calculated corresponding REF cycle points

Namely, the following data are obtained from the systems for the field data analysis:

- For the ejector entrainment inlet: $T_{\mathrm{ej,e}}$ and p_{disc} (and the actual pressure $p_{\mathrm{ej,e}}$ measured after the gas cooler for VEJ-B due to small deviations from pressure losses)

- For the ejector suction inlet: $T_{\mathrm{ej,s}}$ and $p_{\mathrm{ej,s}}$ (generally equal to p_{evap})
- The opening degree for each ejector
- For the liquid receivers: p_{rec} for the HPrec and the liquid levels
- For the evaporator: T_{evap} and p_{evap}
- For the compressors: $T_{\mathrm{comp,suc}}$ and $T_{\mathrm{comp,disc}}$
- The electrical compressor power or the electrical total power consumption of the system (depending on data availability)
- The run indication for each compressor and the capacity of the frequency-controlled compressor
- For heat recovery and gas cooler: $T_{\mathrm{HR,out}}$, $T_{\mathrm{gc,out}}$ and the External Reference voltage

The External Reference voltage is an input parameter from the heating system to the refrigeration system for the control of the heat recovery. Based on the heating demand, the External Reference is set to a value between 0 and 10V, with 0V indicating no heating demand and 10V indicating maximum heating demand.

The obtained raw synchronized data are then mainly evaluated in Python, using Coolprop [36]. As first step of the evaluation, the system data are filtered to ensure that only time periods are evaluated when the system is actually running. For this purpose, data points are only considered for further evaluation if at least one of the four compressors is running during the current and the previous minute. For the frequency-controlled compressor, the condition of more than 20 % capacity during the current and the previous minute is set, to exclude the beginning of system start-up processes with low capacity and unstable parameters.
For system VEJ-A, additional filters for p_{disc} below 65 bar(a) and for any valve opening above 0 % of the valve connecting to the borehole evaporator are applied. The pressure filtering is useful to further exclude any system start-up processes from the data, in addition to the compressor power filter.

The filtered system data are then used for further evaluation with the following steps:

- The atmospheric pressure of 1 bar is added to the measured gauge pressures in the system to obtain absolute pressure values.
- The actual compression power input from the compressors to the system is estimated by multiplying the power data with the relevant efficiencies (see below)
- The enthalpies at the compressor inlet and outlet are calculated from the respective temperature and pressure and used together with the compressor power to calculate $\dot{m}_{\mathrm{comp}}$
- The gas cooler outlet enthalpy is calculated from temperature and pressure and used to calculate the COP_1 by dividing the full gas cooler and heat recovery enthalpy difference by the compressor enthalpy difference.

- the COP_2 is calculated as $COP_1 - 1$ and used to calculate the cooling capacity Q_2 from the compressor power P_{comp}
- The evaporator inlet enthalpy is calculated from the receiver pressure at the vapor quality x=1, assuming isenthalpic expansion to the evaporation pressure level
- The evaporator outlet (and ejector suction inlet) enthalpy is calculated from pressure and temperature and used together with Q_2 to calculate $\dot{m}_{\text{evap}}$. For the case of very low superheat at the ejector inlet as seen particularly in VEJ-B, the suction enthalpy is calculated for T_{evap} and the vapor quality x=1
- The enthalpy at the ejector entrainment inlet is calculated from pressure and temperature and used together with the ejector suction inlet enthalpy and the mass flows to calculate the ejector outlet enthalpy via an energy balance over the ejector.
- The ejector parameters ω, Δp_{lift}, the maximum recoverable work $W_{\text{r,max}}$ and the ejector efficiency η_{ej} are calculated from the other parameters based on the introduced equations in section 2.

For the evaluation of the systems, an efficiency of $\eta_{\text{elm}} = 0.95$ is assumed for the electrical compressor motor. This is expected to be a good approximation for large systems based on Granryd et al. [37]. Furthermore, a fixed factor of 0.7 from the total refrigeration system power input to the compressor power input needs to be assumed for system VEJ-A based on data from other systems. This adds an uncertainty to the calculated absolute values of the system mass flow rates $\dot{m}_{\text{comp}}$ and $\dot{m}_{\text{evap}}$. Both mass flow rates are however calculated based on this assumption, which minimizes the effect on the calculated mass entrainment ratio.
The coefficients of performance COP_2 and COP_1 are here thus defined as the evaporation and condensing capacity relative to the actual compression power input to the system, i.e. the remaining compressor power after accounting for losses in the compressor.
It is necessary to calculate the cooling capacity Q_2 from the energy balance over the system using the COPs here, as the evaporator mass flow is not equal to the compressor mass flow in the vapor ejector system, as figure 3.3 shows.

From a general analysis of both systems VEJ-A and VEJ-B, it is found that there is no significant superheat between the ejector suction inlet and the evaporator outlet.
In system VEJ-A, this is because the ice rink surfaces are connected via a receiver tank to which the evaporator mass flow in the ice rink surface returns. The ejectors are connected to this tank with two-phase conditions, leading in theory to saturated vapor with temperature T_{evap} at the ejector suction inlet when the respective ejector is operating. Depending on the ambient conditions, a small superheat of less than 1 K is found in reality at the ejector inlet, though without visible impact on the ejector operation.
Similarly, there is no relevant superheat in system VEJ-B at the ejector suction inlet, which appears to be a result of the evaporator control here. In addition, oil from the liquid line before the evaporator is injected at the ejector suction inlet, possibly causing even small amounts of liquid at the ejector inlet which might cause issues for the ejector. The oil injection at this point was added to the system later on, it is however not clear why oil is moved to the ejector suction inlet.

Comparison to Reference Case without Ejector

For the comparison to the theoretical reference (REF) case, the cooling capacity Q_2, the evaporation pressure and outlet temperature, the discharge pressure p_{disc}, the gas cooler temperature $T_{\mathrm{gc,out}}$, the ejector entrainment temperature/expansion valve inlet temperature $T_{\mathrm{ej,e}}$ and the isentropic compressor efficiency are set as equal to the VEJ model.
The following steps are then used to calculate the REF system performance in python:

- In the theoretical REF model, the receiver has no impact on the system performance but is modelled for a better comparability to the VEJ system with a pressure difference of 0 bar to the evaporation pressure.
- Based on this receiver assumption, the evaporator inlet enthalpy is calculated from T_{evap} and the vapor quality x=0 and then used together with the outlet enthalpy and Q_2 (equal to VEJ) to calculate $\dot{m}_{\mathrm{evap}}$
- The vapor quality at the expansion valve outlet is calculated from the entrainment enthalpy (equal to VEJ) and p_{rec}
- For the assumed case of stationary conditions and no actual refrigerant storage in the receiver, $\dot{m}_{\mathrm{fg}}$ can then be directly concluded from $\dot{m}_{\mathrm{evap}}$ and vapor quality at the expansion valve outlet
- The compressor mass flow follows directly as sum of $\dot{m}_{\mathrm{evap}}$ and $\dot{m}_{\mathrm{fg}}$
- The enthalpy difference in the liquid-suction heat exchanger is used to calculate the compressor suction enthalpy, from which the ejector discharge conditions are then found using the isentropic compressor efficiency (equal to VEJ)
- The compressor power is calculated from the compressor enthalpy difference and $\dot{m}_{\mathrm{comp}}$ and can then be used to calculate the COP of the reference system in combination with Q_2. The electrical power consumption and COP can be found by dividing by the assumed motor efficiency

For system VEJ-A, two time periods with different ambient temperatures are evaluated, namely the full month of September 2020 and the second half of February 2021 (15/02/2021 to 28/02/2021). From a general annual analysis, these two months are found to be representative for most of the different operating conditions with respect to the ejector. Furthermore, they fulfil the condition that the additional borehole evaporator is not, or only occasionally, used. This is necessary, as a determination of the ejector entrainment and suction mass flow rates is otherwise not possible from the system data. The few occasions during which the additional borehole evaporator is operating are removed from the data during the filtering process.

For system VEJ-B, relatively stable operating conditions and particularly no significant changes in the very low ejector pressure lift are found during stable operating conditions, thus the analysed time periods are limited to 2 days each. Similar to the choice in system VEJ-B, a time period in September 2020 (01/09/2020 to 02/09/2020) for the system operation at warmer ambient temperatures and in February 2021 (01/02/2021 to 02/02/2021) for cold ambient temperatures are selected as representative cases.

Seasonal Energy Savings Evaluation in VEJ

The evaluation of the VEJ system data shows good correlations between Δp_{lift} and $Incr_{\text{COP2}}$. For a certain Δp_{lift} which can be easily obtained from the field data, $Incr_{\text{COP2}}$ can thus be estimated roughly without the necessity for the full described calculation steps above. Based on a linear regression obtained for this correlation in the systems, an estimation of the seasonal energy savings in the systems by the ejector is therefore possible. The estimated savings are defined in comparison to the corresponding REF system which for every minute in the season operates at the same conditions as the VEJ system, as described before.
For the calculation, the power input P_{comp} to the VEJ system is obtained from the data logging platform in addition to the Δp_{lift} for each minute in the season. With the estimated $Incr_{\text{COP2}}$ from the regression and Δp_{lift}, the theoretical power input $P_{\text{comp,ref}}$ of the corresponding REF system can then directly be estimated with equation 3.1 for each minute.

$$P_{\text{comp,ref}} = P_{\text{comp}} \cdot \frac{COP_2}{COP_{2,\text{ref}}} = P_{\text{comp}} \cdot (Incr_{\text{COP2}} + 1) \tag{3.1}$$

The seasonal energy savings can then be estimated from the compressor power inputs according to equation 3.2.

$$Savings = 1 - \frac{\sum P_{\text{comp}}}{\sum P_{\text{comp,ref}}} \tag{3.2}$$

It should be considered that the calculated value only reflects the savings with respect to the refrigeration side, while the reduction in compressor power also reduces the potentially recoverable heat. As described in section 3.2.4, this has no effect on the system if less heat is required than available for recovery. If more heat is needed than provided by the heat recovery, the amount of required auxiliary heating would be reduced when using the here modelled REF system compared to the VEJ system, at the price of lower efficiency.

For system VEJ-A, the seasonal savings are evaluated between July 2020 and May 2021 (23/07/2020 to 23/05/2021). However, as the effect of the additional borehole evaporator on the ejector in this system cannot be determined quantitatively from the system data, all time periods in which the borehole evaporator is used are excluded for the calculation of the savings. As the borehole evaporator is used during time periods when more heat is necessary than provided by use of the heat recovery alone, it could conversely be concluded that sufficient heating is provided by the heat recovery during the remaining time periods, which are evaluated regarding savings. As described above, the energy savings in the evaluated time periods are thus indeed total energy savings, as additional excess heat produced by the less efficient compared REF system would in these cases not require any replacement by auxiliary heating.
For system VEJ-B, the season between system startup in August 2020 and shut-down at the end of April 2021 (05/08/2020 to 26/04/2021, excluding the time period 24/10/2020-26/10/2020 due to the daylight saving time change which causes problems in the evaluation) is analysed regarding energy savings.
From a data acquisition perspective, it should be noted here that the pressure lift directly calculated

by the respective control systems is not always identical to the actual pressure difference between p_{evap} and p_{rec} which is used here to obtain Δp_{lift}.

3.1.2 LEJ System Evaluation

For the analysed LEJ systems, figure 3.4 shows the common system layout of the medium temperature refrigeration unit in both systems. As explained in section 1, the analysis of the LEJ systems is limited to the medium temperature level as liquid ejectors are only used in this part of the systems.

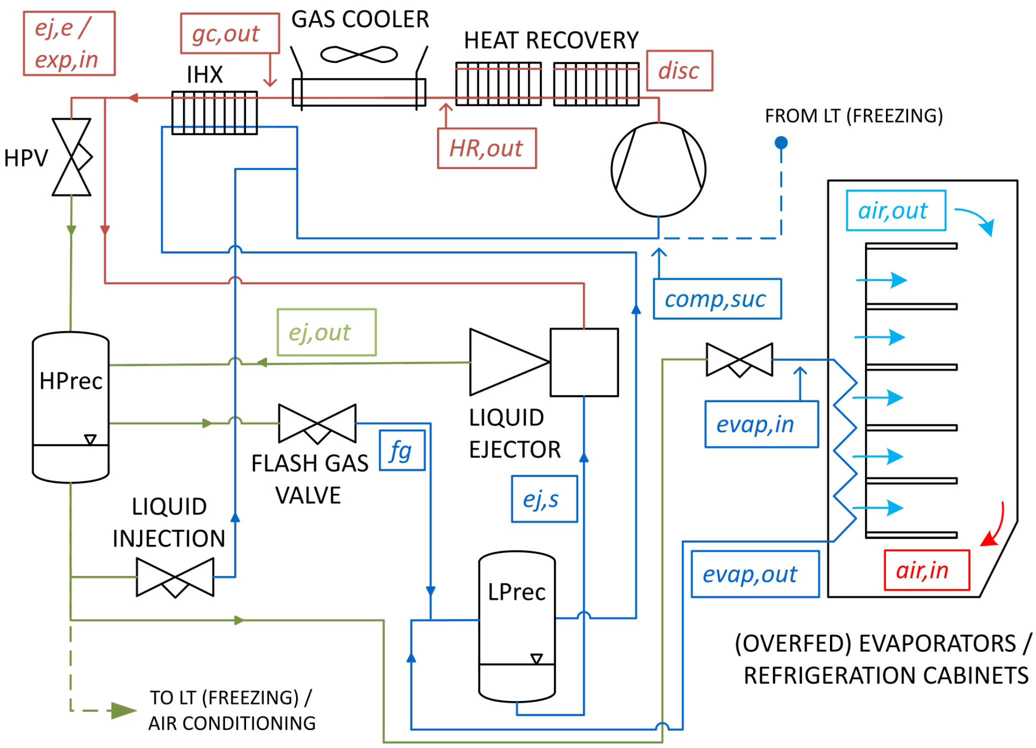

Figure 3.4: System layout of the medium temperature part in LEJ-A and LEJ-B, with indicated parameter subscripts

The performance improvement in LEJ systems is achieved by increasing the evaporation pressure through overfed evaporation rather than by a direct pressure lift from the ejector as in the vapor ejector case. To analyse the evaporator operation conditions and find possible limitations, the analysis of the temperature profiles in the evaporators of the MT refrigeration cabinets forms thus the key part of the LEJ system evaluation.
The MT cabinet evaluation is done by analysing the four temperatures which determine the temperature profile in the evaporator of each cabinet. These are the temperatures at the inlet and outlet of the evaporator for CO2 on the one hand and the air circulating in the cabinet on the other hand. The air temperatures are measured directly in the cabinet in the supply air stream to the cabinet, which

is the evaporator outlet air temperature $T_{air,out}$, and in the return air stream, which is the evaporator inlet air temperature $T_{air,in}$. The temperature of the CO2 leaving the evaporator is measured by a temperature sensor at evaporator outlet in the cabinet, while the evaporation temperature of CO2 T_{evap} is measured as evaporation pressure p_{evap} at the cabinet outlet, which can be converted into the evaporation temperature. The superheat can be determined directly from the CO2 temperatures as the difference between $T_{evap,out}$ and T_{evap}.
In addition, the opening degree of the expansion valve at the evaporator inlet is analysed for the individual MT cabinets.
The LT evaporation is not analysed in further detail, as the ejectors are only used on the MT level. In contrast to the VEJ systems, the actual liquid ejector performance has a relatively minor effect on the system as it is mainly fulfilling the role of a liquid pump. A direct analysis of the ejector performance itself in the liquid ejector systems is furthermore not possible with the available parameters in the system, as the actual mass flows through the ejectors cannot be determined accurately. With respect to the refrigeration unit, the LEJ system analysis focuses therefore on the operation of the liquid ejectors based on the liquid level in the LPrec and the liquid flow based on the evaporator and flash gas valve operation, which are the two sources of refrigerant mass flow into the LPrec.

For system LEJ-A, no significant changes in the operating strategy are known or could be observed visually in the system data. Thus, the first week of April 2021 (01/04/2021 to 07/04/2021) is chosen for a representative evaluation.
For system LEJ-B, the operating mode was changed in October 2020 to an operation with lower superheat. Therefore, two weeks are evaluated for the system, to compare the two different operating modes: The first week of August 2020 (01/08/2020 to 07/08/2020) and the first week of November 2020 (01/11/2020 to 07/11/2020).
As the supermarket systems are both located in Sweden and are open every day including Sundays, no specific differentiation between weekdays is made.

3.2 Ejector Modelling

The literature review shows a range of different ejector behaviours with significant dependence on the actual ejector design. The design of the ejectors in the analysed systems in this work is not known in detail. The focus of the modelling approach in this work is therefore on the interaction of the ejector with the refrigeration system in which it is integrated. The ejector itself is modelled as a black box using mass and energy balances to depict its behaviour based on the surrounding parameters, with a general orientation at the equations given in the work of Lucas and Koehler [14] among others.
The models of the ejector systems are built using the software "Engineering Equation solver" (EES).

Using an energy balance over the ejector, the mass entrainment ratio ω can be directly linked to the ejector outlet enthalpy $h_{ej,out}$ for fixed entrainment and suction conditions, as shown in equation

3.3.

$$\omega = \frac{h_{\text{ej,e}} - h_{\text{ej,out}}}{h_{\text{ej,out}} - h_{\text{ej,s}}} \tag{3.3}$$

A simple mass balance over the ejector is described by equation 3.4.

$$\dot{m}_{\text{ej,out}} = \dot{m}_{\text{ej,e}} + \dot{m}_{\text{ej,s}} \tag{3.4}$$

Together with this mass balance, the mass entrainment ratio ω can be used to relate the mass flows at the ejector entrainment and suction inlets to the ejector outlet mass flow, as in equations 3.5 and 3.6.

$$\frac{\dot{m}_{\text{ej,e}}}{\dot{m}_{\text{ej,out}}} = \frac{1}{1+\omega} \tag{3.5}$$

$$\frac{\dot{m}_{\text{ej,s}}}{\dot{m}_{\text{ej,out}}} = \frac{\omega}{1+\omega} \tag{3.6}$$

As the focus of the model is on the interaction of the ejector with the system, a fixed isentropic compressor efficiency of $\eta_{\text{comp,is}} = 0.64$ and a fixed efficiency of $\eta_{\text{elm}} = 0.95$ for the compressor motor are used in the modelling process. The value for $\eta_{\text{comp,is}}$ is the mean value for the isentropic efficiency found in VEJ-A, while the value for η_{elm} is chosen as for the field data evaluation.

3.2.1 Vapor Ejector Modelling

The VEJ system is shown in figure 2.4, in accordance with the thermodynamic cycle shown in the log(p)-h chart in figure 3.3 for example conditions. The pressure of the entire evaporator mass flow $\dot{m}_{\text{evap}}$ is lifted by the ejector and the entire compressor mass flow $\dot{m}_{\text{comp}}$ is used for the entrainment in the ejector. A balanced system operation is therefore only possible in this system design if the liquid mass flow at the ejector outlet is equal to the evaporator mass flow and the vapor mass flow at the ejector outlet is equal to the compressor mass flow. Thus, the vapor quality at the ejector outlet is directly linked to the ejector mass entrainment ratio ω in this case, as described in equation 3.7.

$$x_{\text{ej,out}} = \frac{\dot{m}_{\text{comp}}}{\dot{m}_{\text{comp}} + \dot{m}_{\text{evap}}} = \frac{1}{1+\omega} \tag{3.7}$$

Further modelling assumptions for the VEJ case are based on literature findings in combination with the parameters in system VEJ-A, as the system with the most detailed measurement data. In particular, an ejector efficiency of 0.3 is used as this corresponds to the upper range of ejector efficiencies found in literature and also is found as upper range of the ejector efficiencies in system VEJ-A during stationary operating conditions. A similar assumption is taken in the study by Biner [31]. For the analysis of the entrainment conditions, the mean evaporation temperature in VEJ-A

of $T_{\mathrm{evap}} = -10.4\,°\mathrm{C}$ is used in the model. Furthermore, no heat exchange in the liquid suction heat exchanger is assumed for this modelling case. The effect of the liquid suction heat exchanger is evaluated separately instead.
For these fixed parameters, particularly for the ejector efficiency and the evaporation temperature, a sensitivity analysis is done as part of the model evaluation to analyse the impact of these parameters on the results.

3.2.2 Liquid Ejector Modelling

The modelled liquid ejector system is shown in figure 2.6 and the corresponding thermodynamic cycle is visualized in the log(p)-h chart in figure 3.5 together with the corresponding REF cycle for example conditions.

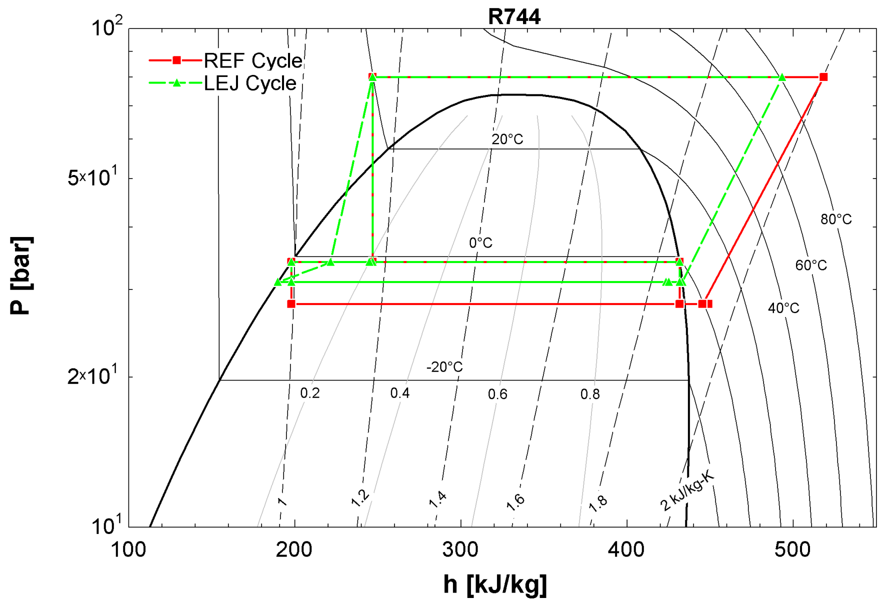

Figure 3.5: Cycles of LEJ and REF model with example conditions of 10 K superheat in the REF model and an evaporation temperature increase of 3.7 K, $T_{\mathrm{evap}} = -8\,°\mathrm{C}$ in REF, no IHX

The compressor mass flow $\dot{m}_{\mathrm{comp}}$ is in this case not entirely used for entrainment in the ejector, but instead split into ejector entrainment mass flow $\dot{m}_{\mathrm{ej,e}}$ and a mass flow through the HPV $\dot{m}_{\mathrm{HPV}}$, as expressed in equation 3.8.

$$\dot{m}_{\mathrm{comp}} = \dot{m}_{\mathrm{ej,e}} + \dot{m}_{\mathrm{HPV}} \tag{3.8}$$

The vapor quality in the LPrec after the mixing of evaporator mass flow $\dot{m}_{\mathrm{evap}}$ and flash gas mass flow $\dot{m}_{\mathrm{fg}}$ is described by equation 3.9, as the vapor mass flow in the LPrec is equal to the compressor mass flow $\dot{m}_{\text{comp}}$.

$$x_{\text{LPrec}} = \frac{\dot{m}_{\text{comp}}}{\dot{m}_{\text{evap}} + \dot{m}_{\text{fg}}} = 1 - \frac{\dot{m}_{\text{ej,s}}}{\dot{m}_{\text{evap}} + \dot{m}_{\text{fg}}} \tag{3.9}$$

The vapor quality in the HPrec can be used similarly to express the ratio of the flash gas mass flow $\dot{m}_{\text{fg}}$ to the total HPrec mass flow $\dot{m}_{\text{evap}} + \dot{m}_{\text{fg}}$.

$$x_{\text{HPrec}} = \frac{\dot{m}_{\text{fg}}}{\dot{m}_{\text{evap}} + \dot{m}_{\text{fg}}} \tag{3.10}$$

In the liquid ejector cycle, liquid flows into the receiver either from the ejector $\dot{m}_{\text{ej,out}}$ or the HPV $\dot{m}_{\text{HPV}}$. The liquid is then fed to the evaporator $\dot{m}_{\text{evap}}$ and the flash gas mass flow $\dot{m}_{\text{fg}}$ is bypassing the evaporator. The ratio of the ejector outlet mass flow to the total mass flow through the receiver can thus be expressed independently of the actual mass flow rates as shown in equation 3.11, using equations 3.6 and 3.9.

$$\begin{aligned} Rel_{\text{ej/rec}} = \frac{\dot{m}_{\text{ej,out}}}{\dot{m}_{\text{evap}} + \dot{m}_{\text{fg}}} &= \frac{\dot{m}_{\text{ej,s}}}{\dot{m}_{\text{evap}} + \dot{m}_{\text{fg}}} \cdot \left(1 + \frac{1}{\omega}\right) \\ &= \left(1 - x_{\text{LPrec}}\right) \cdot \left(1 + \frac{1}{\omega}\right) \end{aligned} \tag{3.11}$$

The ratio of the HPV mass flow to the total receiver mass flow follows directly as the remaining mass flow into the receiver, as shown in equation 3.12.

$$\frac{\dot{m}_{\text{HPV}}}{\dot{m}_{\text{evap}} + \dot{m}_{\text{fg}}} = 1 - \frac{\dot{m}_{\text{ej,out}}}{\dot{m}_{\text{evap}} + \dot{m}_{\text{fg}}} = 1 - Rel_{\text{ej/rec}} \tag{3.12}$$

To calculate COP_2, the ratio between the evaporator mass flow $\dot{m}_{\text{evap}}$ and the compressor mass flow $\dot{m}_{\text{comp}}$ is needed. Using equations 3.8, 3.9, 3.10 and 3.11, it can be expressed independently of the actual mass flow rates as shown in equation 3.13. The equation starts from the vapor quality in the LPrec, i.e. equation 3.9. The compressor mass flow is then replaced using equation 3.8 and the flash gas mass flow is replaced using equation 3.10. Equations 3.6 and 3.11 can then be used to replace the ratio of $\dot{m}_{\text{ej,e}}$ to the total HPrec mass flow and equation 3.12 can be used to replace the ratio of $\dot{m}_{\text{HPV}}$ to the total HPrec mass flow.

$$\begin{aligned} \frac{\dot{m}_{\text{evap}}}{\dot{m}_{\text{comp}}} &= \frac{1}{x_{\text{LPrec}}} - \frac{\dot{m}_{\text{fg}}}{\dot{m}_{\text{comp}}} \\ &= \frac{1}{x_{\text{LPrec}}} - x_{\text{HPrec}} \cdot \frac{\dot{m}_{\text{evap}} + \dot{m}_{\text{fg}}}{\dot{m}_{\text{ej,e}} + \dot{m}_{\text{HPV}}} \\ &= \frac{1}{x_{\text{LPrec}}} - x_{\text{HPrec}} \cdot \frac{1}{\frac{1}{1+\omega} \cdot Rel_{\text{ej/rec}} + \left(1 - Rel_{\text{ej/rec}}\right)} \end{aligned} \tag{3.13}$$

For the LEJ system model, the increase in evaporation temperature does not directly depend on the ejector. Instead, the heat transfer characteristics in the evaporator play a key role in combination

with the removed superheat [2]. Therefore, literature data for a change to overfed conditions in a typical cabinet as stated by Karampour and Sawalha is used for the LEJ model, i.e. an increase in evaporation temperature by 3.7 K from $T_{\text{evap}} = -8\,^{\circ}\text{C}$ by removing 10 K superheat [18].
Furthermore, a vapor quality of 0.96 as stated by Minetto et al. (2014) [19] is assumed for the evaporator outlet in the LEJ system. For the liquid ejector, a fixed mass entrainment ratio of $\omega = 0.8$ is set, as no relevant impact of this parameter on the performance is seen during initial model test runs. A sensitivity analysis is done to see the effect of changing these parameters on the model.

3.2.3 VPC System Modelling

In comparison to the VEJ system (Figure 2.4), the VPC system (Figure 2.5) has two additional possible mass flow paths: One through the main compressors, as the main compressors of the VEJ system are replaced by the parallel compressors in the VPC system, and the second through the HPV, as possible option for the expansion of the high pressure refrigerant, parallel to the expansion in the ejector. In addition to the input variables used in the VEJ system, two more input variables are therefore fixed in the VPC model to achieve an unambiguous system definition:

- The ratio of the HPV mass flow to the gas cooler mass flow
- The ratio of the MC mass flow to the evaporator mass flow

If these parameters are both set to 0, the VPC system is theoretically identical with the VEJ system. Thus, the VPC system can be seen as a more general case of the VEJ system. The VPC system can then be modelled using mass and energy balances for the ejector, the receiver and the mixing point of MC and PC compressor discharge. In addition, two mass balances for the gas cooler outlet and the evaporator outlet can be formulated, as mass flows are split up at these points. As for the previous cases, the model is built for stationary conditions, i.e. no change in liquid level in the receiver is assumed. The energy and mass balances for the ejector are already formulated in equations 3.3 and 3.4. The mass balance for the receiver in the VPC system is shown in equation 3.14, the energy balance in equation 3.15.

$$\dot{m}_{\text{ej,out}} + \dot{m}_{\text{HPV}} = \dot{m}_{\text{PC}} + \dot{m}_{\text{evap}} \tag{3.14}$$

$$\dot{m}_{\text{ej,out}} \cdot h_{\text{ej,out}} + \dot{m}_{\text{HPV}} + h_{\text{ej,e}} = \left(\dot{m}_{\text{ej,out}} + \dot{m}_{\text{HPV}}\right) \cdot h_{\text{rec,mixed}} \tag{3.15}$$

The enthalpy of the mixed flow in the receiver together with the receiver pressure is directly linked to a specific vapor quality of the flow into the receiver. As no change in the receiver liquid level is assumed, this is directly determining the mass flows to evaporator and PC, as the liquid flows from the receiver into the evaporator and the vapor to the PC as described in equation 3.10 for the LEJ case, with the difference that the flash gas mass flow is instead compressed by the parallel compressor in the VPC system.

For the mixing point of the two compressor discharge flows, the mass balance is formulated in equation 3.16 and the energy balance in equation 3.17.

$$\dot{m}_{\mathrm{MC}} + \dot{m}_{\mathrm{PC}} = \dot{m}_{\mathrm{gc}} \tag{3.16}$$

$$\dot{m}_{\mathrm{MC}} \cdot h_{\mathrm{MC,disc}} + \dot{m}_{\mathrm{PC}} + h_{\mathrm{PC,disc}} = \dot{m}_{\mathrm{gc}} \cdot h_{\mathrm{disc,mixed}} \tag{3.17}$$

The mass balance at the evaporator outlet is formulated in equation 3.18.

$$\dot{m}_{\mathrm{ej,s}} + \dot{m}_{\mathrm{MC}} = \dot{m}_{\mathrm{evap}} \tag{3.18}$$

Equation 3.19 shows the mass balance at the gas cooler outlet.

$$\dot{m}_{\mathrm{ej,e}} + \dot{m}_{\mathrm{HPV}} = \dot{m}_{\mathrm{gc}} \tag{3.19}$$

For a systematic analysis without fixed values for the mass flow rates, all mass flow rates in the system are expressed relative to the evaporator mass flow rate. These mass flow rates are marked with "rel" in the subscript, as shown for the example of the gas cooler mass flow rate in equation 3.20.

$$m_{\mathrm{gc,rel}} = \frac{\dot{m}_{\mathrm{gc}}}{\dot{m}_{\mathrm{evap}}} \tag{3.20}$$

3.2.4 Comparison to Reference System

To quantify how the ejector affects the system performance, indicators are evaluated relative to a reference system REF without ejectors, shown in figure 3.6. As refrigeration is seen as the key service provided by the systems, the main comparison is done for equal cooling load Q_2 and equal temperature and pressure conditions. In particular, the evaporation pressure p_{evap} and outlet temperature $T_{\mathrm{evap,out}}$, the superheat provided by the IHX, the discharge pressure p_{disc} and gas cooler outlet temperature $T_{\mathrm{gc,out}}$ are set as equal in the compared systems.
Regarding the discharge pressures, there is theoretically an optimal discharge pressure for maximum system performance for a fixed gas cooler outlet temperature, as shown by Sawalha [38]. From a practical perspective, the analysed systems as well as comparable systems without ejectors are however currently found to be controlled for fixed discharge pressures over a wide range of gas cooler outlet temperatures. This is not optimal from a system performance perspective but appears to be an easier control approach particularly in combination with heat recovery. Based on this situation, the systems are evaluated for a range of equal gas cooler outlet conditions which are considered as representative cases for the conditions found in actual systems, despite possibly being suboptimal operating conditions from a theoretical perspective.

The chosen way of comparison is related to the assumption that more heating than necessary is available for heat recovery, with the remaining heat released to the ambient in the gas cooler. As

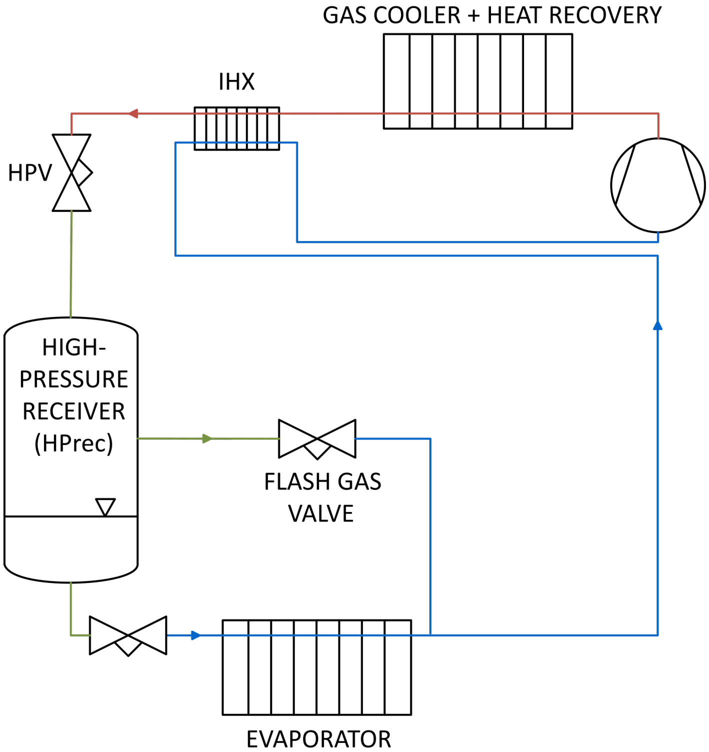

Figure 3.6: Reference System (REF)

all system efficiencies used in the model are assumed to be independent of the system capacity, the COPs can directly be compared between the ejector systems and the reference systems.

$$Incr_{\mathrm{COP2}} = \frac{COP_2 - COP_{2,\mathrm{ref}}}{COP_{2,\mathrm{ref}}} \tag{3.21}$$

For the case of an increasing COP at equal cooling capacity Q_2, the heating capacities are naturally decreasing with the lower compressor power. The relative increase in Q_1 ($Incr_{\mathrm{Q1}}$) as parameter defined in equation 3.22 in parallel to the definition of $Incr_{\mathrm{COP2}}$ can be used to quantify this decrease in total heating capacity (including possible heat recovery and gas cooler) on the discharge side.

$$Incr_{\mathrm{Q1}} = \frac{Q_1 - Q_{1,\mathrm{ref}}}{Q_{1,\mathrm{ref}}} = \frac{COP_1 \cdot COP_{2,\mathrm{ref}}}{COP_2 \cdot COP_{1,\mathrm{ref}}} \tag{3.22}$$

As the heat recovery options of the system are particularly not only characterised by the amount of available heat but also by the temperature at which the heat is available, the impact of the ejector application on the discharge temperature plays an important role and is also analysed.

It should be considered that the assumption that a greater heat availability than heating demand is not valid for every system. Instead, in several cases it is also of interest to produce a certain amount of both cooling and heating or as much heat as efficiently possible for a given cooling demand. For

the analysis of this case, it is assumed that the energy balance of the system, i.e. both heating and cooling capacity, and thus also the energy input to the compressor, should be kept equal for the comparison between ejector and reference system. A short analysis is done regarding alternative system improvements by the ejector possible in this case.
In fact, a third case of systems with the primary purpose of heat production can also be imagined, i.e. heat pumps. If a specific heating demand needs to be met by the system while the cooling/heat absorption is flexible, an ejector system would increase the heat absorption in the evaporator while decreasing the energy consumption of the compressor for equal temperatures and pressures on high and low pressure side. This heat pump case is not studied in further detail here.

4 Results and Discussion

The results and discussion are structured in two main parts: the evaluation of the vapor ejector results and of the liquid ejector results. In both cases, the modelling results are presented and discussed first, followed by the field data evaluations which are put in context with the modelling results and literature findings. A general comparison of vapor and liquid ejector case concludes the chapter.

4.1 Vapor Ejector Results

4.1.1 Modelling Results

The modelled VEJ and REF cycles are plotted in the log(p)-h-chart in figure 4.1 for example conditions of 80 bar and 20 °C at the ejector entrainment inlet, $T_{\mathrm{evap}} = -10.4\,°\mathrm{C}$ and $\eta_{\mathrm{ej}} = 0.3$, no superheat and no internal heat exchange. These conditions are generally linked to conditions found in system VEJ-A.

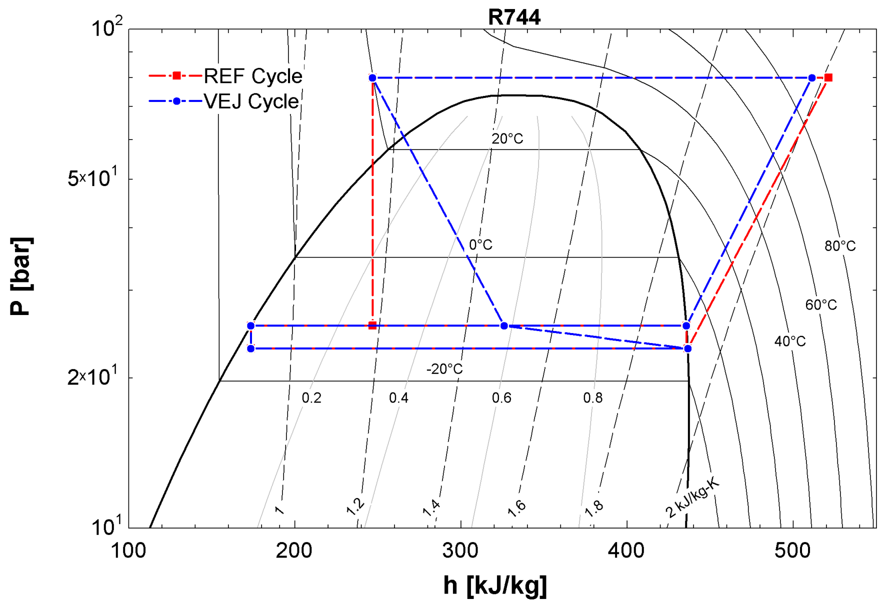

Figure 4.1: Modelled VEJ and REF cycle plotted in the log(p)-h-chart for example conditions

Effect of Parameters at the Ejector Entrainment Inlet

For the modelled case of $T_{evap} = -10.4\,°C$, $\eta_{ej} = 0.3$ and no heat exchange in the IHX, the increase in COP_2 shown in figure 4.2 is found for the comparison of VEJ and REF.

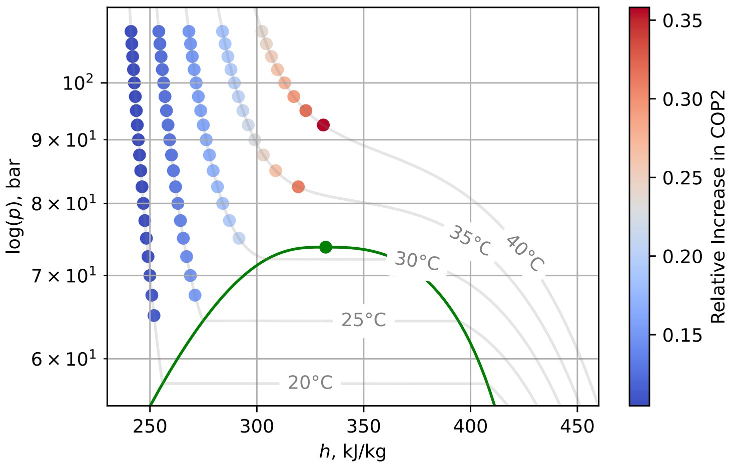

Figure 4.2: $Incr_{COP2}$ at different entrainment conditions for $T_{evap} = -10.4\,°C$ and $\eta_{ej} = 0.3$ in VEJ

For the gas cooler outlet conditions which are expected for floating condensing, i.e. close to the vapor dome for subcritical pressures and at the optimum discharge pressures (lowest evaluated points) for supercritical pressures, the $Incr_{COP2}$ is found to be increasing for higher gas cooler outlet temperatures.
For the individual temperature levels, the $Incr_{COP2}$ is generally decreasing with higher p_{disc}, an effect which is more significant for high temperatures $T_{ej,e}$, especially for the modelled cases of 35 and 40 °C. This is due to the fact that the compressor power consumption increases faster for higher p_{disc} than the amount of recovered work by the ejector, as later explained in more detail. From this, it can be concluded that an increase in p_{disc} beyond the optimum pressure for a certain temperature is generally not able to provide additional system improvements. In specific cases, improvements might however be achieved if the system could be operated at a better compressor efficiency for an adapted p_{disc}.
Together with figure 4.3a, it becomes furthermore clear that higher increases in COP_2 are generally achieved for higher ejector entrainment temperatures $T_{ej,e}$ (here equal to the gas cooler outlet temperatures $T_{gc,out}$, as no heat exchange in the IHX is modelled).

Figure 4.3a shows that efficiency improvements in the range of 10 to 20 % for entrainment temperatures below 30 °C and in the range of 20 to 35 % for entrainment temperatures between 30 and 40 °C are found for the respective optimal discharge pressures in the model.
Figure 4.3b shows the maximum recoverable work $W_{r,max}$ for the analysed conditions at an example cooling capacity of 130 kW. It should be noted that this trend is independent of the actual cooling capacity Q_2 in the theoretical model, as the Q_2 only affects the absolute mass flows, while the enthalpies and relative mass flows are not affected based on the theoretical assumptions. It can

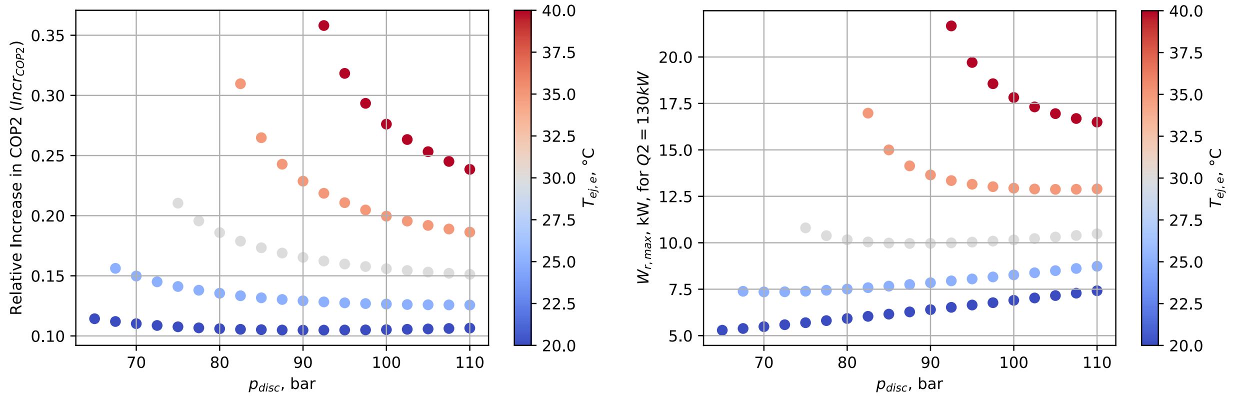

(a) $Incr_{\text{COP2}}$ (same data as in 4.2)

(b) $W_{\text{r,max}}$ for $Q_2 = 130\,\text{kW}$ (relative effects independent of Q_2)

Figure 4.3: $Incr_{\text{COP2}}$ and $W_{\text{r,max}}$ at varying entrainment conditions for $T_{\text{evap}} = -10.4\,°\text{C}$ and $\eta_{\text{ej}} = 0.3$ in VEJ

be seen that the recoverable work is increasing almost linearly with increasing pressures p_{disc} at low $T_{\text{ej,e}}$ with almost constant enthalpies for constant $T_{\text{ej,e}}$. As the ejector efficiency is fixed in the model, the recovered work is proportional to $W_{\text{r,max}}$. Despite this increasing amount of recovered work at low $T_{\text{ej,e}}$, the $Incr_{\text{COP2}}$ is not increasing for increasing pressures. In a similar way, for higher $T_{\text{ej,e}}$ with varying enthalpies for higher pressures, $Incr_{\text{COP2}}$ is found to decreased more significantly for higher p_{disc} in contrast to the smaller decrease in $W_{\text{r,max}}$.
The reason of this can be found in the analysis of relative decrease in compressor enthalpy difference, shown in figure 4.4.

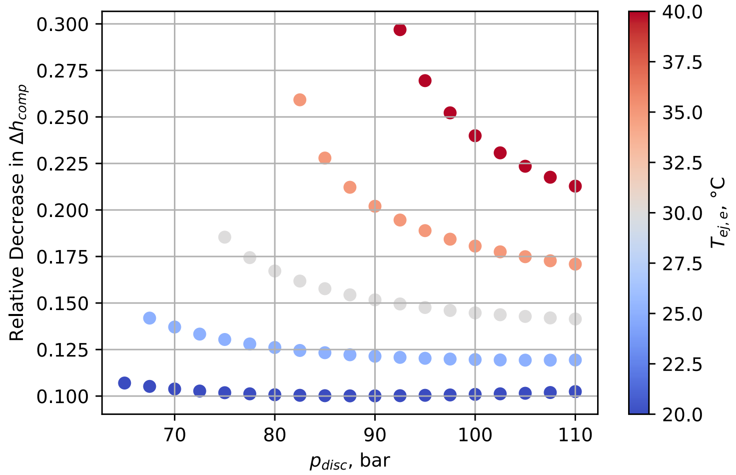

Figure 4.4: Relative **decrease** in compressor enthalpy difference at varying entrainment conditions for $T_{\text{evap}} = -10.4\,°\text{C}$ and $\eta_{\text{ej}} = 0.3$ in VEJ

The figure illustrates the strong correlation of Δh_{comp} with $Incr_{\text{COP2}}$ if compared to figure 4.3a.

This indicates that the effect of the increasing work recovery seen in figure 4.3b is in fact outweighed by the effect of the higher compressor enthalpy difference at higher p_{disc} as a result of the shape of the isentropes (lines of equal entropy) at higher pressures in combination with the isentropic compressor efficiency.

When comparing the trends of the $Incr_{\text{COP2}}$ with the ones of the actual COP_2 for the VEJ and REF system, an almost opposite trend can be seen particularly regarding the effect of $T_{\text{ej,e}}$, with lower temperatures resulting in higher COP_2 but lower $Incr_{\text{COP2}}$ achieved by the ejector.
In general, the discharge pressure appears to have a more significant effect on the COP_2, particularly for low entrainment temperatures $T_{\text{ej,e}}$ which are analysed for a wide pressure range.
For high temperatures $T_{\text{ej,e}}$, particularly for the highest modelled temperature of 40 °C, the variation in COP_2 over p_{disc} is generally small. Nevertheless, it is visible that the discharge pressure for which the maximum COP_2 is reached is shifted to about $3-5$ bar lower discharge pressures p_{disc} in the VEJ system compared to the REF system, as shown by the yellow circles in figure **??** for 35 °C entrainment temperature. This is as a consequence of the significantly higher $Incr_{\text{COP2}}$ achieved by the ejector for lower p_{disc}.

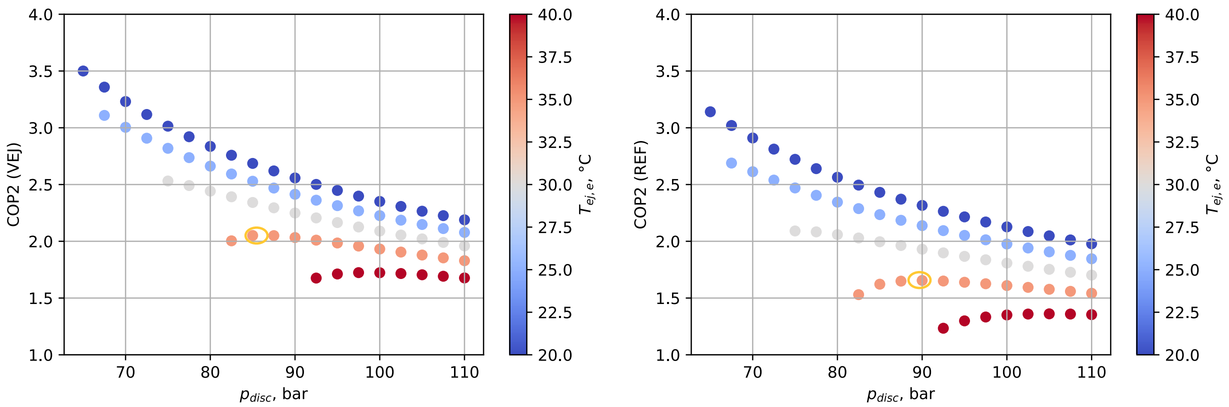

(a) COP_2 for VEJ system

(b) COP_2 for REF system

Figure 4.5: Comparison of COP_2 of VEJ and REF at varying entrainment conditions for $T_{\text{evap}} = -10.4$ °C and $\eta_{\text{ej}} = 0.3$

The analysis of the changes in ejector pressure lift Δp_{lift} and mass entrainment ratio ω in figure 4.6 shows that for low temperatures $T_{\text{ej,e}}$ both Δp_{lift} and ω increase with higher pressures. In contrast, for high temperatures $T_{\text{ej,e}}$, Δp_{lift} decreases while ω increases with higher pressures. When evaluating the change in Δp_{lift} and ω over p_{disc} for equal entrainment enthalpies $h_{\text{ej,e}}$ in figure 4.7 instead of temperatures, it becomes clear that ω is strongly related to $h_{\text{ej,e}}$, with almost no change over p_{disc} for constant $h_{\text{ej,e}}$. Furthermore, Δp_{lift} is increasing almost linearly with p_{disc} for constant enthalpies $h_{\text{ej,e}}$ in the model. The decreasing Δp_{lift} and $Incr_{\text{COP2}}$ at high pressures p_{disc} for high constant temperatures $T_{\text{ej,e}}$ is thus found to be mainly a consequence of the shape of the temperature profiles in the supercritical region.

The theoretical correlation between Δp_{lift} and $Incr_{\text{COP2}}$ for the fixed ejector efficiency in the model is shown in figure 4.8 for the modelled entrainment conditions. Figure 4.8a illustrates the general

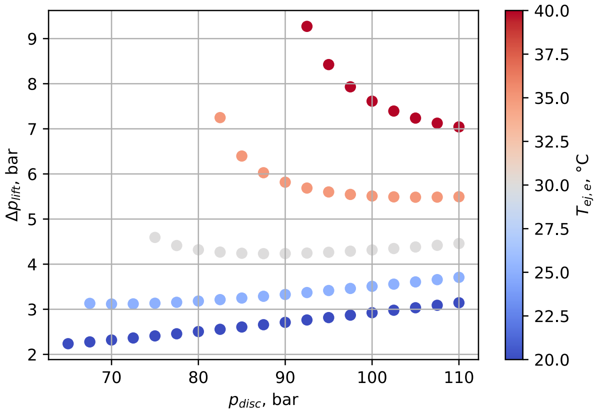

(a) Δp_{lift} for VEJ

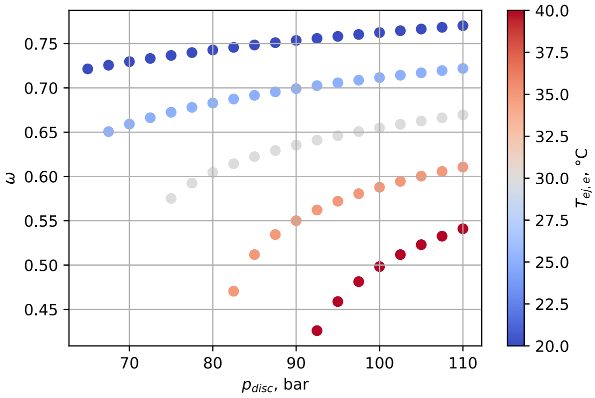

(b) ω for VEJ

Figure 4.6: Δp_{lift} and ω at varying entrainment conditions for $T_{\text{evap}} = -10.4\,°\text{C}$ and $\eta_{\text{ej}} = 0.3$ in VEJ

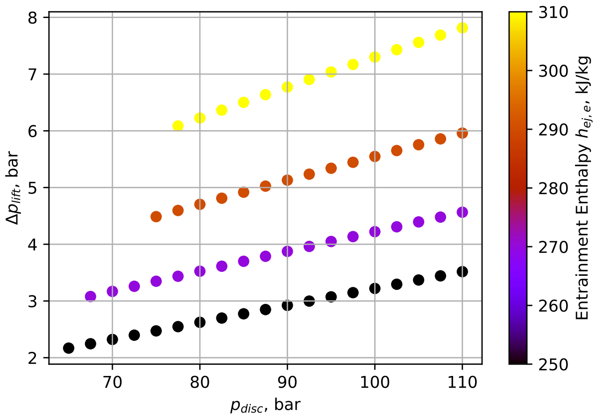

(a) Δp_{lift} for VEJ

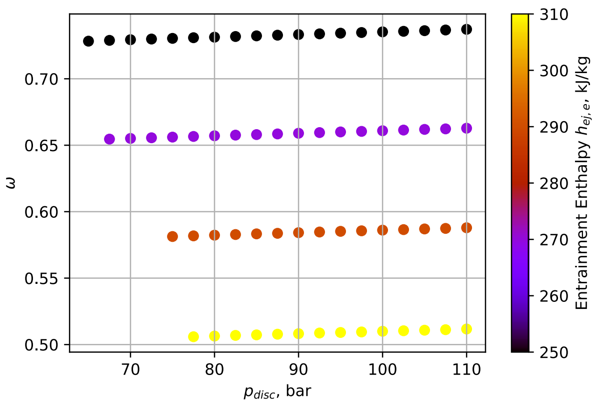

(b) ω for VEJ

Figure 4.7: Δp_{lift} and ω at varying entrainment conditions for $T_{\text{evap}} = -10.4\,°\text{C}$ and $\eta_{\text{ej}} = 0.3$ in VEJ, colors indicating equal enthalpies

trend of higher Δp_{lift} and higher $Incr_{\text{COP2}}$ for higher $T_{\text{ej,e}}$. This differs from the effect of p_{disc} shown in figure 4.8b, which indicates a slightly steeper increase of $Incr_{\text{COP2}}$ over Δp_{lift} for lower p_{disc}. This is due to the fact that the same pressure lift Δp_{lift} has a larger relative effect on the compressor enthalpy difference Δh_{comp} if this enthalpy difference is smaller, which is the case at lower p_{disc}.

The analysis of the effects of the ejector on the high-pressure side, particularly with respect to the heat recovery, show two particular trends indicated in figure 4.9, in comparison to the REF system. Regarding the available heat on the high-pressure side, the total system energy balance leads to a decrease in Q_1 in parallel to the decrease in compressor power for equal cooling capacity Q_2. Figure 4.9a confirms this, showing a decrease by $4-7\,\%$ in Q_1.

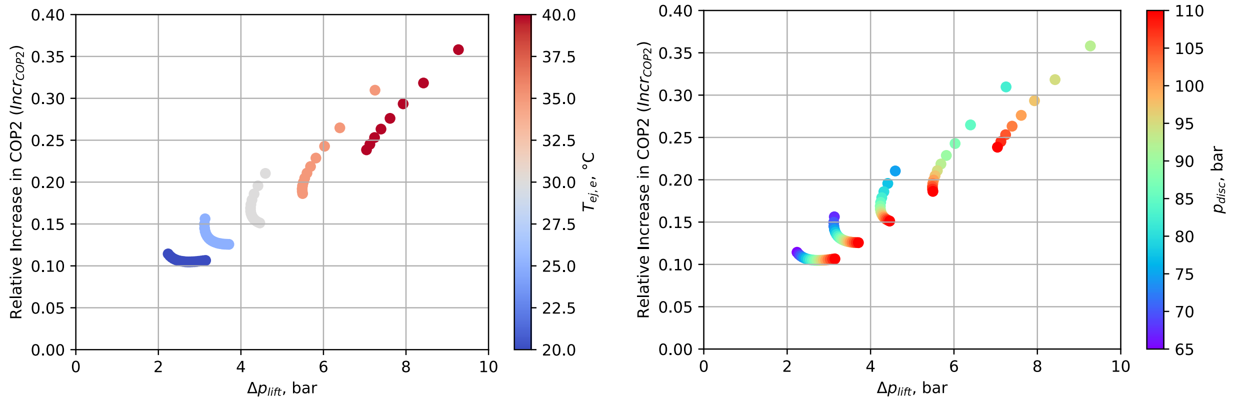

(a) Effect of $T_{\mathrm{ej,e}}$ (b) Effect of p_{disc}

Figure 4.8: Correlation between Δp_{lift} and $Incr_{\mathrm{COP2}}$ at varying entrainment conditions for $T_{\mathrm{evap}} = -10.4\,°\mathrm{C}$ and $\eta_{\mathrm{ej}} = 0.3$ in VEJ

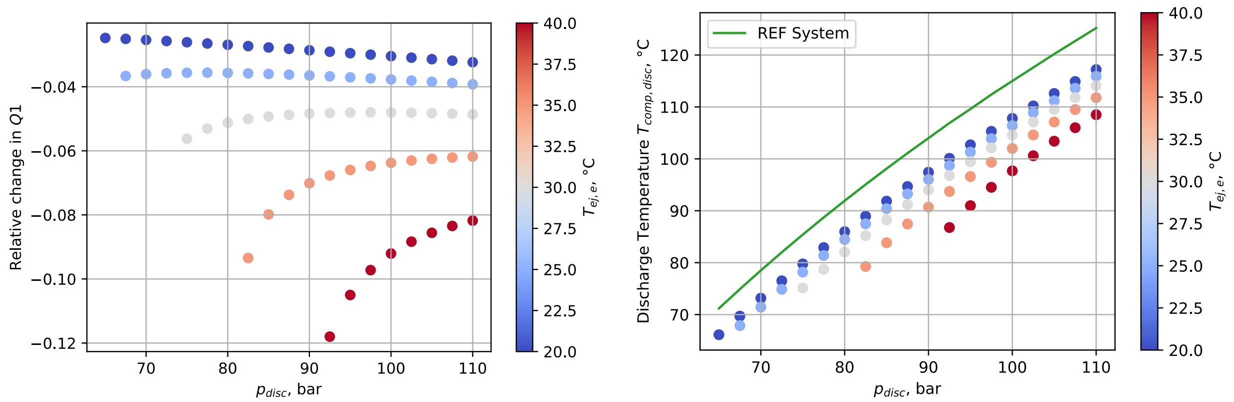

(a) Relative change in total high-pressure side capacity ($Incr_{\mathrm{Q1}}$) (b) $T_{\mathrm{comp,disc}}$

Figure 4.9: Ejector effect on the high-pressure side at varying entrainment conditions for $T_{\mathrm{evap}} = -10.4\,°\mathrm{C}$ and $\eta_{\mathrm{ej}} = 0.3$ in VEJ

Furthermore, the smaller compressor enthalpy difference due to the ejector pressure lift causes the discharge temperature to decrease in the VEJ system compared to the REF system, as indicated in figure 4.9b.
Depending on the actual temperature requirements of the heat recovery, this can have a negative effect if high temperatures are specifically required. On the other hand, if peak discharge temperatures are not actually required in the system, the lower temperature in the VEJ system might possibly be beneficial as heat losses might be reduced and the component design temperature particularly for the cases of high p_{disc} might in fact be less critical.

Effect of Evaporation Temperature and IHX

Figure 4.10 shows the effect of varying $T_{\mathrm{ej,e}}$ and T_{evap} for a fixed discharge pressure of $p_{\mathrm{disc}} = 80\,\mathrm{bar}$ in the model. The figure clearly indicates that high increases in COP_2 are achieved for high

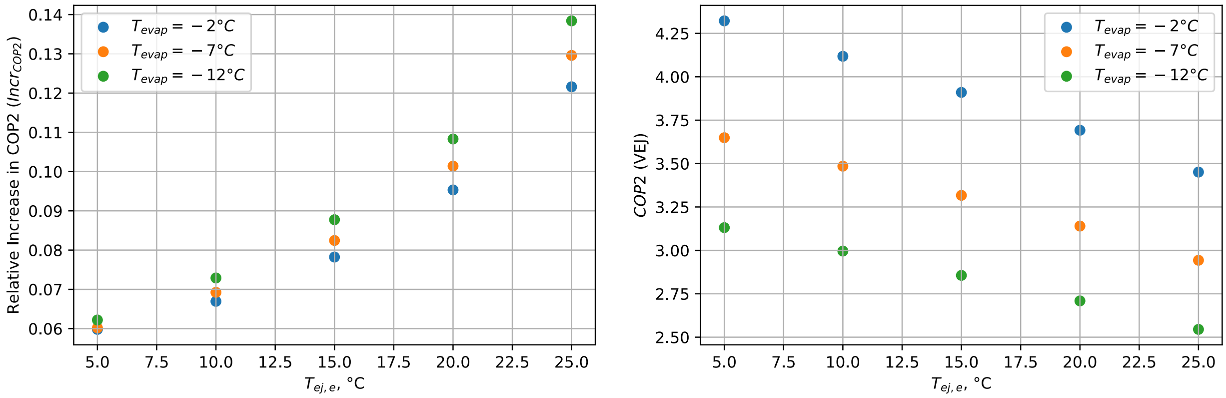

(a) $Incr_{\mathrm{COP2}}$ (b) COP_2

Figure 4.10: Effect of $T_{\mathrm{ej,e}}$ at three different T_{evap}, for $p_{\mathrm{disc}} = 80\,\mathrm{bar}$, $\eta_{\mathrm{ej}} = 0.3$ and no IHX in VEJ

$T_{\mathrm{ej,e}}$ and low T_{evap}. This is in contrast to the actual COP_2 which is decreasing for high $T_{\mathrm{ej,e}}$ and low T_{evap}. Relative to the effect of $T_{\mathrm{ej,e}}$ it can be observed that $T_{\mathrm{ej,e}}$ has a strong effect on the COP_2, as generally expected due to the direct effect on the compressor pressure ratio. The effect of T_{evap} on $Incr_{\mathrm{COP2}}$ is in contrast found to be generally less significant compared to $T_{\mathrm{ej,e}}$.
As the evaporation temperature influences the ejector suction enthalpy due to the shape of the vapor dome, it also has an effect on ω as shown in figure 4.11. The effect of T_{evap} is smaller than the effect of $T_{\mathrm{ej,e}}$ on ω, as $T_{\mathrm{ej,e}}$ is more directly related to the ejector entrainment enthalpy.

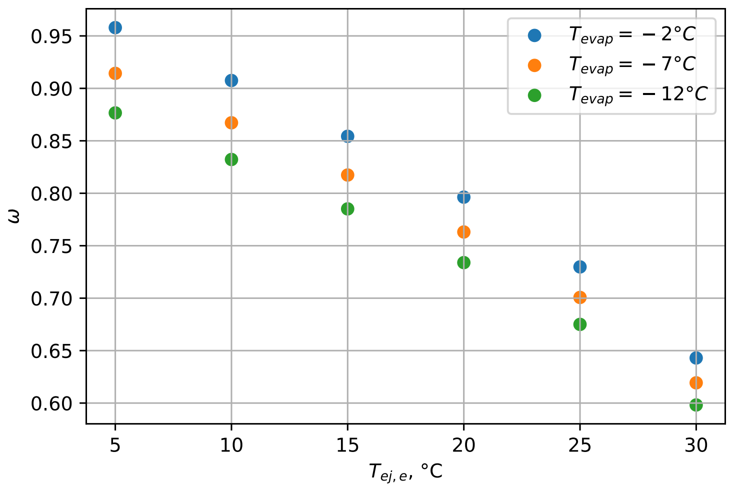

Figure 4.11: Effect of $T_{\mathrm{ej,e}}$ and T_{evap} on ω, for $p_{\mathrm{disc}} = 80\,\mathrm{bar}$ and $\eta_{\mathrm{ej}} = 0.3$ in VEJ

An evaluation of the effect of the superheat from the IHX shows that a change from no internal heat exchange to 5 K superheat provided by the IHX causes a 7 – 13 % drop in $Incr_{COP2}$. In fact, the increasing internal heat exchange is found to decrease the COP_2 of the VEJ system by about 2 % for most of the analysed cases. The negative effect is however decreasing with higher $T_{ej,e}$. In contrast, the effect of the IHX in the REF system is found to cause an insignificant increase in COP_2 for higher heat exchange in the internal heat exchanger, i.e. does not show a relevant effect. The described trends are likely linked more to the provided subcooling from the IHX after the gas cooler and subsequent lower $T_{ej,e}$, rather than to the increase in superheat. A reduction of the internal heat exchange in the VEJ system therefore seems interesting from a performance perspective in the modelled cases. The provided superheat though also serves the practical purpose of preventing liquid in the compressor, which is to be taken into account when considering a removal of the IHX in the VEJ system. For a change from no internal heat exchange to 10 K superheat provided by the IHX, the observed trend continues with 16 – 22 % lower $Incr_{COP2}$.
In contrast, if the internal superheat in the evaporator is increased at equal evaporation temperatures (theoretical case), the $Incr_{COP2}$ is also increasing, supporting the previous point that the negative impact of the internal heat exchanger is related to the subcooling side. The sensitivity analysis indicates an increase of $Incr_{COP2}$ by up to 1 % for a 1 K higher evaporator superheat (starting at 10 K).

Sensitivity to other parameters

The ejector efficiency η_{ej} as a key parameter naturally shows a significant effect on $Incr_{COP2}$. In fact, $Incr_{COP2}$ is almost directly proportional to η_{ej}, with a 10 % increase in η_{ej} (equal to 0.03 percentage points of η_{ej}) causing 8.5 – 10 % increase in $Incr_{COP2}$, which in turn leads to up to 3 % increase in the COP_2 of the VEJ system, with the highest effect at high $T_{ej,e}$ and low p_{disc}.
The sensitivity analysis for the increase of T_{evap} by 1 K is found to increase the COP_2 of both VEJ and REF system by up to 4 %, which corresponds to the expectations as the compressor pressure ratio is decreased for a higher evaporation temperature. The $Incr_{COP2}$ is in contrast found to decrease by up to 1.5 % for the increase of the evaporation temperature by 1 K.
The analysis of the sensitivity of the assumed compressor isentropic and motor efficiencies on the modelling results shows a negligible effect on $Incr_{COP2}$, as equal efficiencies are assumed for both the VEJ and the REF. For the actual COPs, the compressor efficiency shows a directly proportional effect, i.e. the COPs increase by 10 % for a 10 % higher compressor efficiency.

Vapor Ejector System with Parallel Compression (VPC)

The here presented VPC system comprises two additional components in comparison to the VEJ system: the parallel compression and the HPV. Both components can be added independently to the system, as they fulfil different purposes.
The HPV in parallel to the ejectors can be used to control p_{disc}, instead of relying on the ejectors for this control task as is necessary in the VEJ system.
The parallel compression allows to compress some of the evaporator mass flow directly, which

enables a control of the mass entrainment ratio and pressure lift of the vapor ejector independent of the system conditions. This allows more flexibility compared to the VEJ system, in which the vapor quality at the evaporator outlet based on the entrainment and suction conditions directly determines the ratio of $\dot{m}_{\text{evap}}$ and $\dot{m}_{\text{comp}}$ as previously explained.

The model of the system is evaluated to make a basic theoretical comparison to the VEJ system. For the test run, 50 % of the evaporator mass flow is compressed by the MC while the remaining 50 % is entrained by the ejector, with the resulting improvements in COP2 compared to the VEJ shown in figure 4.12. While the evaluation generally shows similar improvement trends in the VPC

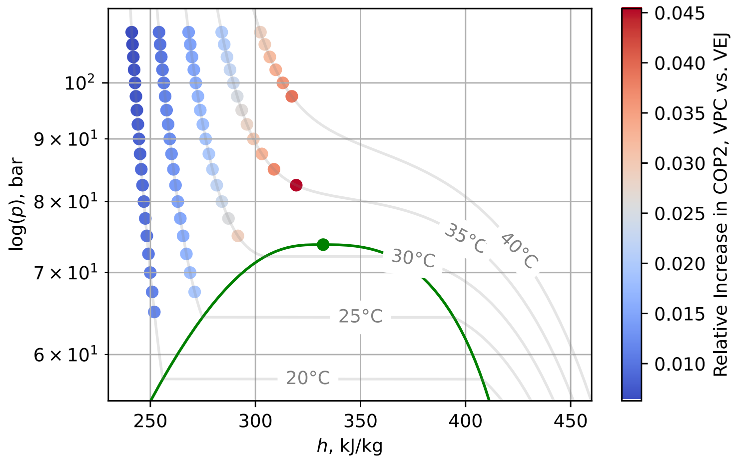

Figure 4.12: Relative increase in COP2 of the VPC model *in comparison to the VEJ model findings* at varying entrainment conditions for $T_{\text{evap}} = -10.4\,°\text{C}$, $\eta_{\text{ej}} = 0.3$ and $\dot{m}_{\text{MC}} = 0.5 \cdot \dot{m}_{\text{evap}}$

and VEJ systems compared to the REF system, the direct comparison of the system for the tested conditions indicates an additional performance improvement in the VPC system of 1.0 – 4.5 %. When comparing to the $Incr_{\text{COP2}}$ trends of the VEJ system compared to the REF system, it can be seen that the highest additional improvements of the VPC system occur in fact at conditions which also show the highest improvements of VEJ compared to REF system.
For the case of 40 °C, it can be seen that the evaluation starts only 97 °C, i.e. the optimal pressure of about 93 bar, which is due to the fact that the ejector outlet conditions would be located outside of the vapor dome for low pressures, as a result of the high pressure lifts as shown in figure 4.13.

The improvements seen for the VPC system are generally linked to significantly higher pressure lifts Δp_{lift} compared to the VEJ system, as figure 4.13 indicates for the analysed case. The higher pressure lifts result from the fact that the recovered work is provided to the system with a lower mass entrainment ratio ω, which in turn increases Δp_{lift}.
For a more detailed comparison of the example case of 75 bar and 25 °C entrainment conditions, resulting in a pressure lift of 5.6 bar in VPC, it is found that the entrainment mass flow is nearly equal in VEJ and VPC. As a consequence, it can be concluded that the maximum recoverable work $W_{\text{r,max}}$ in the VPC system is in fact reduced in comparison to the VEJ system by about 11 % due to the higher receiver pressure which decreases the net pressure difference available for work

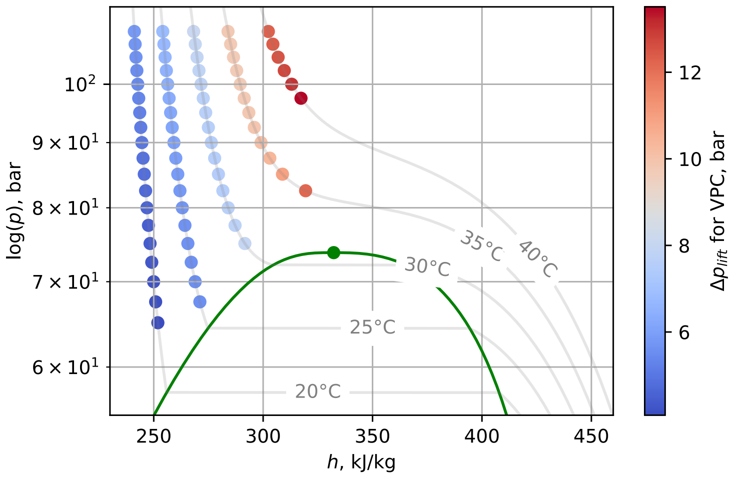

Figure 4.13: Pressure lift at varying entrainment conditions for $T_{\mathrm{evap}} = -10.4\,°\mathrm{C}$, $\eta_{\mathrm{ej}} = 0.3$ and $\dot{m}_{\mathrm{MC}} = 0.5 \cdot \dot{m}_{\mathrm{evap}}$ in VPC

recovery. Despite this fact, the reduction in enthalpy difference in the PC appears to outweigh both the additional work for the MC compression and the reduced recoverable work. It is found that 34.5 % of the entrainment mass flow of the VPC system are compressed in the MC with the remaining 65.5 % compressed in the PC. While the enthalpy difference of the MC is 15 % smaller and of the PC only 11 % higher compared to the ethalpy difference over the single compressor in VEJ, this still results in a total efficiency improvement of 1.7 % for the VPC.
The findings indicate that the efficiency of the PC is particularly important to achieve this relatively small improvement. For this reason amongst others, it might be difficult to actually achieve the modelled improvements in reality. Especially the operation at very high pressure lifts could itself pose additional challenges, e.g. on the operational range of the parallel compressor. Furthermore, the more difficult control of the system, as found in the literature review, possibly leads to further general system instabilities which might affect the performance.
It can be concluded from the indicated results in direct comparison to the VEJ system, that the VPC potentially offers further improvements from an energy perspective, which could be particularly interesting in combination with the possibility to adapt the operating conditions regarding ω and Δp_{lift}, giving more flexibility in optimizing the efficiency of the ejector.

4.1.2 Field Data Evaluation

In general, the analysis of the February case of both systems show conditions of high heat recovery demands, with the external reference at 9.8 or 9.9 V (of a maximum of 10 V) for all analysed time steps in system VEJ-A and at 10 V for almost the full February time range in VEJ-B. As a consequence, the system is found to be mostly controlled for a fixed p_{disc} in these time periods, with a pressure of 80 bar in system VEJ-A and 85 bar in system VEJ-B.
In contrast, the value of the external reference shows variations in the full range of 0 – 10 V for the September case in VEJ-A, while being on a constant low value of 1 V in system VEJ-B for the

analysed time period in September. In accordance with that, p_{disc} is also found to vary significantly in the September time periods, including also subcritical pressures.
Due to the seasonal temperature changes, the February cases also generally show lower gas cooler outlet and entrainment temperatures $T_{\mathrm{ej,e}}$ in comparison to the September cases.

System VEJ-A, February 2021

The analysis of the February case in system VEJ-A is generally representative for low ambient temperatures and high heat recovery in the system. Figure 4.14a shows the $Incr_{\mathrm{COP2}}$ and η_{ej} in correlation to different pressure lifts Δp_{lift}, indicating about 15 % increase in COP_2 for a pressure lift of 4 bar, with an approximately linear correlation in line with the modelling expectations.
Figure 4.14b shows the mass entrainment ratio ω in dependence of $T_{\mathrm{ej,e}}$ and T_{evap}, with a range of 0.6 to 0.95. While the direct effect of $T_{\mathrm{ej,e}}$ on ω is clearly visible as expected from the modelling results, only a minor effect can be seen by T_{evap}.

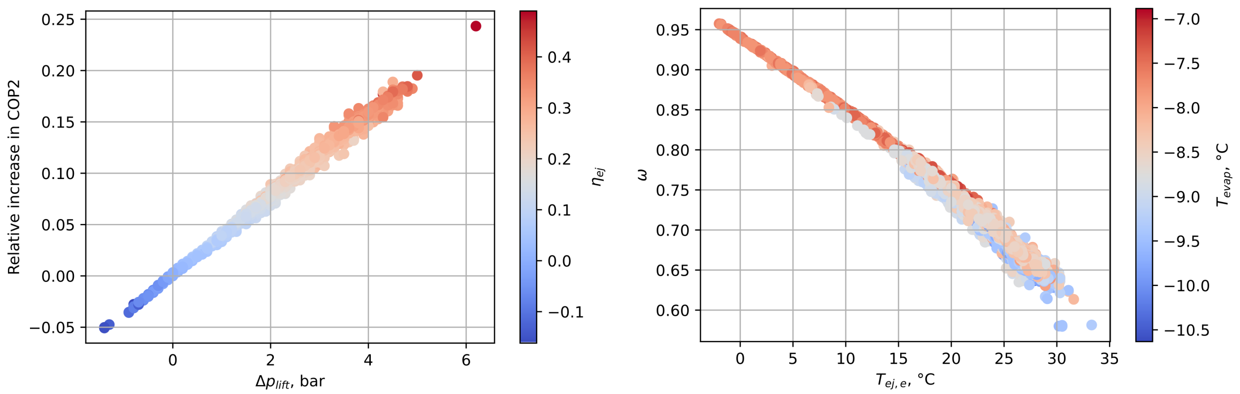

(a) Correlation of Δp_{lift}, $Incr_{\mathrm{COP2}}$ and η_{ej}

(b) Correlation between $T_{\mathrm{ej,e}}$ and ω for different T_{evap}

Figure 4.14: Basic ejector parameters in VEJ-A (Feb)

A common daily operation pattern likely related to the use of the system can be seen for the analysed time period in February, and continues to occur in the following weeks. The pattern is shown for three days in Figure 4.15.
It can be seen that power input P_{tot} commonly drops to a value below 50 kW between 21:00 and 24:00 in the evening before re-increasing between 09:00 and 12:00 in the morning. The pattern is closely linked to the evaporation temperature, which is lower during the higher power demands.
Furthermore, a similar trend can be seen for the $Incr_{\mathrm{COP2}}$, with values around 0 during most of the time periods of low power, but significantly higher values in the range of 0.05 to 0.015, i.e. a 5 – 15 % relative increase in COP_2, during the periods of higher power. During the hours around 12:00 on day 1, a high $Incr_{\mathrm{COP2}}$ can be observed despite low compressor power. The occasion indicates a direct link of $Incr_{\mathrm{COP2}}$ to the entrainment temperature $T_{\mathrm{ej,e}}$, which is increasing in parallel with $Incr_{\mathrm{COP2}}$.
Figure 4.16 confirms the correlation between $T_{\mathrm{ej,e}}$ and $Incr_{\mathrm{COP2}}$, showing a closely connected trend

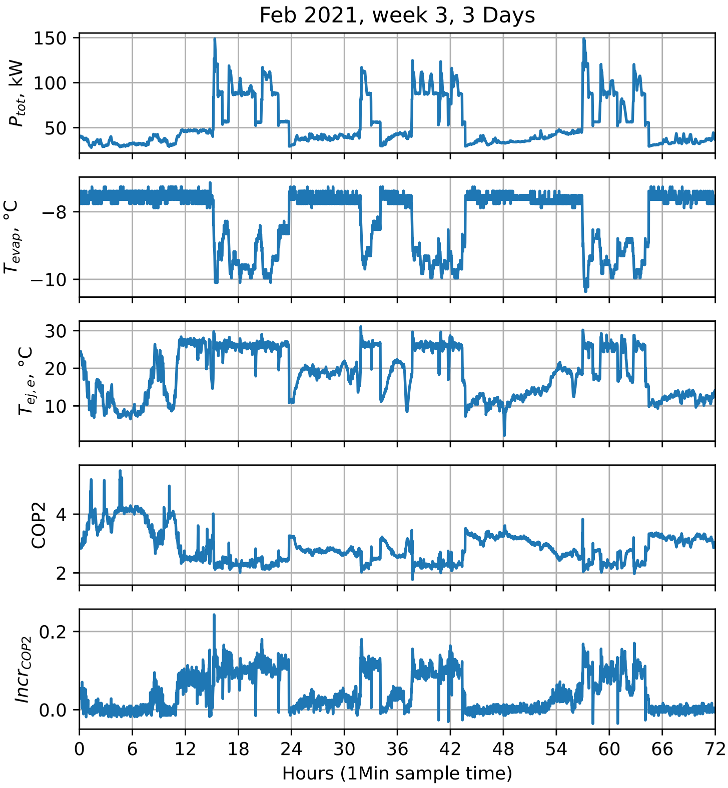

Figure 4.15: Pattern for 3 days in VEJ-A (Feb)

for η_{ej} and Δp_{lift} over $T_{ej,e}$.

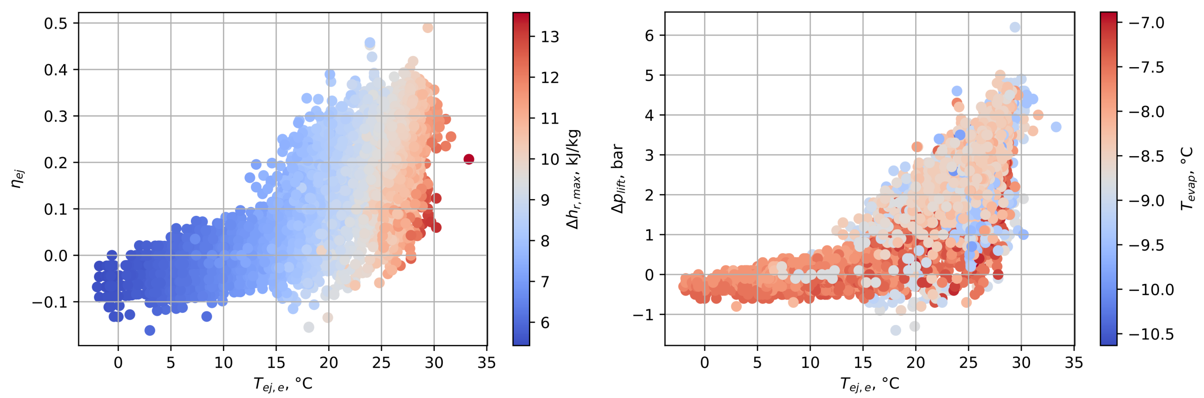

(a) Effect of $T_{ej,e}$ on η_{ej} and $\Delta h_{r,max}$

(b) Effect of $T_{ej,e}$ and T_{evap} on Δp_{lift}

Figure 4.16: Effect of $T_{ej,e}$ and T_{evap} on η_{ej}, recoverable work and Δp_{lift} in VEJ-A (Feb)

For $T_{ej,e}$ below 15 °C, Δp_{lift} is found to be unstable and fluctuating in a range of about 1 bar around $\Delta p_{lift} = 0$ bar. In relation to that, η_{ej} is also unstable in this range. Negative ejector efficiencies occurring together with negative pressure lifts during time periods when the ejector is not functioning as intended. In these cases the compressor suction pressure is actually below the evaporation pressure, i.e. the performance of the system is decreased. This results. For system VEJ-A, this is however found to occur only during a small number of short-term occasions. It is suspected that these occur in relation to a change in operating conditions in the system which lead to pressure fluctuations.

For higher $T_{\mathrm{ej,e}}$, a general continuously increasing trend Δp_{lift}, η_{ej} and $Incr_{\mathrm{COP2}}$ can be seen in the figures up to a pressure lift of $4-5$ bar and an ejector efficiency around 0.3 , achieving results in a similar range as the previously presented modelling results.

The evaporation temperature T_{evap} is found to have high values during the low Δp_{lift}, while lower values appear to occur generally during higher $T_{\mathrm{ej,e}}$ and higher Δp_{lift}. This is in line with the expectations from the model findings, according to which high T_{evap} decrease the work recovery potential.

The main effect on the work recovery potential comes from $T_{\mathrm{ej,e}}$, as figure 4.16a clearly indicates. The isentropic enthalpy difference available for work recovery is decreasing for the low $T_{\mathrm{ej,e}}$, in line with the modelling results. In combination, it is found that the low Δp_{lift} is mostly occurring at low entrainment mass flow rates during low $T_{\mathrm{ej,e}}$ as figure 4.17b shows. This generally results in a minimal work recovery potential and subsequently a low pressure lift for these conditions, even independent of the ejector efficiency.

Regarding the actual ejector efficiency η_{ej}, the analysis of the effect of the opening degree of ejector EJ1 on Δp_{lift} in figure 4.17a shows that the low pressure lifts occur during low opening degrees of mostly below 20 % for ejector EJ1, while the ejectors EJ2 and EJ3 are fully closed for these cases. In combination with the low $\dot{m}_{\mathrm{comp}}$ at these occurrences, and based on the literature findings on the off-design operation of needle-controlled ejectors, it can be suspected that the ejectors are possibly over-dimensioned for the operation at these conditions, causing a significant decrease in η_{ej} due to the off-design operation.

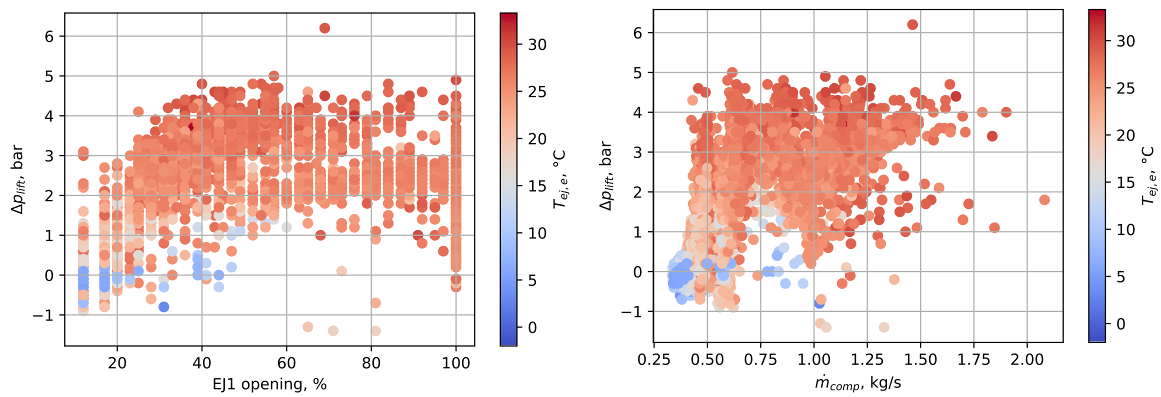

(a) Effect of the opening degree of Ejector EJ1 (b) Effect of the entrainment mass flow $\dot{m}_{\mathrm{comp}}$

Figure 4.17: Effect of the entrainment mass flow $\dot{m}_{\mathrm{comp}}$ and the opening degree of Ejector EJ1 in VEJ-A (Feb)

For the analysed case, $T_{\mathrm{ej,e}}$ appears thus to have a major impact on Δp_{lift} and the resulting performance improvements in the system, with low Δp_{lift} corresponding to low $T_{\mathrm{ej,e}}$. While this is in line with the decrease of the work recovery potential for low $T_{\mathrm{ej,e}}$, the field data shows that a

decrease of η_{ej} at low $T_{ej,e}$ intensifies this affect additionally.
The low $T_{ej,e}$ is found to be mainly caused by a significant temperature drop in the gas cooler, i.e. as a result of the low ambient temperatures. From an energy perspective for the refrigeration part, it can however be concluded that this operation is still more efficient in comparison to the option of reducing the gas cooler temperature difference in order to operate the ejector at higher $T_{ej,e}$. This is because a higher $T_{ej,e}$ would reduce the enthalpy difference on the high-pressure side which would in turn require an increase in $\dot{m}_{comp}$ to achieve the same cooling capacity from an energy balance perspective. The modelling results in figure 4.5 confirm that the work recovery in the ejector is not able to compensate for the reduction in COP_2 resulting from a higher $T_{ej,e}$ even for a continuously high ejector efficiency of 0.3 . Figure 4.15 is in line with this, indicating that the COP_2 is in fact higher during the periods with low $T_{ej,e}$ and low $Incr_{COP2}$ by the ejector.

System VEJ-A, September 2020

In comparison to February 2021, the analysis of September 2020 generally shows lower mass entrainment ratios ω in the range of about 0.5 to 0.85 due to the higher $T_{ej,e}$ as figure 4.18b illustrates in line with the modelling findings. For high $T_{ej,e}$, the effect of the shape of the equal temperature lines relative to the enthalpy can be seen, causing a more rapid decrease of ω over $T_{ej,e}$ as the enthalpy difference between temperature lines increases. The high $T_{ej,e}$ results from the higher ambient temperatures in September, which set the lower temperature limit in the gas cooler.
Figure 4.18b also indicates an effect of p_{disc} on ω. ω is generally increasing for higher p_{disc} at equal $T_{ej,e}$ due to the reduction in entrainment enthalpy, which is however small compared to the effect of $T_{ej,e}$. This trend is in accordance with the expectations from the model.

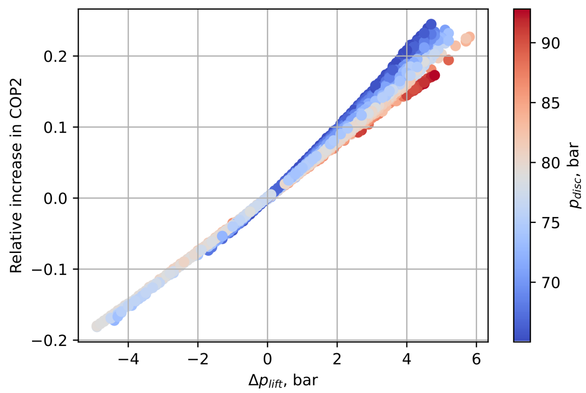

(a) Correlation of Δp_{lift} and $Incr_{COP2}$ for different p_{disc}

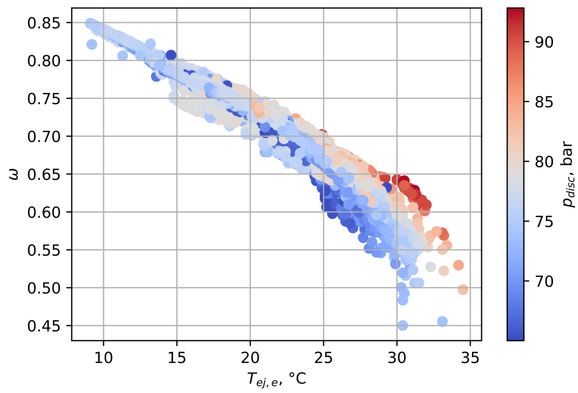

(b) Correlation between $T_{ej,e}$, ω and p_{disc}

Figure 4.18: Basic ejector parameters in VEJ-A (Sep)

The clear correlation between the pressure lift Δp_{lift} and the relative increase in COP_2 can be seen in figure 4.18a similarly to February. In addition, the effect of the changing p_{disc} in September on the slope can be seen in this figure in accordance with the modelling findings, showing up to 20 % relative increase in COP_2 for the lower limit of p_{disc} here.

Regarding the evaporation temperature T_{evap}, stable ejector efficiencies η_{ej} up to 40 % are found down to an evaporation temperature of −12 °C in figure 4.19, with only a small number of points found below this temperature. Furthermore, there appears to be a different trend below an evapora-

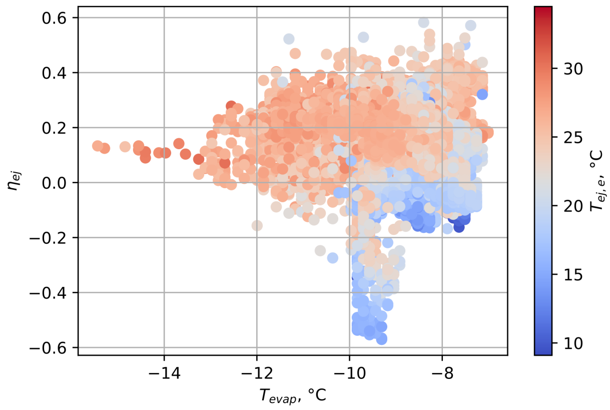

Figure 4.19: Effect of low T_{evap} and $T_{\mathrm{ej,e}}$ on η_{ej} in VEJ-A (Sep)

tion temperature of −10 °C compared to above, with a generally wider range of η_{ej} and dependency on $T_{\mathrm{ej,e}}$ above −10 °C, while $T_{\mathrm{ej,e}}$ appears to remain on a high level for T_{evap} below −10 °C. The different trends are analysed separately in the following step.

A more detailed analysis of all cases in September at low evaporation temperatures between -12 and −10 °C shows a specific behaviour of η_{ej} and Δp_{lift} over the discharge pressure in figure 4.20. For p_{disc} below 73 bar, an almost stable high ejector efficiency in a small range of about 0.25 to

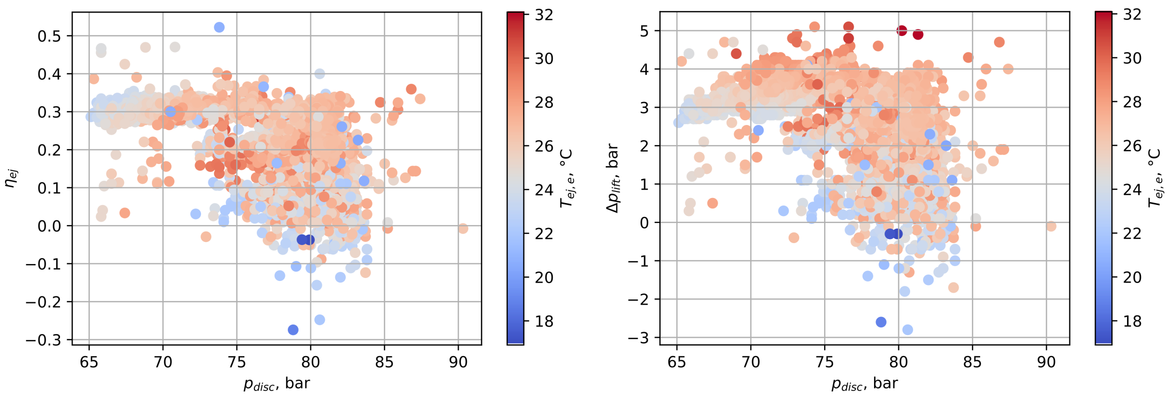

(a) η_{ej} (b) Δp_{lift}

Figure 4.20: Effect of p_{disc} and $T_{\mathrm{ej,e}}$ on η_{ej} and Δp_{lift} for T_{evap} between -12 and −10 °C in VEJ-A (Sep)

0.35 can be seen for the large majority of cases. For higher p_{disc} contrast, ejector efficiencies are found to occur in a much wider range including significantly lower efficiencies.
A corresponding stable trend can be observed for the pressure lift at p_{disc} below 73 bar, with

increasing Δp_{lift} from 2.5 up to 4.5 bar for higher p_{disc} and higher $T_{\mathrm{ej,e}}$ as expected from the model and corresponding to an $Incr_{\mathrm{COP2}}$ between 15 and 20 %. For higher pressures in contrast, the Δp_{lift} is also found to be varying in a wide and mostly lower range.

As possible reason for this trend, it is found that the low p_{disc} corresponds to low compressor powers and thus also low $\dot{m}_{\mathrm{comp}}$ compared to the cases at higher p_{disc}. In combination with this, a difference in the ejector operation is found to possibly have an impact. This is illustrated for an example time period of two hours in figure 4.21 which shows a common pattern occurring during low T_{evap} in this system.

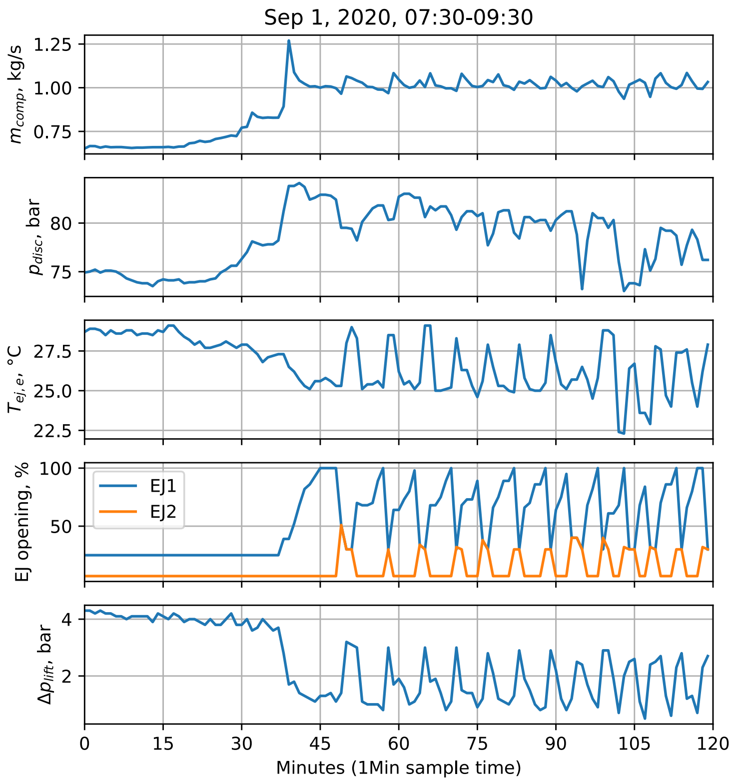

Figure 4.21: Typical control patterns for T_{evap} between -12 and $-10\,°\mathrm{C}$ in VEJ-A (Sep)

In the analysed time period, the system power input P_{tot} is changing from 55 kW to a short time period of 75 kW and then to 100 kW, parallel to the change seen for $\dot{m}_{\mathrm{comp}}$ in figure 4.21. P_{tot} is relatively stable at all of these three power levels, in contrast to $\dot{m}_{\mathrm{comp}}$ which shows a stable initial value but higher fluctuations at the higher $\dot{m}_{\mathrm{comp}}$ after 45 min.
Corresponding to this compressor behaviour, it can be seen that the ejector operation is initially stable with medium use of EJ1 and no use of EJ2 at the lower power and subcritical p_{disc}, creating a continuous pressure lift Δp_{lift} of about 4 bar. The ejectors react to the increase in compressor power and mass flow first by increasing the opening degree of EJ1 to 100 % at strongly decreasing Δp_{lift} before EJ2 is turned on in parallel with a reduction in the opening degree of EJ1 and a re-increase to about 3 bar pressure lift. This state is however not maintained. Instead, the ejector operation starts to fluctuate between the two cases of 100 % opening of EJ1 and a closed EJ2 on

the one hand and about 40 % opening in both EJ1 and EJ2. EJ3 is not used during the entire plotted time period.
The use of equal opening degrees for all used ejectors appears to be a general control strategy in the system.
The ejector fluctuations appear to correlate with the changes in $T_{\mathrm{ej,e}}$, with low pressure lift and high opening degrees of ejector EJ1 during low $T_{\mathrm{ej,e}}$. The changes in $T_{\mathrm{ej,e}}$ in turn are in fact caused by a changing subcooling in the borehole heat exchanger before the IHX. While the borehole heat exchanger is generally aimed to be controlled in order to facilitate stable ejector operation according to the manufacturer, this seems not to be the case here. The general possibility to impact the ejector pressure lift Δp_{lift} by controlling this heat exchanger can though be seen clearly.

As a consequence of the observed ejector control, the fluctuating pressure lift creates a changing receiver pressure level p_{rec} while p_{evap} remains relatively stable. The changing p_{rec} in turn affects the refrigerant density at the compressor inlet and thus $\dot{m}_{\mathrm{comp}}$, which is likely followed by the fluctuations seen in p_{disc} and possibly also the results in the subcooling control leading to the fluctuating $T_{\mathrm{ej,e}}$ at the ejector inlet. As the ejector is likely trying to control the high-side pressure, this is possibly a situation of hunting, where the parameters affect each other in a cycle, creating an unstable control situation which is neither beneficial for the ejector performance nor for the overall system.
With reference to the later presented findings in system VEJ-B on the effect of T_{evap}, it could furthermore be suspected that the ejector itself has difficulties to achieve a stable operation at the low T_{evap} in combination with the supercritical p_{disc}.
In total, an efficient and stable ejector operation for subcritical conditions is found for the case of T_{evap} below $-10\,°\mathrm{C}$. In contrast, the low pressure lifts at supercritical conditions are found for these low evaporation temperatures mainly as a result of unstable ejector control and fluctuating $T_{\mathrm{ej,e}}$.

For the cases with evaporation temperatures above $-10\,°\mathrm{C}$, figure 4.22 generally shows a broader range of Δp_{lift} and similarly for η_{ej} (not shown) over p_{disc}, with a clear effect of $T_{\mathrm{ej,e}}$, which generally varies in a wider range here compared to the case at low T_{evap}. In contrast to the findings for the case of low T_{evap} (figure 4.20b), the pressure lift seems not affected by p_{disc} here. The found pressure lifts correspond to an $Incr_{\mathrm{COP2}}$ of up to 25 % here with a generally decreasing trend for higher p_{disc} in accordance with the findings in figure 4.18a. However, a number of cases with significantly lower, negative Δp_{lift} seem to occur, as previously mentioned likely related to short-term control changes.
A more detailed analysis is therefore done for the range of p_{disc} between 78 and 80 bar in which the majority of points with this very low Δp_{lift} is found. Figure 4.23a shows the general trend of increasing Δp_{lift} for higher $T_{\mathrm{ej,e}}$. In line with this, very low Δp_{lift} occur at the lower $T_{\mathrm{ej,e}}$. Furthermore, the figure shows for these low $T_{\mathrm{ej,e}}$ that the points with negative Δp_{lift} correlate with high compressor mass flows $\dot{m}_{\mathrm{comp}}$, resulting from a higher capacity.
In combination with this, figure 4.23b indicates that the ejector EJ1 shows higher opening degrees in combination with the higher compressor mass flows $\dot{m}_{\mathrm{comp}}$, presumably to handle the higher capacity. Ejectors EJ2 and EJ3 are found not to be used during the occurrences of negative Δp_{lift} at low $T_{\mathrm{ej,e}}$, in contrast to their apparent usage for cases of higher capacity at higher $T_{\mathrm{ej,e}}$.
In addition, despite analysing only evaporation temperatures above $-10\,°\mathrm{C}$ in this case, figure

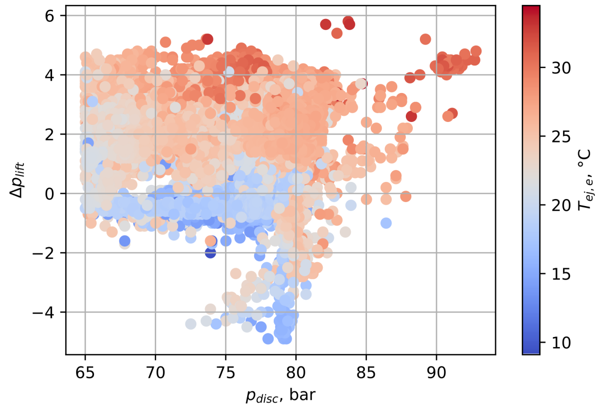

Figure 4.22: Δp_{lift} over p_{disc} for varying $T_{\text{ej,e}}$ in VEJ-A (Sep)

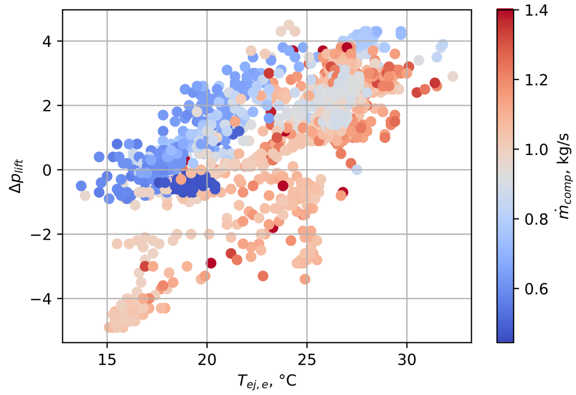

(a) $\dot{m}_{\text{comp}}$

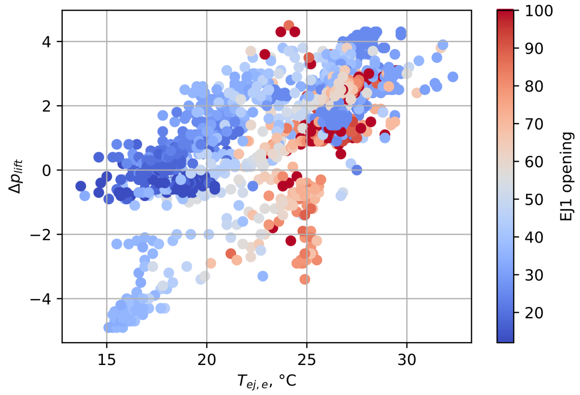

(b) EJ1 opening degree

Figure 4.23: Effect of $\dot{m}_{\text{comp}}$ and EJ1 on Δp_{lift} at varying $T_{\text{ej,e}}$ for T_{evap} above $-10\,°\text{C}$ in VEJ-A (Sep)

4.24 indicates still a negative effect of low evaporation temperatures T_{evap} at low $T_{\text{ej,e}}$ in relation to the occurrence of the low Δp_{lift}.
In total, the very low pressure lifts in this time period appear to result from the combination of these aspects, particularly at high capacities in combination with low evaporation temperatures. Based on the findings by Lucas and Koehler [14], it can be suspected that the low evaporation temperatures in combination with the ejector design and control are causing the very low pressure lifts, as a result of the high velocity and increased friction pressure drop at these conditions in the ejector.

System VEJ-A, Seasonal Savings

To estimate the seasonal energy savings in system VEJ-A, a linear regression is made for the correlation between Δp_{lift} and $Incr_{\text{COP2}}$ seen in both figure 4.14a and figure 4.18a. As both cases

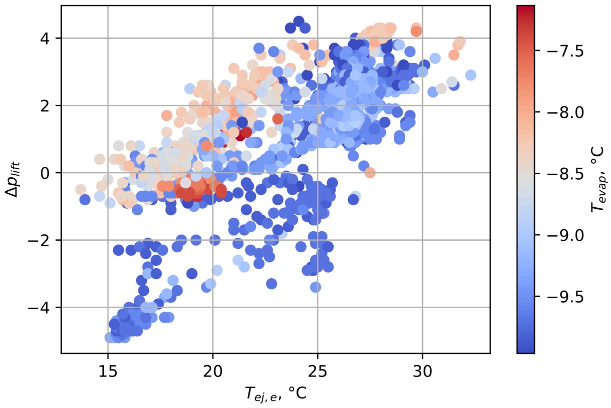

Figure 4.24: Effect of $T_{\text{ej,e}}$ and T_{evap} on Δp_{lift} for T_{evap} above $-10\,°\text{C}$ in VEJ-A (Sep)

are expected to be representative for about half of the season, the average of the obtained factors between Δp_{lift} and $Incr_{\text{COP2}}$ is used for the seasonal savings calculation, resulting in equation 4.1.

$$Incr_{\text{COP2}} = 0.0418 \cdot \Delta p_{\text{lift}} \tag{4.1}$$

When comparing the savings calculated with this equation to the actual savings calculated based on the detailed calculation of $Incr_{\text{COP2}}$ for September and February, the equation is found to give a close approximation, with 3 % underestimation of the savings in September and 5 % overestimation of the savings in February.
In total, the evaluation of the season for the time periods without operation of the borehole evaporator shows 7 % energy savings in comparison to a REF system operating at the same conditions. In comparison to the literature findings, this is within the range of the findings by Corrazzol et al. [17] for needle-controlled ejectors and above the findings of 5 % improvement for a multi-ejector in Trondheim, Norway in 2014 by Hafner [16].

System VEJ-B, February 2021

Similar to system VEJ-A, system VEJ-B operates in February at mostly constant p_{disc} and comparatively low entrainment temperatures $T_{\text{ej,e}}$ and thus with high mass entrainment ratios ω in the range of 0.7 to 1, as figure 4.25b shows. The modelling results indicate that this leads to lower pressure lifts and theoretically a smaller system improvement potential by the ejector. Indeed, figure 4.25a confirms generally lower Δp_{lift} and $Incr_{\text{COP2}}$ for lower $T_{\text{ej,e}}$ compared to the findings in VEJ-A.
In contrast to the according figures for system VEJ-A, figure 4.25b also shows a clear effect of T_{evap} on ω, in line with the expectations from the model. This is likely due to the significantly wider range of T_{evap} seen in system VEJ-B compared to system VEJ-A. It is furthermore clearly visible that T_{evap} in system VEJ-B is generally lower compared to system VEJ-A, as expected due to the indirect evaporation in VEJ-B.

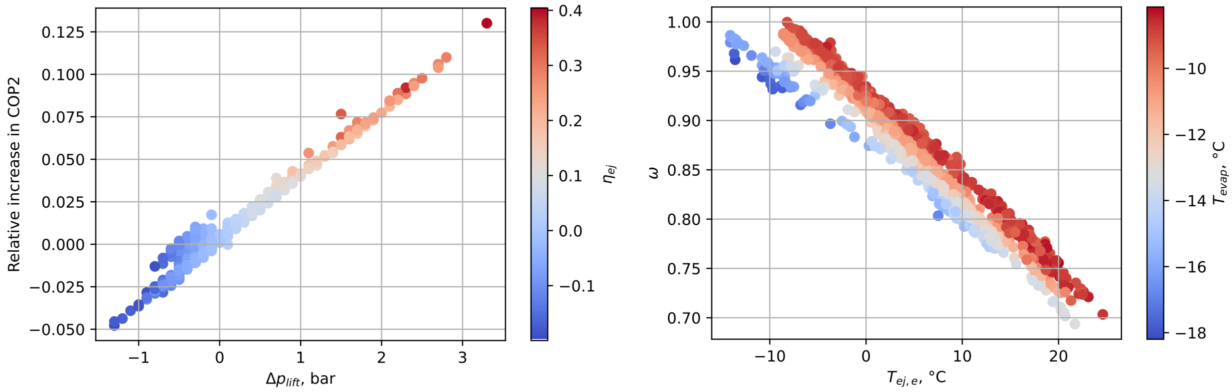

(a) Correlation of Δp_{lift} and $Incr_{\mathrm{COP2}}$ for different $T_{\mathrm{ej,e}}$ (b) Correlation of $T_{\mathrm{ej,e}}$ and ω for different T_{evap}

Figure 4.25: Basic ejector parameters in VEJ-B (Feb)

A more detailed analysis of the effect of T_{evap} in figure 4.26 shows a significant impact on the performance in system VEJ-B. The figure reveals in fact a relatively sharp cut at an evaporation

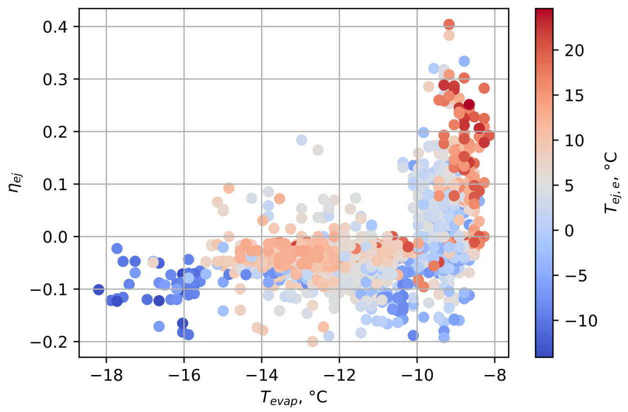

Figure 4.26: Effect of low T_{evap} in VEJ-B (Feb)

temperature $-10\,°\mathrm{C}$, with the large majority of cases with lower T_{evap} showing negative ejector efficiencies as the result of negative pressure lifts. The clear effect at $-10\,°\mathrm{C}$ indicates that the ejector is not able to operate properly below this evaporation temperature. Based on the findings by Lucas and Koehler [14] described in section 2.3, it can be suspected that the effect is linked to the mixing section of the ejector, where a pressure below the evaporation pressure is needed to achieve proper suction. For the analysed case, it is likely that the ejector is not designed for such low mixing pressures.

At the same time, the low $T_{\mathrm{ej,e}}$ and the high p_{disc} might play a key role in combination with the low T_{evap} as cause for the instable ejector operation here. This can be concluded from the comparison with the effect of low T_{evap} in system VEJ-A (figure 4.19), where high ejector efficiencies are found even for evaporation temperatures between -10 and $-12\,°\mathrm{C}$ in contrast to the performance drop at

−10 °C in VEJ-B. The specific comparison of these two cases of low T_{evap} shows that system VEJ-A is operating at a significantly higher $T_{ej,e}$ and mostly subcritical p_{disc} in contrast to the lower temperatures $T_{ej,e}$ in VEJ-B in this context.

For the case of evaporation temperatures above −10 °C in February, the effect of the enthalpy difference $\Delta h_{r,max}$ and the ejector efficiency η_{ej} analysed for different $T_{ej,e}$ is shown in figure 4.27.

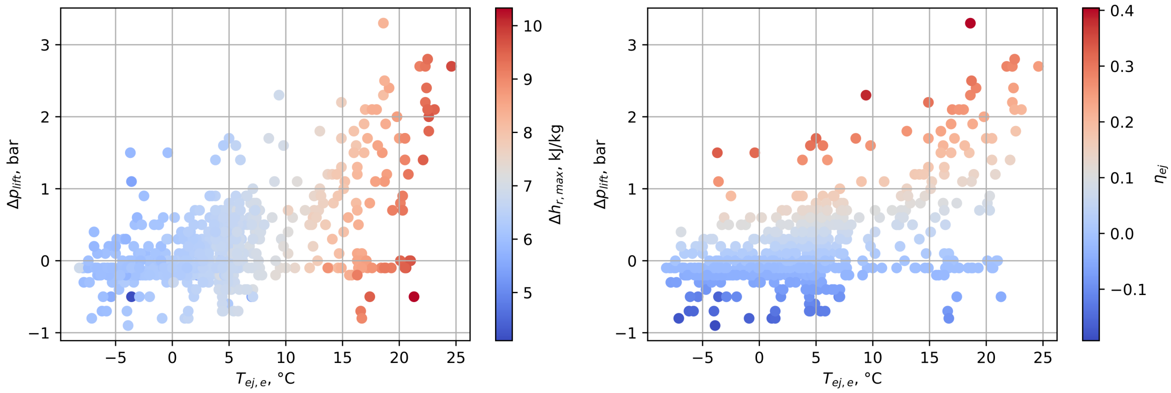

(a) Effect of $\Delta h_{r,max}$ (b) Effect of η_{ej}

Figure 4.27: Effect of $\Delta h_{r,max}$ and η_{ej} on Δp_{lift} for varying $T_{ej,e}$ at T_{evap} above −10 °C in VEJ-B (Feb)

Regarding η_{ej}, a clear effect on Δp_{lift} can be seen. From a work recovery perspective, as the capacity and thus the compressor mass flow rate are approximately constant during the here analysed cases of high T_{evap}, the maximum recoverable work $W_{r,max}$ is approximately proportional to $\Delta h_{r,max}$ as shown in 4.27a. Thus, a close correlation between $T_{ej,e}$ and the maximum recoverable work is in fact indicated in the figure 4.27a, similar to the findings for system VEJ-A in figure 4.16a. It can be concluded that the low pressure lifts Δp_{lift} at low $T_{ej,e}$ are a result of the low recoverable work in combination with the ejector design which is likely operating at off-design conditions for these temperatures.

Even for high $T_{ej,e}$ and subsequent high $W_{r,max}$, the actual recovered work, illustrated by the pressure lift Δp_{lift} (for equal ω at equal $T_{ej,e}$) is found to be varying. As the work recovery is thus excluded as possible reason, the ejector efficiency is causing the variation as seen in figure 4.27b. While no further effect of the evaporation temperature T_{evap} or fluctuations of p_{disc} can be identified as direct cause for this, figure 4.28 suggests that the ejector control plays a role.

It is visible in figure 4.28b that the ejectors EJ2, EJ3 and EJ4 are more than 40 % opened for the majority of the cases of low Δp_{lift} at $T_{ej,e}$ above 10 °C, while they are turned off during higher Δp_{lift} at these $T_{ej,e}$. Even ejector EJ1 is operated at the same opening degree during the opening of ejectors EJ2 to EJ4, in accordance with the control strategy which appears to control all used ejectors for equal opening degrees if not turned off. In contrast, EJ1 shows smaller opening degrees during the cases of higher Δp_{lift} even though ejectors EJ2 to EJ4 are in fact turned off in these cases. As $\dot{m}_{comp}$ is not varying significantly during these cases and ω is also approximately constant for equal $T_{ej,e}$, the high increase in ejector capacity seems unjustified here and likely a

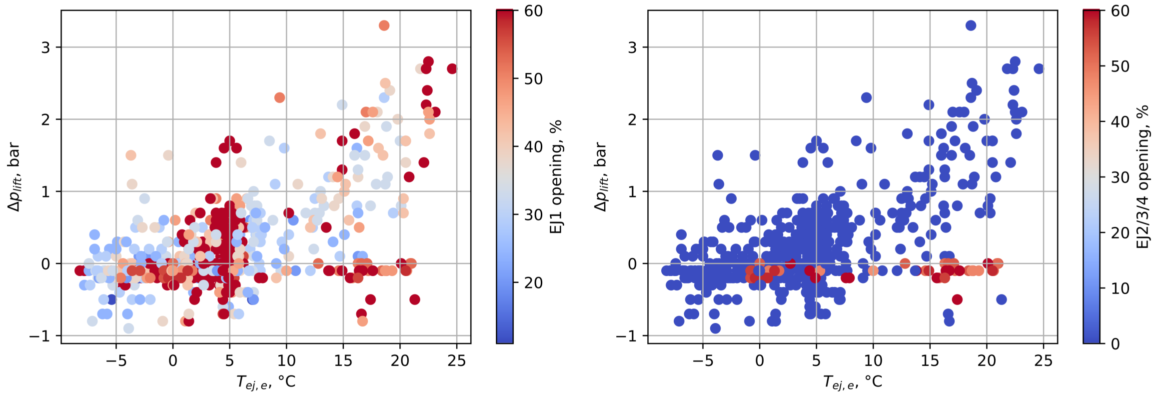

(a) Opening degree of EJ1

(b) Opening degree of EJ2, EJ3 and EJ4 (equal opening degrees)

Figure 4.28: Effect of the ejector opening on $Incr_{\mathrm{COP2}}$ for varying $T_{\mathrm{ej,e}}$ at T_{evap} above $-10\,°\mathrm{C}$ in VEJ-B (Feb)

reason for the low ejector performance at these occurrences. It is unclear why the ejectors are operated in this way.

System VEJ-B, September 2020

For the analysed data in September for system VEJ-B, the relative increase in COP_2 is generally found to be in a low range between -4 and 6 %, showing a performance decrease for a substantial number of points as figure 4.29a indicates. In addition, it can be seen that the pressure is in a subcritical range during the full analysed time period. Similar to the September case in system

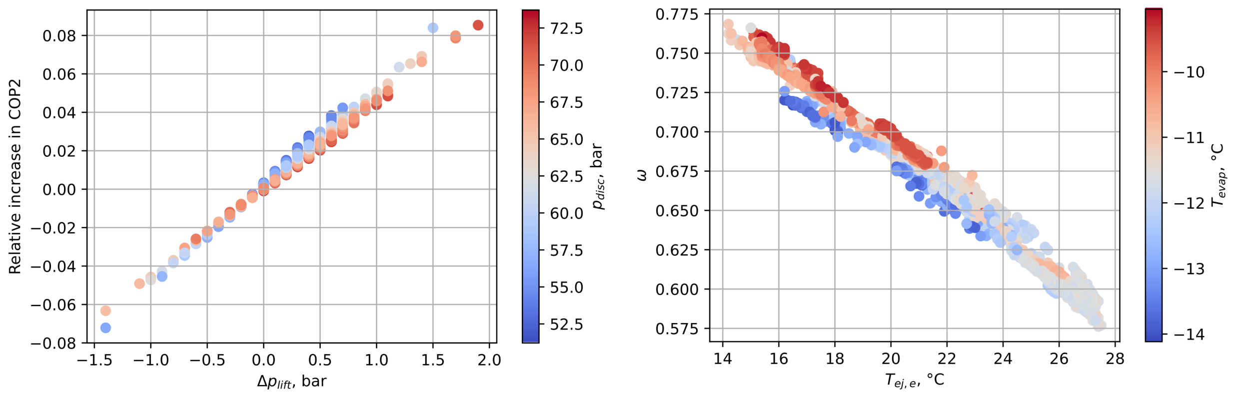

(a) Correlation of Δp_{lift} and $Incr_{\mathrm{COP2}}$ for different p_{disc}

(b) Correlation between $T_{\mathrm{ej,e}}$ and ω for different T_{evap}

Figure 4.29: Basic ejector parameters in VEJ-B (Sep)

VEJ-A, the mass entrainment ratio ω is here also in a lower range compared to the February case due to the higher $T_{\text{ej,e}}$. Furthermore, ω is varying in a smaller range with T_{evap} as seen in figure 4.29b.

An analysis of the evaporation temperature T_{evap} in figure 4.30a shows evaporation temperatures generally below $-9\,°\text{C}$, with most values below the limit of $-10\,°\text{C}$ seen in the February case as minimum T_{evap} for a possible ejector operation. In contrast to the February case, there is no improvement of Δp_{lift} visible above $-10\,°\text{C}$ here. From figure 4.30b, it can be observed that η_{ej} is in

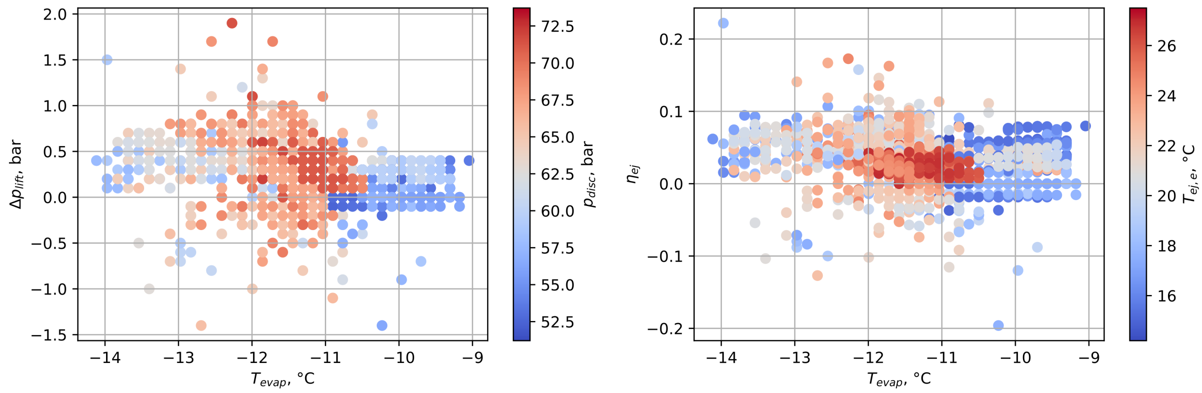

(a) Effect of T_{evap} on Δp_{lift} for different p_{disc} (b) Effect of T_{evap} and η_{ej} for different $T_{\text{ej,e}}$

Figure 4.30: Conditions at low T_{evap} for VEJ-B (Sep)

the range of -5 to 10 % with an average η_{ej} of 3 % corresponding to the fact that η_{ej} is positive for the larger part of the time. Despite the low T_{evap}, these are in fact higher η_{ej} compared to the ones found for February in system VEJ-B for similar low T_{evap}, possibly as a result of the generally higher $T_{\text{ej,e}}$ which has been previously found to improve the ejector performance. An additional reason might be the subcritical operation, which appears to achieve better performances for low T_{evap} in system VEJ-A in September. The ejector efficiencies seen here in system VEJ-B are however significantly below the ones seen for the compared September case in VEJ-A.
While no direct cause for the observed low pressure lifts can be found from the surrounding parameters, the discharge pressure p_{disc} seems to have a minor effect in combination with a varying ejector control, as figure 4.31 shows. As in the previous cases, it can be seen that all used ejectors are almost exclusively operated at equal opening degrees. From the figure 4.31, two major cases of ejector operation can be identified. On the one hand, If ejector EJ4 is turned off (dark blue region in figure 4.31b, the remaining three ejectors are operated at comparatively high opening degrees here. On the other hand, if ejector 4 is also used and all four ejectors are operating at a common lower opening degree (light blue region in both figures), it can be observed that Δp_{lift} is in fact increasing to a certain extend for higher p_{disc} in the majority of the cases, appearing to generally enable the comparatively higher pressure lifts of about $0.5 - 1$ bar seen for p_{disc} above 65 bar.
From these observations, it might be suspected that an optimized ejector control might be able to increase the performance in the observed case, possibly achieving higher pressure lifts as possible in VEJ-A for comparable conditions.

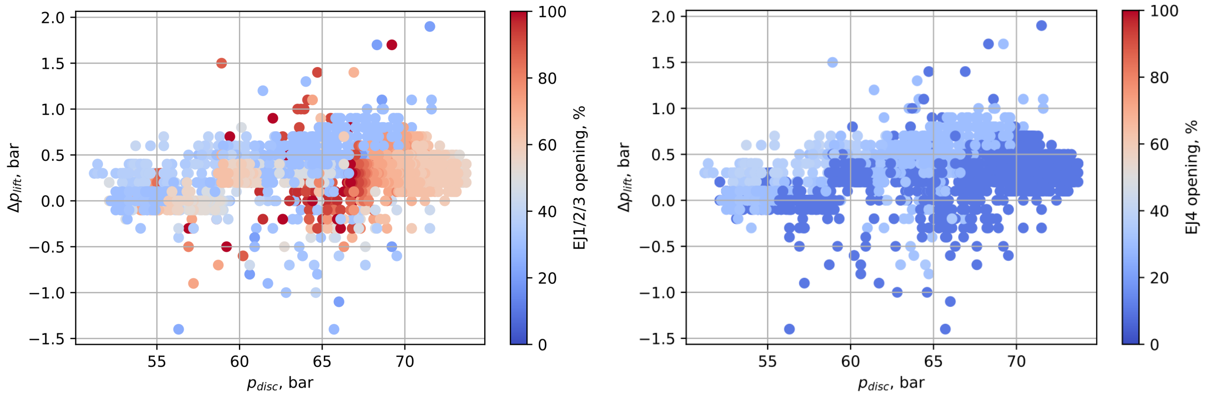

(a) Ejectors EJ1/2/3 (equal openings)

(b) Ejector EJ4

Figure 4.31: Effect of the ejector opening over p_{disc} on Δp_{lift}

System VEJ-B, Seasonal Savings

The regression of the correlation between Δp_{lift} and $Incr_{\text{COP2}}$ is done similar to VEJ-A by using the mean value of the factors obtained from figure 4.25a and figure 4.29a to find equation 4.2.

$$Incr_{\text{COP2}} = 0.0425 \cdot \Delta p_{\text{lift}} \tag{4.2}$$

The actual savings found from the detailed calculation in VEJ-B are 1.5 % for September and −0.4 % for February. For February, this is in fact a small performance decrease as a result of the ejector in comparison to a REF system operating at the same conditions, due to the unstable ejector operation seen as a consequence of the low T_{evap} in combination with the low $T_{\text{ej,e}}$ in winter, leading to a situation requiring the receiver pressure (which is the compressor suction pressure) to be slightly lower than the evaporation pressure.
Due to the generally small values here, higher deviations between the savings calculated from the regression and the savings obtained from the detailed calculation are found here, increasing the uncertainty of the total savings estimation. The found deviations for the calculated savings are 13 % for September and 88 % for the small absolute value in February.
For the full seasonal estimation, an insignificant performance increase of 0.16 % is found, showing no relevant gain in system performance by the ejector in VEJ-B as a result of the unfavourable conditions for the used ejector design.
Despite the uncertainties in system VEJ-B, it can be noticed that the factor in the obtained regression equations is in a similar range for both systems VEJ-B and VEJ-A.

4.1.3 Consequences and Possible Improvements

The analysed ejectors particularly in system VEJ-B show clear difficulties to achieve benefits at low T_{evap}. The model findings indicate that this is not related to the theoretical work recovery potential, which increases in fact for lower T_{evap} due to the higher pressure differences. Instead,

the operational difficulties at low T_{evap} appear to be related to the design and control of the used ejectors, likely particularly to the design of the mixing chamber, which could be adapted in order to operate at lower mixing pressures and thus also lower T_{evap}.
In comparison to the negative effect of T_{evap} in VEJ-B, system VEJ-A shows in fact a stable ejector efficiency in a range of equally low evaporation temperatures and otherwise comparable conditions. This reinforces the point that an adapted ejector design and control would be able to overcome the low ejector efficiency in VEJ-B at these conditions.

Another challenge for the VEJ system, particularly for the operation at low $T_{\text{ej,e}}$, lies within the direct coupling of ω to $T_{\text{ej,e}}$. This is leading to low pressure lifts due to the high ω at low $T_{\text{ej,e}}$, which is related to a significant decrease of the work recovery by the ejectors in the analysed systems. On the one hand, this can be linked to the lower work recovery potential at lower $T_{\text{ej,e}}$ as found in the model. On the other hand, the system data evaluation shows also strongly decreasing work recovery efficiencies in the ejectors for low $T_{\text{ej,e}}$.
While the amount of recoverable work cannot be increased for fixed conditions, an improved ejector efficiency particularly at low entrainment temperatures would allow for a higher amount of recovered work. One option could be the adaption of the ejector design more specifically to the relevant conditions, i.e. to a higher mass entrainment ratio and low pressure lifts for the use at low $T_{\text{ej,e}}$.
Alternatively, the VPC system (with or without the HPV parallel to ejectors) offers possibly an interesting solution to decouple ω from the entrainment temperature $T_{\text{ej,e}}$ and using the available work recovery potential to operate the ejector at optimum conditions with a suitable ω and higher Δp_{lift} for energy savings in the parallel compressor, while compressing the remaining part of the evaporator mass flow in the main compressors. A techno-economic analysis would be required to analyse the additional investment for parallel ejectors here.

4.2 Liquid Ejector Results

4.2.1 Modelling Results

Figure 4.32 maps the increase in COP_2 in the LEJ system for an increase in T_{evap} by 3.7 K in parallel with the reduction of the superheat by 10 K to overfed conditions, based on the findings by Karampour and Sawalha [18]. It can be observed that the liquid ejector has a more significant improvement effect on the COP_2 for lower entrainment temperatures $T_{\text{ej,e}}$ under the used modelling assumptions. Furthermore, for low $T_{\text{ej,e}}$ a higher improvement by the ejector can be seen for lower discharge pressures p_{disc}.
The analysis of the LEJ and REF cycles for an example case in the log(p)-h-chart as shown in figure 3.5 can give a further understanding of the reason for this trend. As T_{evap} and thus also $p_{\text{comp,suc}}$ is increased by a fixed value in LEJ compared to REF independent of p_{disc}, the relative effect of this increase is decreasing for higher discharge pressures. Thus, as the effect of the achieved indirect pressure lift in LEJ is decreasing compared to the total compressor pressure ratio, the impact on the COP_2 is also decreasing.

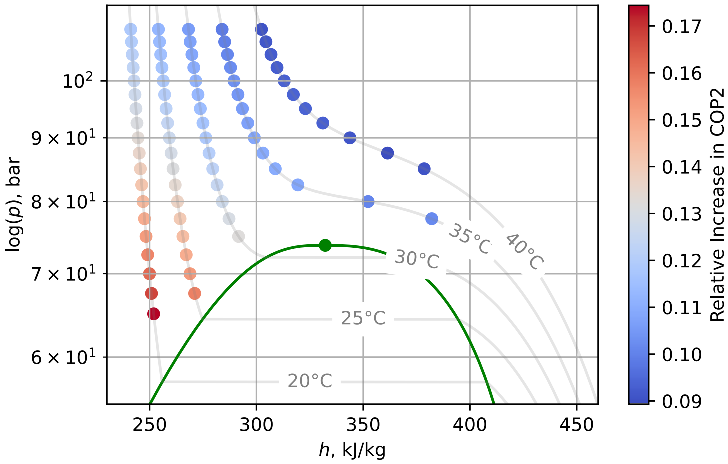

Figure 4.32: $Incr_{\mathrm{COP2}}$ in LEJ for varying entrainment conditions for 10 K superheat in the REF model and an evaporation temperature increase of 3.7 K

As the $Incr_{\mathrm{COP2}}$ is calculated for equal cooling capacity Q_2, it is directly related to a difference in compressor power consumption in the model. Figure 4.33 therefore shows the relative increases in the compressor mass flow and the compressor enthalpy difference, i.e. the two parameters which result in the compressor power as a product. The plot confirms the described trend of the reduced

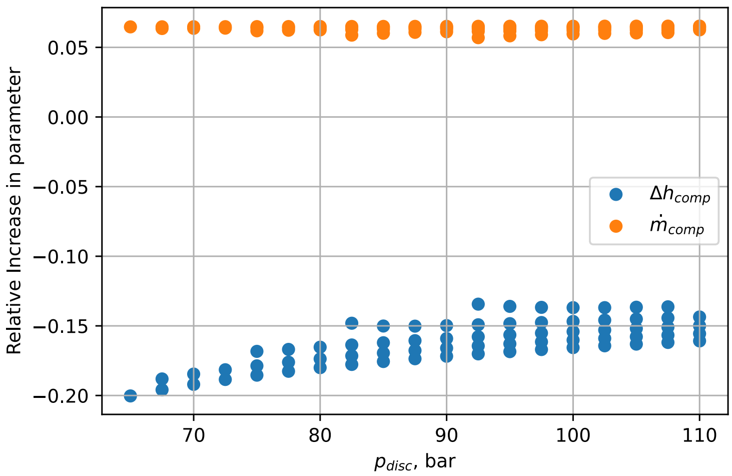

Figure 4.33: Comparison of the contribution of compressor enthalpy difference and mass flow to the increase in COP_2 in LEJ

impact of the fixed pressure lift, as the relative decrease of the enthalpy difference is reduced for higher discharge pressures. The mass flow in the compressor is found to be generally $6 - 7\,\%$ higher in the LEJ case compared to the REF case due to the reduced evaporator enthalpy difference in the LEJ case. This effect is counteracting the decrease in enthalpy difference, however only with about one third of the impact, as the figure indicates.
The trends found in figure 4.32 can also be seen in the direct plot of the increase in COP2 $Incr_{\mathrm{COP2}}$

over the discharge pressure p_{disc} in figure 4.34. The theoretical model shows efficiency improvements above 15 % for subcritical pressures and the modelled entrainment temperatures of 20 and 25 °C, but a clear decrease for higher pressures. For the two highest modelled entrainment temperatures of 35 and 40 °C, the model indicates that an optimal increase in COP_2 can be found for a certain optimal discharge pressure p_{disc}.

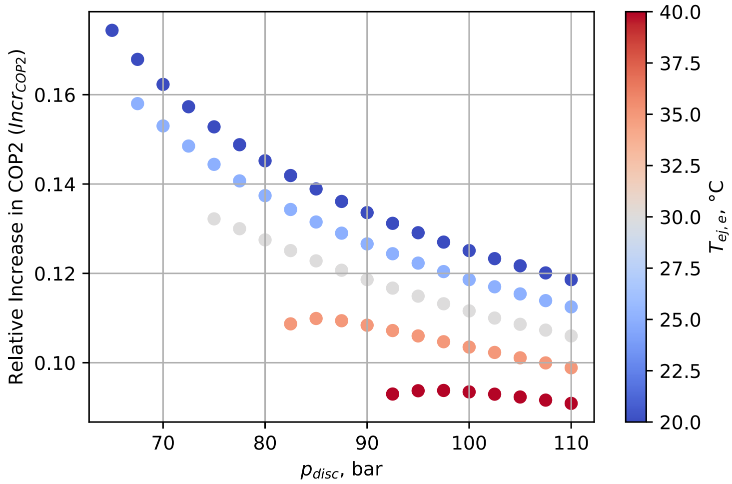

Figure 4.34: $Incr_{\text{COP2}}$ at varying entrainment conditions in LEJ (same data as in figure 4.32)

The plots of the actual COP_2 for the LEJ and the REF system in figure 4.35 show that high improvements from the liquid ejector correspond to high values for COP_2, in contrast to the trend seen for the VEJ model in section 4.1.1. In particular, the discharge pressures for optimal COP_2 for the two highest tested entrainment temperatures of 35 and 40 °C are in a similar pressure range as the respective discharge pressures for the highest $Incr_{\text{COP2}}$ here. In both cases, this optimum is likely related to the shape of the respective supercritical temperature profiles.

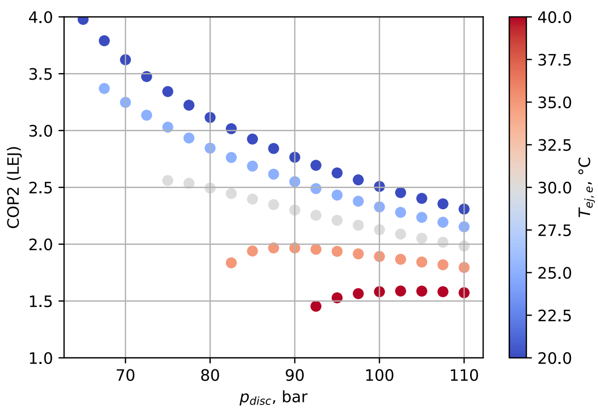

(a) COP_2 for LEJ system

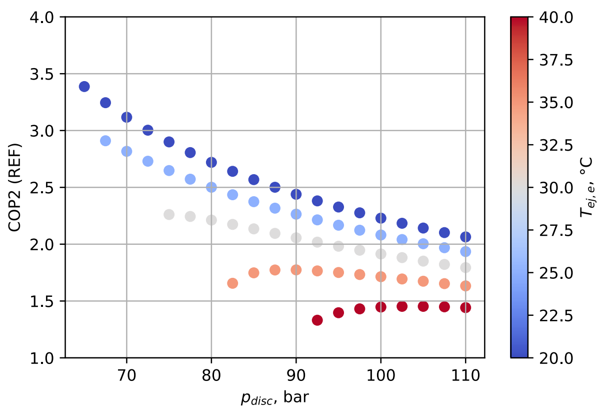

(b) COP_2 for REF system

Figure 4.35: Comparison of COP_2 for LEJ and REF at varying entrainment conditions for 10 K superheat in the REF model and an evaporation temperature increase of 3.7 K

From a mass flow perspective, the model data show that the mass flow from the liquid ejector into the HPrec is only 3 – 8 % of the total mass flow through the HPrec, generally with an increasing share for increasing p_{disc}. This confirms that the liquid ejector itself only plays a minor direct role in the LEJ system, compared to the direct effect of the vapor ejector.
Furthermore, for most of the modelled cases, 80 – 97 % of the liquid entering the LPrec comes from the evaporator, i.e. the remaining liquid mass flow coming from the flash gas expansion is found to be only a minor contributor to the liquid inflow into the LPrec. A deviation from this trend is found only for high temperatures and low pressures, as the flash gas mass flow increases substantially for these conditions. These cases are however unlikely to occur in reality due to suboptimal performance.

Regarding the high-pressure side and heat recovery, a more homogenous effect for the varying entrainment conditions can generally be seen in figure 4.36 compared to the effect of the vapor ejector. This is a consequence of the fixed increase in compressor suction pressure in the liquid

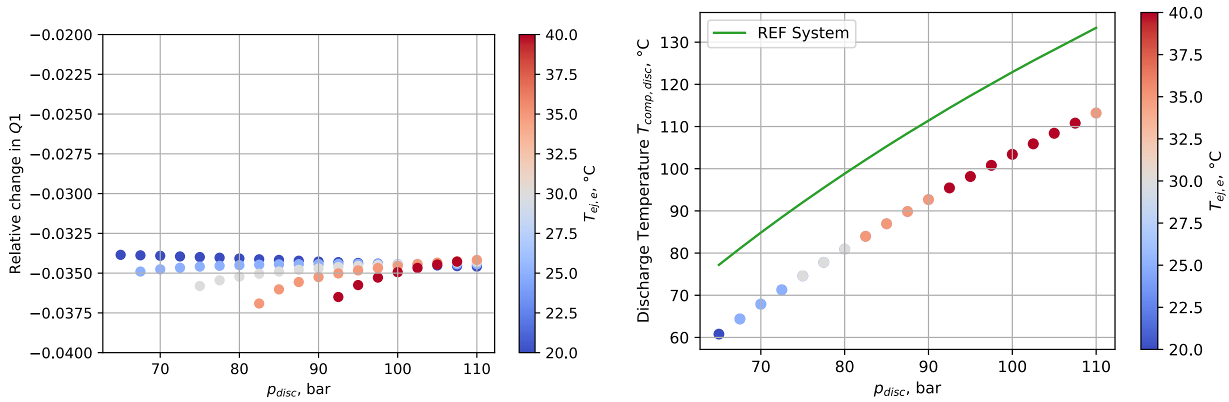

(a) Relative change in total high-pressure side capacity ($Incr_{Q1}$)

(b) $T_{\text{comp,disc}}$

Figure 4.36: Ejector effect on the discharge side in LEJ compared to REF at varying entrainment conditions for 10 K superheat in the REF model and an evaporation temperature increase of 3.7 K

ejector case in contrast to the varying pressure lift caused by the vapor ejector. The general trend of a lower Q_1 and a lower discharge pressure resulting from the reduced compressor capacity at equal Q_2 is however the same for both LEJ and VEJ cycle.
For the modelled LEJ cycle, Q_1 decreases by 3 – 4 %, while the compressor discharge temperature is generally found to be 14 – 20 K lower in the LEJ system compared to the REF system. The higher $T_{\text{comp,disc}}$ shown for the REF in figure 4.36 compared to $T_{\text{comp,disc}}$ in the corresponding plot for the VEJ system (figure 4.9) results from the modelled superheat of 10 K for the REF system in the here shown comparison to the LEJ system.

Model Sensitivity to Input Parameters

The sensitivity analysis for the input parameters shows that the $Incr_{\mathrm{COP2}}$ is generally most sensitive to a change in the evaporation temperature difference between LEJ and REF system, which is in line with expectations as the system improvement is directly affected by this difference. For an increase in the evaporation temperature difference by 10 % (equal to a 0.37 K higher difference), an increase of 9.6 – 12.4 % in $Incr_{\mathrm{COP2}}$ is found for the analysed conditions.
Another key assumption of the model is the evaporation temperature of the REF system. It should be noted that the difference between the evaporation temperatures of LEJ and REF is set as a fixed value, i.e. the evaporation temperature of the LEJ system is changed accordingly here. The increase of evaporation temperature of the REF system by 1 K results in an increased efficiency improvement $Incr_{\mathrm{COP2}}$ by 0.9 – 2.7 % for the evaluated cases. The sensitivity is nearly proportional to the actual $Incr_{\mathrm{COP2}}$, with the highest sensitivity at conditions with the highest $Incr_{\mathrm{COP2}}$.
The assumed value for the superheat in the REF system is found to have an effect of up to 4 % decrease in $Incr_{\mathrm{COP2}}$ for a 1 K increase in the superheat, particularly for conditions with high $T_{\mathrm{ej,e}}$ and low p_{disc}. As the superheat is set independently from the evaporation temperature in the theoretical model, an increase benefits the $COP_{2,\mathrm{ref}}$ as the evaporation enthalpy difference is increased.
No significant sensitivity of the results is found for the variation of the assumed vapor quality at the outlet of the overfed evaporator, i.e. the effect of a parameter change by 10 % resulted in a change of the output parameters several magnitudes below the respective actual output parameter values in the EES Model. Similarly, no significant sensitivity was found for the assumed liquid ejector mass entrainment ratio ω.
Similar to the VEJ case, the assumed compressor isentropic and motor efficiencies show a negligible effect on $Incr_{\mathrm{COP2}}$ if an equal efficiency is used for both the LEJ and the REF case. However, the effect on an efficiency variation of the COPs of the respective systems is found to be directly proportional to the change in efficiency, i.e. an efficiency change of 10 % equally changes the respective COP by 10 %.

4.2.2 Field Data Evaluation

Evaluation of System LEJ-A

The analysis of the MT cabinets for the first week in April 2021 is carried out based on the CO2 and air inlet and outlet temperatures in the individual cabinets of supermarket system LEJ-A. Figure 4.37 shows the weekly mean values of these four temperatures for each MT cabinet. The measured T_{evap} indicates that the cabinets have only small differences in the mean evaporation temperature, which corresponds to the expectations due to the fact that all evaporator outlets are connected to the same MT return line in the refrigeration unit. The mean evaporation temperature over the whole week for all cabinets is found to be −4.6 °C.
An unexpected result is that the measured evaporator CO2 outlet temperature $T_{\mathrm{evap,out}}$ is found to be higher than the measured air temperatures $T_{\mathrm{air,in}}$ and $T_{\mathrm{air,out}}$ in some of the cabinets. Furthermore, the mean air outlet temperature $T_{\mathrm{air,out}}$ is measured to be higher than the mean air inlet

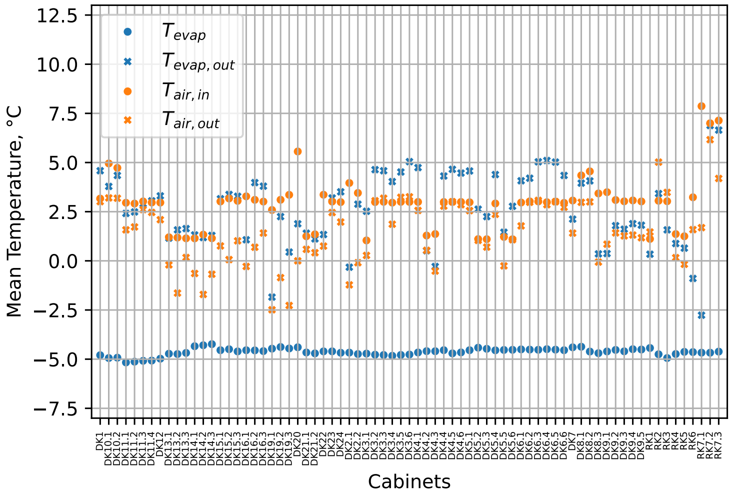

Figure 4.37: Mean CO2 and air inlet and outlet temperatures in the evaporator for each cabinet in LEJ-A

temperature $T_{\text{air,in}}$ measurement in a number of these cabinets. In theory, this would correspond to an increase in air temperature in these cabinets and thus a net heating effect, which is not realistic and therefore likely a measurement error. While the cabinets for which this effect is found thus require a more thorough check of the temperature sensors, which is a potential limitation of the following results.

A more detailed analysis of the air temperatures in the individual cabinets for the analysed week is shown in figure 4.38, where the mean temperatures are indicated as dots for each cabinet, while the range of occurring values (minimum to maximum) is indicated as line. Figure 4.38a shows that the

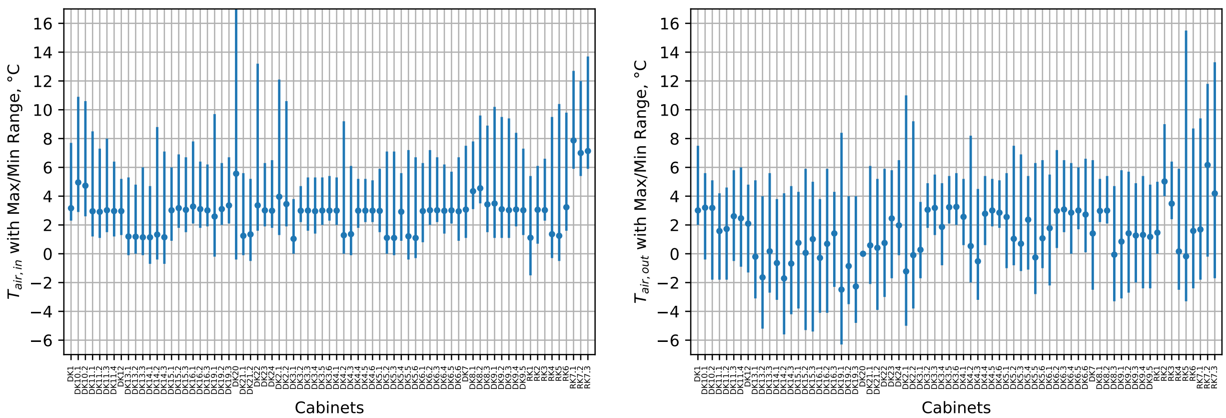

(a) $T_{\text{air,in}}$ (b) $T_{\text{air,out}}$

Figure 4.38: Air inlet and outlet mean temperatures with Max/Min range for each cabinet in LEJ-A

air inlet temperature $T_{\text{air,in}}$ for the majority of the cabinets is at either 1, 3 or 5 °C, which confirms

an information from the manufacturer that most cabinets are controlled based on this parameter. The setpoint for this temperature is one of these three temperature levels in most cabinets, depending on the food type stored in the respective cabinet.
Figure 4.38b indicates that the air outlet temperature $T_{\text{air,out}}$ is varying more significantly between the different cabinets compared to $T_{\text{air,in}}$, showing mean temperature of less than $-2\,°\text{C}$ for the cabinets DK19.1 and DK19.3 and minimum temperatures down to $-6\,°\text{C}$ for cabinet DK19.1.

Figure 4.39a gives an overview of the mean superheat in all cabinets during the first week of April 2021, with the range between the maximum and minimum value indicated as lines. While the mean superheat in the cabinets is in the range between 2 and 12 K, it can be seen that the majority of the cabinets also achieves low superheat of less than 1 K.

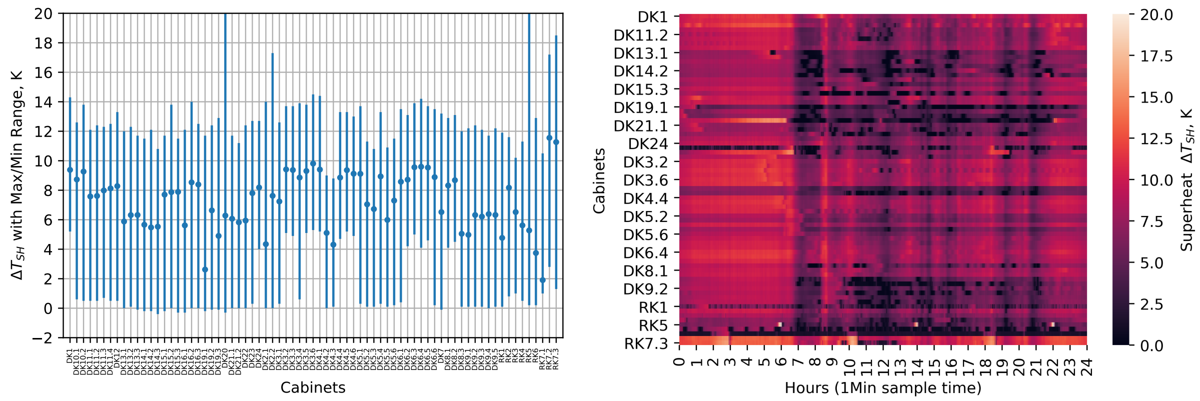

(a) Mean $\Delta T_{\text{SH,evap}}$ with Max/Min Range (b) $\Delta T_{\text{SH,evap}}$ for one day, all cabinets

Figure 4.39: Superheat $\Delta T_{\text{SH,evap}}$ for each cabinet in LEJ-A (the heatmap covers also the cabinets which are not explicitly indicated on the y-axis)

Over the first analysed day, a common pattern can be observed for many cabinets as shown in in the heat map in figure 4.39b, with a decrease in superheat around 07:00 and a re-increase after 22:00, which corresponds to the opening times of the store.

As an upper limit for T_{evap} in order to achieve the intended heat exchange, the air outlet temperature $T_{\text{air,out}}$ from the evaporator is of particular interest. Therefore, the temperature profile over a one-day time period of the temperatures in cabinet DK19.1 with the lowest mean air outlet temperature is shown in figure 4.40. The figure indicates that the evaporator outlet temperature difference between $T_{\text{air,out}}$ and T_{evap} is in the range of 2 – 4 K before 07:00, but mostly smaller with partly almost no temperature difference later during the day. With the current control strategy, a further increase in evaporation temperature T_{evap} does not seem possible in this cabinet after 07:00, as the evaporation temperature T_{evap} needs to be below the air outlet temperature $T_{\text{air,out}}$ in order to provide cooling to the air.
Regarding the superheat which is found in figure 4.40 as the difference between $T_{\text{evap,out}}$ and T_{evap}, the cabinet temperatures in DK19.1 indicate a fluctuating superheat with values from no superheat up to 10 K. A comparable pattern is also found for the cabinets DK19.2 and DK19.3 with similar low $T_{\text{air,out}}$. While this indicates that there would be further potential for a higher T_{evap} with regard

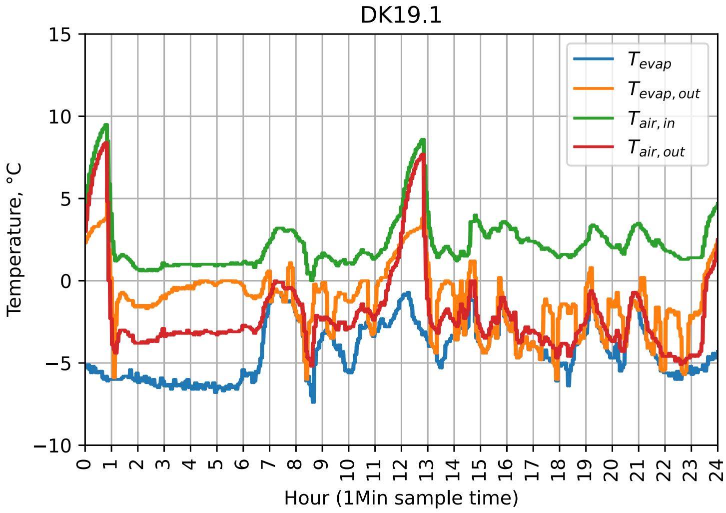

Figure 4.40: Temperatures in the evaporator for 1 day in cabinet DK19.1 in LEJ-A

to a possible further reduction of the superheat in these cabinets, it appears that in fact the low $T_{\mathrm{air,out}}$ is limiting for a further increase in T_{evap} here.
A possible reason for the low $T_{\mathrm{air,out}}$ could be a high cooling demand in the concerned cabinets, which would be difficult to change. Månsson et al. [39] suggest another possible cause for low $T_{\mathrm{air,out}}$. According to the study, a temperature gradient field occurs close to the cabinet wall in the region of the return air sensor, caused by the warmer ambient air in front of the cabinet doors. An unsuitable placement of the return air temperature sensor (measuring $T_{\mathrm{air,in}}$) close to the cabinet wall within this temperature gradient therefore results in too high temperature measurements. This results in turn in an over-estimation of the cooling demand, likely causing the cabinet control to decrease the supply air temperature into the cabinet $T_{\mathrm{air,out}}$.
An additional possible limitation for a further decrease of the superheat during the time periods with remaining high superheat, the dimensioning of the expansion valves at the evaporator inlets are analysed, as the valve sizes limit the maximum mass flow into the cabinets and thus also the possibility for flooding in the individual evaporators. For system VEJ-A, it is found that the mean opening degree of the valves is at about 60 % at the highest for some cabinets, making it unlikely that this is a limiting factor for the overfed evaporation in LEJ-A.

On a refrigeration unit perspective, the superheat from the individual cabinets results in a combined total superheat in the MT return line. The temperature in this common return line is measured with a separate temperature sensor before the mixing with the refrigerant flow from the flash gas valve in system LEJ-A. For the evaluated time period, a recurring pattern is found for the superheat at this point, which is indicated in figure 4.41 for 3 days and generally corresponds to the superheat pattern in the individual cabinets shown in figure 4.39b. In relation to the pattern in the superheat, higher liquid levels ("LL" in the figure) are found in the LPrec during timer periods with very low superheat of close to 0 K. Furthermore, the liquid ejector EJ1 is operating during these time periods. In contrast, the other liquid ejectors 2 and 3 in the system are not found to be used.
Plotting the LPrec liquid level over the total superheat as in figure 4.42 shows that high liquid

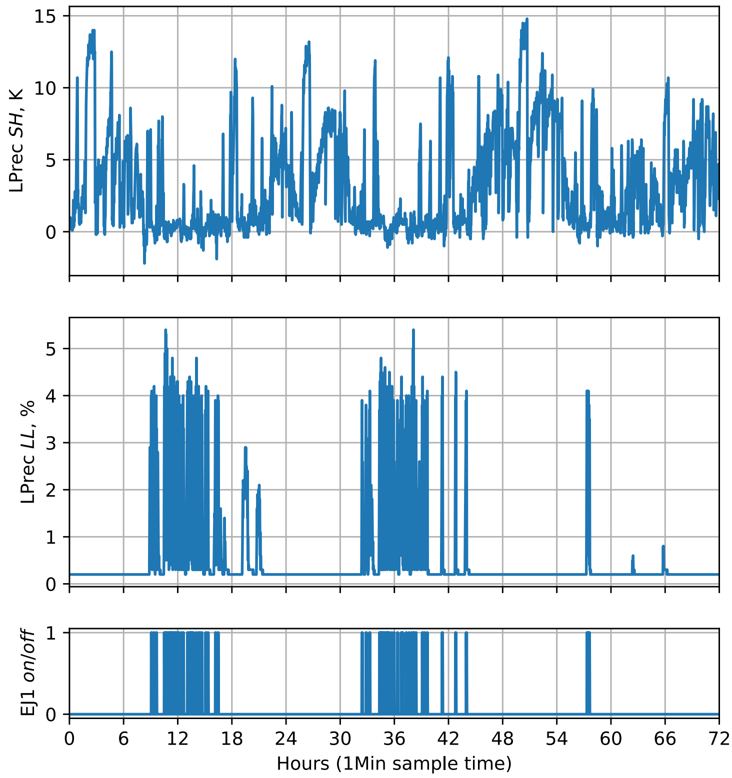

Figure 4.41: Superheat at LPrec inlet and LPrec liquid level for 3 days in LEJ-A

levels occur mostly at a superheat of less than 1.5 K. It can also be observed that the ejector EJ1 operates mostly above a liquid level of 4 % in the LPrec. Only in a few cases does the ejector also operate at lower liquid levels, which is probably due to a time delay fixed in the control system to avoid unstable operating conditions. The ejector has no specific control option, i.e. it is either turned on or off, with the threshold for switching the ejector on likely at 4 % liquid level in this system.

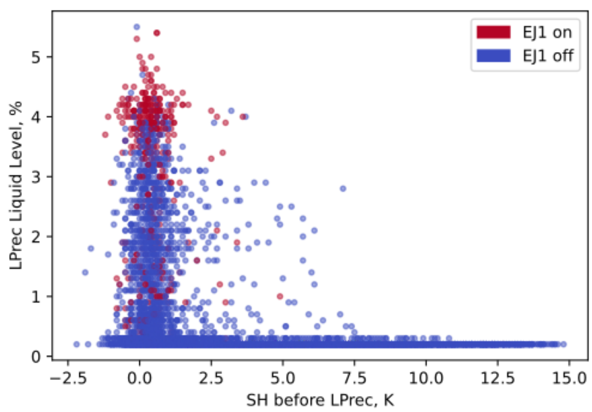

Figure 4.42: LPrec liquid level over total superheat with indicated activity of ejector EJ1 in LEJ-A

Apart from the overfed evaporation, the flash gas flow is to be considered as possible other source of liquid in the receiver, as the shape of the vapor dome for CO2 leads to a small amount of liquid as a result from the flash gas valve expansion process, as visualized in figure 4.43.

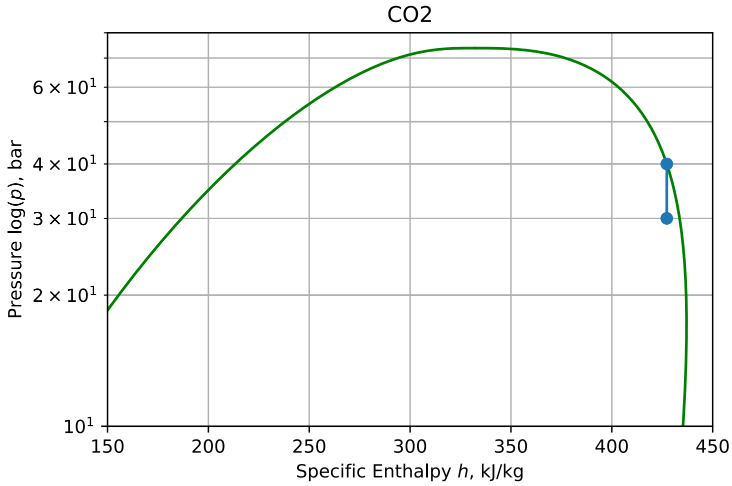

Figure 4.43: The vapor dome for CO2 in the log(p)-h-chart with an example flash gas valve expansion process indicated in blue

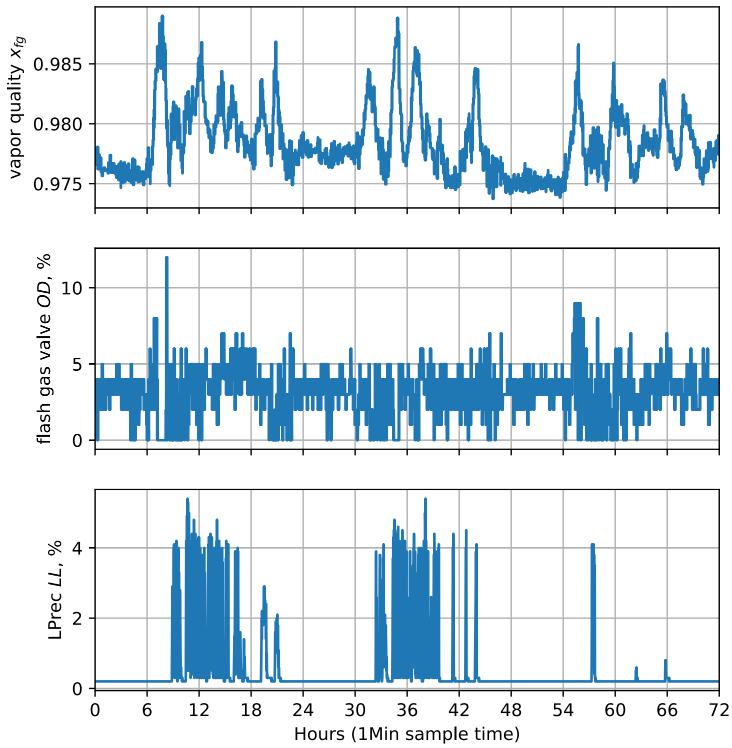

Figure 4.44: Flash gas vapor quality and valve opening, with LPrec liquid level for 3 days in LEJ-A

When analysing the vapor quality x_{fg} of the refrigerant flow expanded in the flash gas valve, it can be observed in figure 4.44 that the vapor quality is in the range of $0.97 - 0.99$. Thus a small amount of liquid is likely also entering the LPrec in this way. When comparing to figure 4.41, it can be noticed that the vapor quality is generally high when the superheat is low and vice versa. This results from the fact that low superheat is corresponding to high evaporation temperatures and thus a lower pressure difference between the pressures in the HPrec and the LPrec, as the pressure in the HPrec is comparatively stable.
While some liquid is thus generated in the flash gas expansion process, no clear correlation between the opening degree (OD) of the flash gas valve and the liquid level in the LPrec can be observed as figure 4.44 shows. In combination with the modelling findings that the liquid flow caused by the flash gas flow is generally low compared to the liquid from the overfed evaporators, it is likely that the liquid seen in the LPrec is mostly a result of overfed evaporation in the cabinets.

Evaluation of System LEJ-B

The analysis of the supermarket system LEJ-B is done in parallel for the two analysed time periods in order to get a direct comparison of the situation before and after the change of control to lower superheat in October 2020. All analysed parameters are therefore shown for both analysed cases in August and November 2020.
The control change seen in the system is achieved by decreasing the measured evaporation pressure p_{evap} in the system control by $2 - 3$ bar. The exact difference is unfortunately not known at the point of this study, thus the plotted evaporation temperatures for November in the following figures are not the real values but the values resulting from this adaption. The real evaporation temperature for November is expected to be $2 - 3.5$ K higher than the indicated values in the data. This also affects the superheat, which is thus decreased by this difference in reality for November.

Comparing the mean temperatures for CO2 and air inlet and outlet in the cabinets in figure 4.45, it can be seen that the mean air temperatures and the evaporator outlet temperature $T_{evap,out}$ are in a similar temperature range for both August and November. The evaporation temperature is in contrast clearly higher in November as intended by the control change, with an average increase in the range of $4.9 - 6.4$ K from an average value of $-6.4\,°C$ in August, likely to a range between $-1.5\,°C$ and $0\,°C$ in November. The mean evaporation temperature found in system LEJ-A for April of $-4.6\,°C$ is thus between these two values. The comparability is though limited due to the different evaluated season.
The data also show that the cabinets DK9A, DK9B and DK9C have an evaporation temperature which is about 1 K below the evaporation temperature in the majority of the cabinets in both August and November. Furthermore, a higher evaporation temperature than in the majority of the cabinets can be seen for the RK2.2, RK6 and RK7, which are possibly separately controlled cold rooms.

While the control change between August and November is aiming at an increase in T_{evap}, it is important to ensure that the system is still able to provide sufficient cooling in the cabinets, i.e. maintain the air temperatures required in the individual cabinets depending on the load and the type of stored food. Figure 4.46 therefore shows a more detailed analysis of the mean air inlet and outlet temperatures (indicated as dot) with the total range of occurring temperatures (indicated as

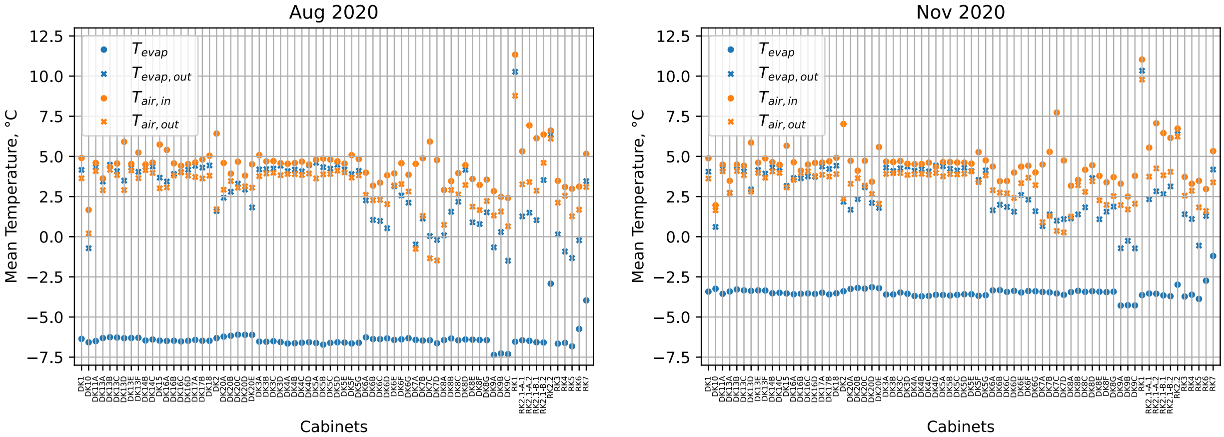

(a) First week of August 2020

(b) First week of November 2020 (T_{evap} *probably higher*)

Figure 4.45: Mean CO2 and air inlet and outlet temperatures in the evaporator for each cabinet in LEJ-B

line) in each cabinet over the respective analysed time period of one week.
From the figures 4.46a and 4.46b, almost no difference between August and November can be found for the mean values of air inlet temperatures $T_{\text{air,in}}$ as well as for the maximum/minimum range in which it occurs.
The air outlet temperatures $T_{\text{air,out}}$ are also generally similar for the majority of the cabinets in both cases as shown in figures 4.46c and 4.46d. However, it can be observed that a few cabinets have higher mean and higher minimum air outlet temperatures. This is the case for the cabinets DK7A, DK7B and DK7B, which show mean values below 0 °C in August, but positive mean values between 0 and 2 °C in November, likely caused by a reduction of the load in these cabinets. In general, this leads to a more equal load distribution in the cabinets.

An evaluation of the mean superheat with occuring range is shown in figure 4.47. It is clearly visible that the intended reduction of the superheat from August to November is achieved, even despite the fact that the here indicated superheat for November is suspected to be 2 – 3.5 °C above the real values due to the control adaption described above. With this knowledge, it is very likely that overfed conditions are reached for the majority of the cabinets in November. The mean superheat is suspected to be in a range of about 1 – 5 K for November, indicating that at least some of the cabinets achieve overfed conditions only part of the time.
In comparison to November, August has a significantly higher superheat with mean values in the range of 6 – 12 K and a minimum superheat of 1 K in part of the cabinets, while other cabinets show continuous high superheat, even with high minimal values.

Figure 4.48 shows the effect of the superheat on the liquid level for the time period of one day for August and November, with a similar pattern occuring in the following days. The heat map for August indicates a higher superheat (indicated by brighter colors) in a number of cabinets between about 00:00 and 07:00 compared to the time between 07:00 and 00:00 which roughly corresponds

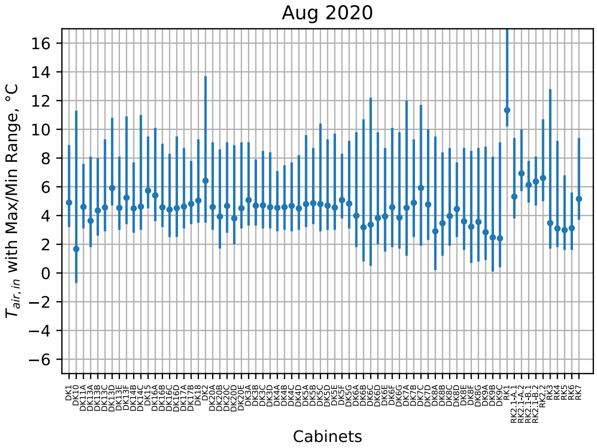

(a) $T_{\text{air,in}}$, August 2020

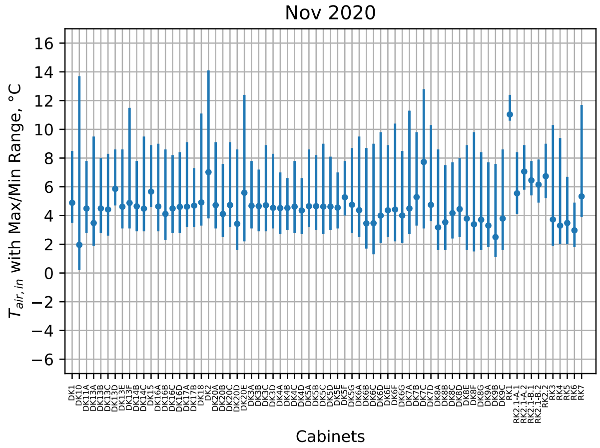

(b) $T_{\text{air,in}}$, November 2020

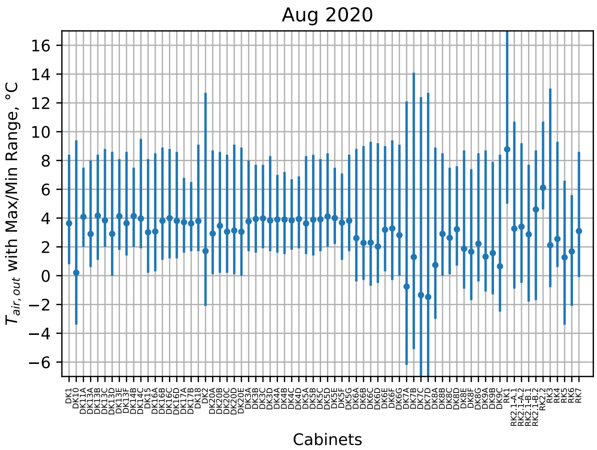

(c) $T_{\text{air,out}}$, August 2020

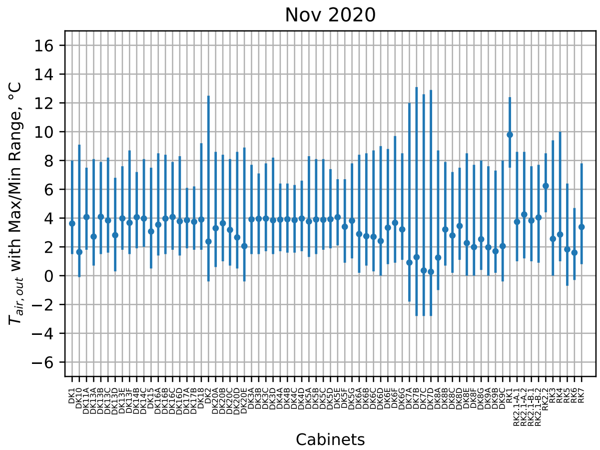

(d) $T_{\text{air,out}}$, November 2020

Figure 4.46: Air inlet and outlet mean temperatures with Max/Min range for each cabinet in LEJ-B

to the opening hours of the supermarket. In a similar way, the liquid level in the LPrec in August is found to start increasing at 07:00 from a level around 5 – 5.5 % liquid level to a level above 5.5 %, which is kept throughout the day, before decreasing back to the previous value between 20:00 and 00:00 of the following day.
For November, the generally lower superheat appears in contrast to be relatively stable, without clear differences between night and daytime operation. Similarly, a relatively stable liquid level, is found for the LPrec, however generally on a higher level than in August.
Despite the high superheat in August, a general correlation between the superheat and the liquid level therefore appears to exist in the system.

Figure 4.49 shows the ejector operation of ejectors EJ1-3 in response to the described liquid level in the LPrec for a time period of three days. A clear ejector operation based on the thresholds set in the system is found for both August and November. The threshold values obtained from the data logging system state that EJ1 is turned on if the liquid level is increasing above 5 % in the LPrec.

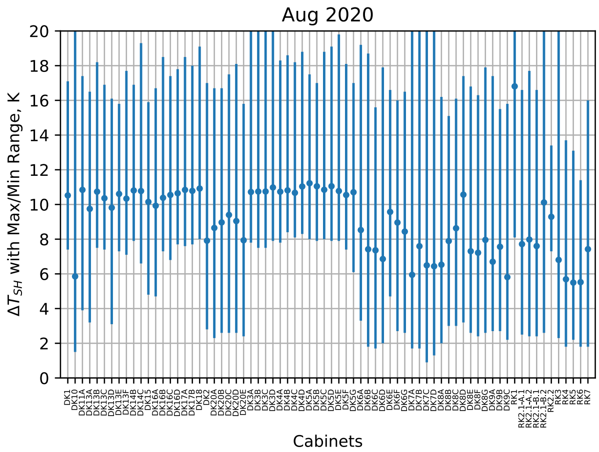

(a) First week of August 2020

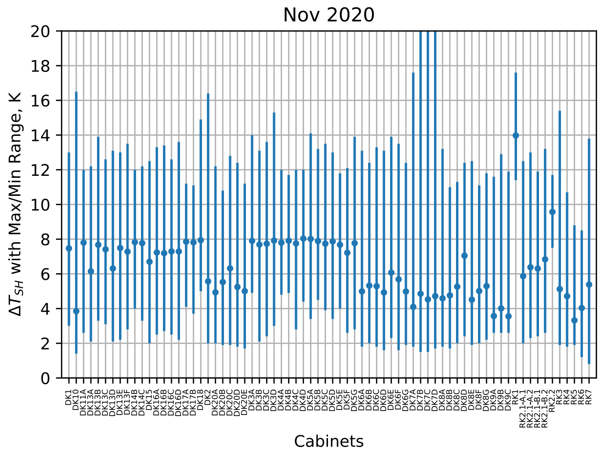

(b) First week of November 2020 ($\Delta T_{\mathrm{SH,evap}}$ *probably lower*)

Figure 4.47: Mean Superheat with Max/Min Range for each cabinet in LEJ-B

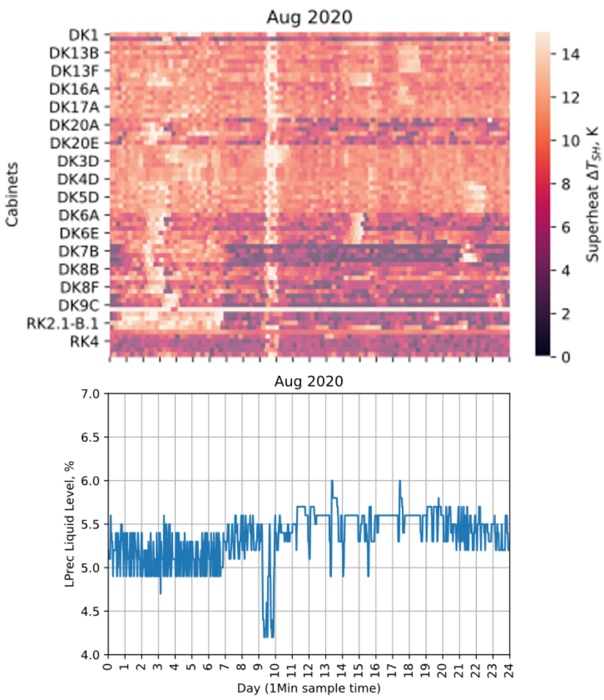

(a) First week of August 2020

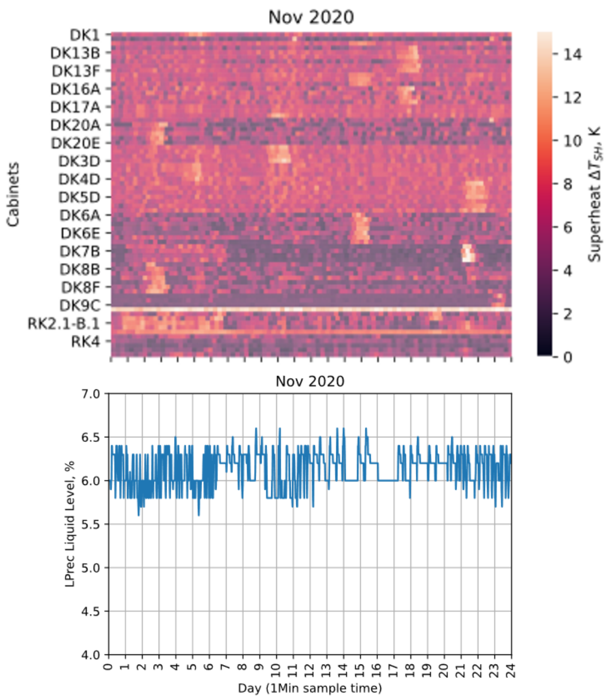

(b) First week of November 2020 ($\Delta T_{\mathrm{SH,evap}}$ *probably lower*)

Figure 4.48: Superheat in each cabinet for one day (heat maps) and LPrec liquid level in LEJ-B

In the August case with liquid levels around this threshold, EJ1 is thus almost always the only used ejector, as the case in the illustrated time period. It is found to operate about 88 % of the time here. In contrast, the higher liquid level in November is causing EJ1 to operate constantly, while EJ2 is

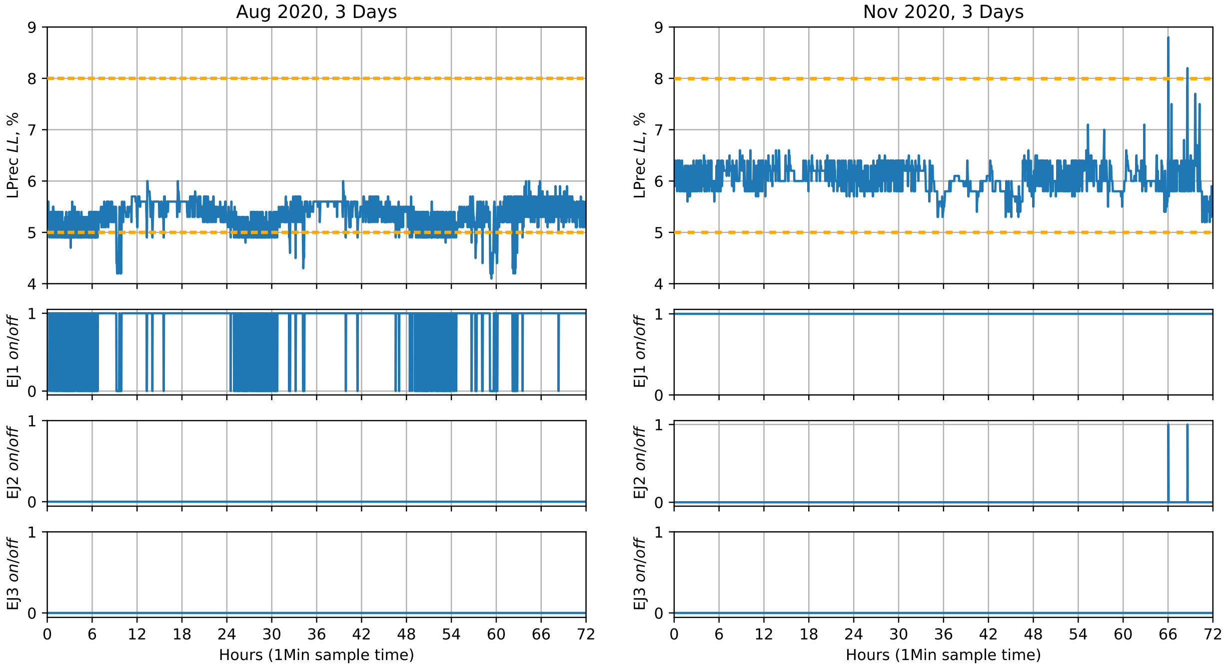

(a) First week of August 2020

(b) First week of November 2020

Figure 4.49: LPrec liquid level and ejector operation in LEJ-B

used in a few occasions when the liquid level of 8 % is crossed in the LPrec. The threshold of 13 % for EJ3 is found to be only very occasionally reached in the November case.
Based on these operational findings, the ejector block appears in fact over-dimensioned, even for the case of November. It seems likely that the rare occurrences of liquid levels above 8 % for short time periods could have been handled by EJ1 when allowing for a higher increase in the LPrec liquid level for these short time periods, which appears feasible due to the generally low liquid levels at which the receiver is kept.

Particularly for the case of August, it is of interest to analyse the flash gas expansion process as possible source for the liquid arriving in the receiver as described for system LEJ-A. The vapor quality at the flash gas outlet x_{fg} and flash gas valve opening degree are therefore shown together with the LPrec liquid level in figure 4.50, respectively for a time period of three days.
The data for November show high vapor qualities due to the increased evaporation temperature and comparatively low flash gas valve opening degrees of mostly below 20 %, indicating no significant or only a minor effect of the flash gas valve expansion on the liquid level in the receiver based on the modelling findings, similar to the case in LEJ-A.
In contrast, significant increases in the flash gas valve opening degree with openings between 25 and 40 % over a time period of several hours are found for the August case in parallel to the time periods of increasing liquid level. Furthermore, the vapor quality is at a slightly lower level of around 0.975 compared to the November case.
These trends for August together with the superheat which shows non-overfed conditions for August indicate possibly a relevant impact of the liquid created during the flash gas expansion process

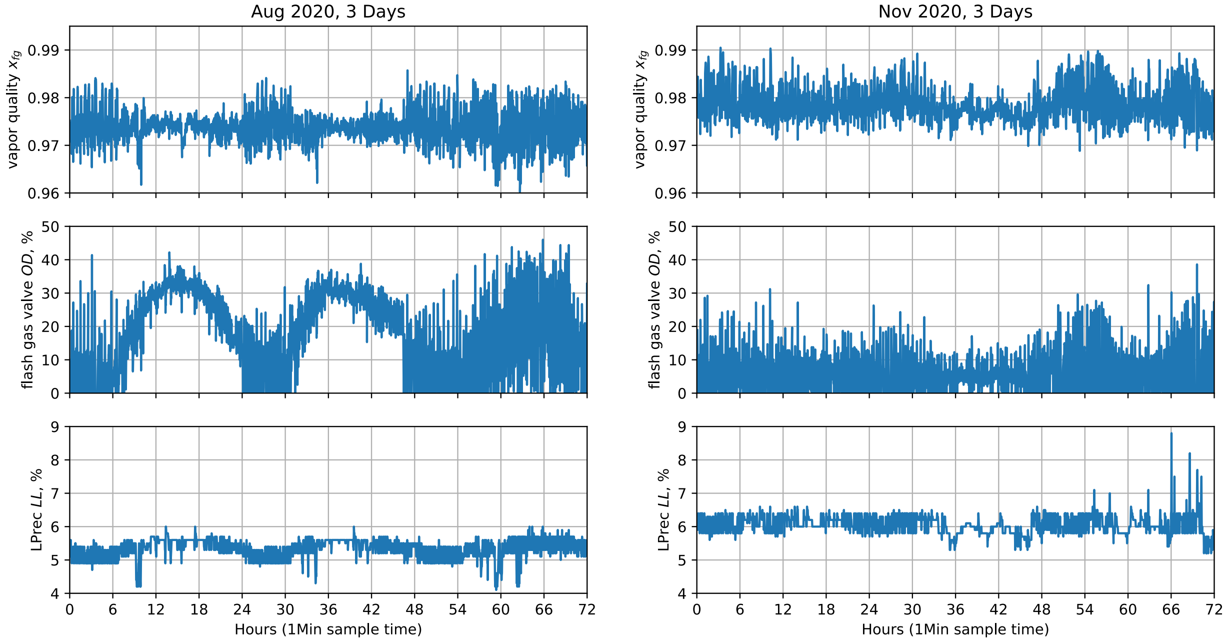

(a) First week of August 2020

(b) First week of November 2020

Figure 4.50: Flash gas vapor quality and valve opening, with LPrec liquid level for 3 days in LEJ-B

on the LPrec liquid level. At the same time, the superheat is suspected to still play an indirect role in the liquid level, as the evaporator return and the flash gas mass flow are mixed before the liquid receiver, which is suspected to evaporate small amounts of liquid in the flash gas mass flow during time periods of high superheat. The lower superheat in a number of cabinets during the daytime operation in August can therefore be assumed to contribute indirectly to the appearance of the flash gas liquid in the LPrec liquid level.

To analyse possible limitations for a further increase of the evaporation temperature, two cabinets of particular interest are analysed in more detail for one day.
As one of the cabinets with the lowest $T_{\text{air,out}}$, cabinet DK7D is analysed in figure 4.51 due to the direct limitation of the evaporation temperature by this temperature as explained in section 4.2.2. The cabinet belongs to the group of cabinets showing a very low $T_{\text{air,out}}$ in August, as found in figure 4.46c. With an evaporator outlet temperature difference of $3-5$ K in August for most of the daytime period, this is possibly an upper limit for the evaporation temperature in this case, as the cabinets appear to be controlled for a small amount of superheat.
For the November case, the measured superheat is again found to be $3-5$ K, however, the actual evaporation temperature is probably higher due to the control adaption. This decreases the evaporator outlet temperature difference between $T_{\text{air,out}}$ and T_{evap} to a very small temperature difference. In fact, the evaporation temperature in November is even higher than $T_{\text{air,out}}$ seen in the August case for a in a number of cases, showing that the reduced load in these specific cabinets likely contributes to the possibility for high evaporation temperatures in the November case.

Regarding the evaporator expansion valve opening, a general analysis indicates high openings

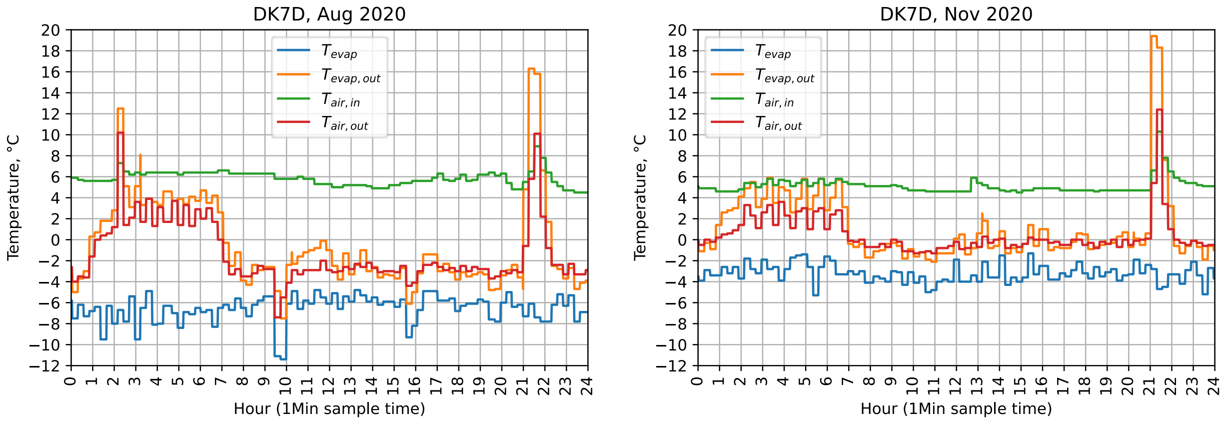

(a) First week of August 2020

(b) First week of November 2020 (T_{evap} *probably higher*)

Figure 4.51: Evaporator temperatures for cabinet DK7D in LEJ-B

for a number of cabinets in November, particularly for cabinet DK9A. The opening degree of the expansion valve at the inlet of this cabinet is therefore shown in figure 4.52. For the case of

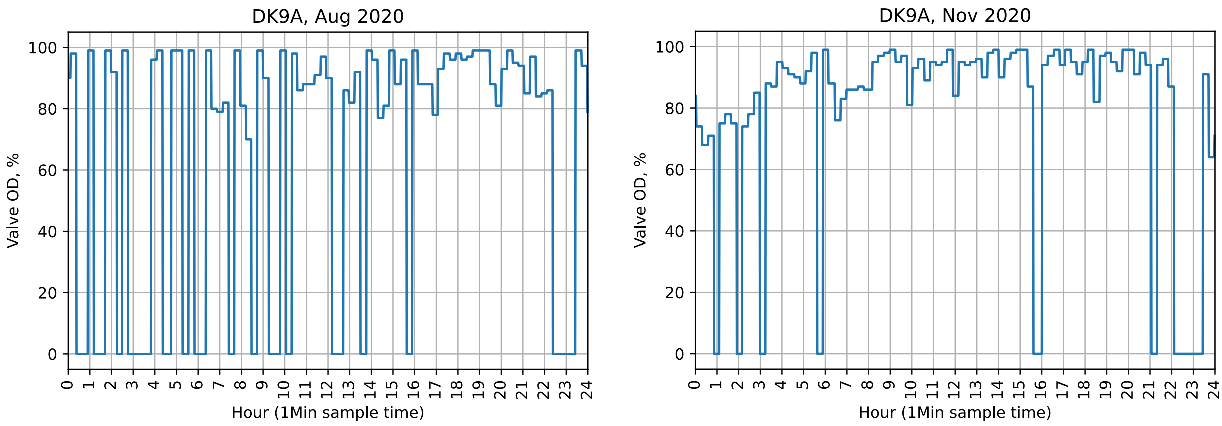

(a) First week of August 2020

(b) First week of November 2020

Figure 4.52: Evaporator expansion valve opening degree for cabinet DK9A in LEJ-B

November, it can be seen that the expansion valve is operating at opening degrees close to 100 % for most of the time during the analysed day. Even for the case of August, the expansion valve in this cabinet is found to be close to 100 % opening for an extended time period between 07:00 and 22:00 in the plot, indicating that larger expansion valves in the cabinets should be considered for overfed conditions to avoid limitations by the maximum flow rate of the valves.

In total, the modelling findings indicate that the liquid ejector is an efficient option to improve the system performance, with particularly high relative performance increases achieved for low

discharge pressures and gas cooler outlet temperatures.
In contrast to the direct impact of the entrainment conditions on the ejector efficiency and operation seen in the vapor ejector case, the performance improvement in the liquid ejector system is less dependent on these conditions, with a stable operation of the liquid ejectors in the removal of liquid from the LPrec found for the analysed field systems.
The actual evaporation conditions in the analysed supermarket systems shows a mixed picture. A substantially higher superheat is found to be achieved in system LEJ-B after a change in control, while system LEJ-A shows an intermediate evaporation temperature in-between the two cases of LEJ-B. Overfed conditions are reached in a number of cabinets temporarily, but higher mean superheat values remain in all systems despite the aim of overfed conditions, indicating possible space for further improvement.
A particular limitation regarding a further increase of the evaporation temperature is seen from the required air supply temperature in the cabinets, possibly resulting from the cabinet load, the system control or from the sensor placement. In addition, the size of the evaporator expansion valve in individual cabinets can be a limiting factor for overfed conditions if designed not sufficiently large to provide the required mass flow into the evaporator.

4.3 Comparison of the Modelling Results for VEJ and LEJ System

Figure 4.53 shows the results of a performance comparison of the VEJ and LEJ system under different entrainment conditions, indicating whether the VEJ or LEJ system provides higher performance for the respective condition.
The colors in the plot indicate which system (VEJ or LEJ) performs better for the respective condition. As factor with significant impact and strong variation in the field data evaluation, η_{ej} is set to three different levels in VEJ. Naturally, conditions which show better improvements from the VEJ system at low η_{ej} are showing even higher performance for higher η_{ej}. For instance, the cases in which VEJ is found to show higher performance improvements than LEJ at $\eta_{ej} = 0.1$ also show higher performance improvements in VEJ than LEJ for ejector efficiencies for the cases of $\eta_{ej} = 0.2$ or 0.3.
The comparison is made for equal conditions of $T_{evap} = 8\,°C$ and 10 K superheat in the evaporator, which is though changed in the LEJ system case due to the increase in T_{evap} in accordance with the previously mentioned specific modelling assumptions.
While the evaluation is not necessarily representative for all cases, it clearly indicates preferable conditions for LEJ systems at low p_{disc} and particularly low $T_{ej,e}$. High entrainment temperatures $T_{ej,e}$ are in contrast found to be preferable conditions for the VEJ system with substantial performance improvements compared to the REF system, while only small improvements are found from the LEJ system in these conditions as indicated in the separate modelling section.

Based on the findings for the LEJ model showing that only a small amount of the compressor mass flow is actually used as entrainment mass flow in the liquid ejector, it can also be concluded that

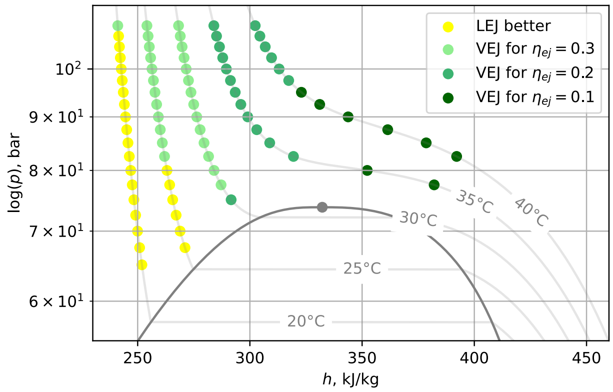

Figure 4.53: Comparison of VEJ and LEJ system for equal system conditions at three different η_{ej} in VEJ

vapor and liquid ejectors likely complement each other in an efficient way, which is in line with research on multi-ejectors combining liquid and vapor ejector elements [16][3].

Comparison for Equal Cooling and Equal Heating Capacity

The previous comparison between the different system cases and the REF system focused on the refrigeration system and the possible efficiency increase $Incr_{\mathrm{COP2}}$, which comes with the assumption that a reduction of the available heat on the discharge side is not relevant for the system. As explained in section 3.2.4, the amount of recoverable heat in the system is however important in systems with higher heating demand than the recoverable heat from the system, requiring an increase in auxiliary heating in the considered case of a compressor power reduction by the ejector in VEJ. Instead of reducing the compressor and heating power, the work recovered by the ejector might instead be used in a different way in the system to improve the overall performance.
Two possible benefits of the ejector in the VEJ and LEJ system for the cases of equal cooling *and* equal heating capacity Q_1 and thus naturally also equal COPs and P_{comp} are illustrated for an example case in figure 4.54 with fixed conditions in REF.
The cases are modelled for $-8\,°\mathrm{C}$ and $10\,\mathrm{K}$ superheat in VEJ and REF, while the previously described modelling assumptions are used for all other input parameters, particularly a fixed ejector efficiency, fixed compressor efficiencies and no IHX. As a result, a COP_2 of 3.4 is calculated for all shown cases. It can be seen that the vapor ejector outlet pressure in VEJ and the evaporation pressure achieved in LEJ are on a similar level for the example case.
Figure 4.54a indicates that the VEJ and LEJ systems can possibly benefit from the ejectors by providing heat for heat recovery at a higher p_{disc} compared to the reference system while consuming an equal amount of compressor power. For the shown example case of $p_{\mathrm{disc}} = 80\,\mathrm{bar}$ in the REF system, p_{disc} is found to be about 10 bar higher in VEJ and about 11.5 bar higher in LEJ at fixed $T_{\mathrm{gc,out}} = 20\,°\mathrm{C}$. Possible benefits are the shift of the available heating capacity to slightly higher temperature levels, while the total temperature range remains similar. Furthermore, an improved system control is possibly expected from the higher pressure based on previous experience

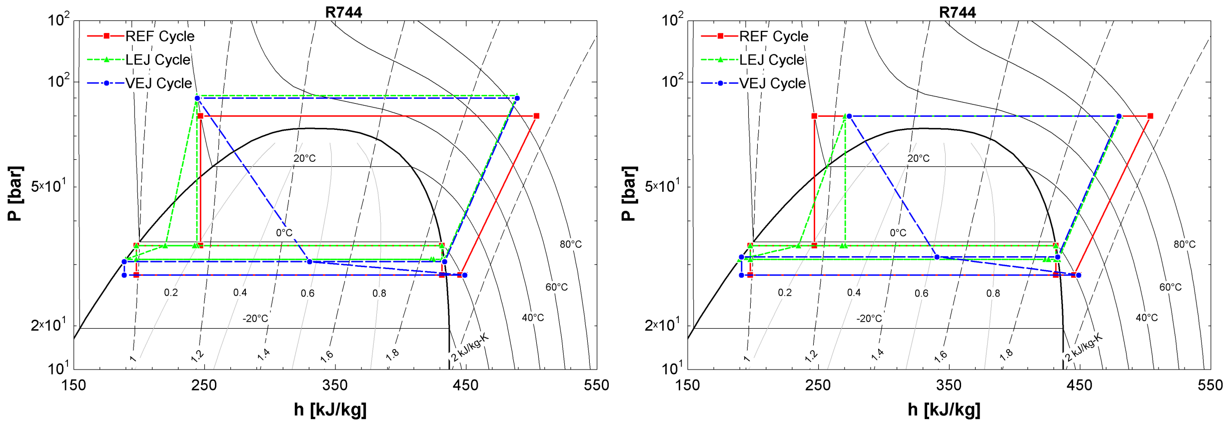

(a) Increasing p_{disc} (b) Increasing $T_{\text{gc,out}}$

Figure 4.54: Possible system benefits for equal COP_2 and Q_1

with the heat recovery control.
Alternatively, for a fixed $p_{\text{disc}} = 80\,\text{bar}$, the gas cooler outlet temperature $T_{\text{gc,out}}$ could possibly be increased as figure 4.54b indicates. Compared to $T_{\text{gc,out}} = 20\,°\text{C}$ in REF, an increase of $T_{\text{gc,out}}$ by 7.8 K in VEJ and by 7 K in LEJ is found from the model. This could for example allow for higher return temperatures in a connected heating system while providing the same amount of heat, which can have a beneficial effect for the heating system control. It should however be noted that the discharge temperature $T_{\text{comp,disc}}$ is also decreased, as generally seen in the ejector systems due to the higher compressor suction pressures, making this adaption particularly interesting if a smaller temperature range at equal heating capacity is suitable, as generally for space heating applications.

5 Conclusions

The installation of two vapor and two liquid ejectors in system installations in ice rinks and supermarkets have been analysed regarding their ability to improve the system performance under practical conditions in comparison to the findings from theoretical models.
For the VEJ system, modelling results show the highest work recovery potential for high ejector entrainment temperatures, with refrigeration efficiency improvements from 10 % at 20 °C up to more than 30 % at 40 °C under ideal conditions for a high assumed ejector efficiency of 0.3 in comparison to a system without ejectors operating at equal conditions.
The field data evaluation of the analysed ice rink VEJ systems confirms this effect of the entrainment temperature while a decreasing ejector efficiency is found in addition for low entrainment temperatures, reinforcing the decrease in work recovery for entrainment temperatures particularly below 15 °C.
The system findings also indicate that an unstable control for certain pressures causes a decrease in ejector performance as well as fluctuations in various other system parameters particularly on the high-pressure side.
In the analysed system VEJ-B, a significant decrease in ejector performance is also found for low evaporation temperatures occurring due to the indirect system configuration on the evaporator side. A drop in performance is particularly visible at about −10 °C, indicating that the used ejectors are not designed for such low evaporation temperatures. In contrast, stable ejector efficiencies of about 30 % are found in VEJ-A in subcritical conditions even for evaporation temperatures below −10 °C.
Despite the challenges, the ejector is estimated to yield system improvements of 7 – 8 % for the refrigeration side of the system VEJ-A for the season 2020/2021. In contrast, the evaluation of the system VEJ-B shows no performance improvement from the ejector, caused by the very low evaporation temperatures combined with the low ejector entrainment temperatures during parts of the year.
Regarding a possible solution for the operation at low evaporation temperatures, it seems likely that an adapted ejector design for these conditions could solve the problem.
In contrast, the aspect of a decreasing work recovery potential at low ejector entrainment temperatures cannot be avoided by an improved ejector performance. Nevertheless, the additional effect of a decreasing efficiency for off-design conditions could possibly be improved by further developments of the control mechanisms.
Alternatively, the use of parallel compressors in combination with the vapor ejector, as shown in the VPC system design, would allow to decouple the system mass flow rates and thus operate the ejector at optimized pressure lifts. This possibly allows to improve the ejector efficiency over a wider range of entrainment temperatures while also moderately increasing the theoretical potential of the recovered work as the VPC model analysis indicates. Due to the limited possible gains

from this, it should however be carefully considered whether such a solution is also economically feasible.
Regarding the found control aspects, a more detailed study with focus on this aspect is recommended in cooperation with the controller developers to better understand and improve the control approach for ejectors in combination with the other component controls.

For liquid ejectors, the model shows the highest benefits for low discharge pressures and low gas cooler outlet temperatures, with performance improvements close to 18 % at 20 °C and 65 bar compared to less than 10 % improvement for 40 °C found for the assumed refrigeration cabinet case. With this, the beneficial conditions for the improvement by the liquid ejector correspond to the beneficial conditions for the actual system COP.
With respect to the field measurements, the liquid ejectors are found to operate as expected in the analysed systems. However, most of the time only one of the three installed ejectors in both analysed systems is used, as the liquid level in the low-pressure receivers is found to cross 10 % only very seldom. This is likely related to the fact that refrigeration cabinets in the systems reach overfed conditions only temporarily, while showing average superheat values of up to 10 K for the considered overfed conditions over the analysed time periods.
From the more detailed analysis of the evaporators in the refrigeration cabinets, a number of possible limitations for a further reduction in superheat and increase in evaporation temperature are identified. On the one hand, these are related to the temperature measurements and their correct depiction of the cooling demand for the control, which is particularly limiting the evaporation temperature by requiring a certain air supply temperature to the cabinets. On the other hand, the size of the expansion valves at certain cabinets in system LEJ-B are found to be operated at almost full capacity for extended time periods, indicating that a larger valve design could benefit the system by enabling higher mass flows and thus further overfeeding in the evaporators.

The general comparison of the modelling results for the VEJ and the LEJ system indicates that the LEJ system is generally a more interesting option for colder climates and low entrainment pressures, while the VEJ system provides higher potential savings in warmer climates with high ejector entrainment temperatures.
If heating and cooling capacities and thus also the power input are fixed in the comparison between the ejector systems and the REF system, the model indicates that the recovered work by the ejectors can be used to increase the discharge pressure and/or the gas cooler outlet temperature by a substantial amount, possibly benefiting heating systems by providing higher temperatures and more stable control.

References

[1] 'World Guide to Transcritical CO2 Refrigeration - Part 1,' *shecco*, 2020. [Online]. Available: https://issuu.com/shecco/docs/r744-guide-part1 (visited on 27/05/2021).

[2] G. Grazzini, A. Milazzo and F. Mazzelli, *Ejectors for Efficient Refrigeration: Design, Applications and Computational Fluid Dynamics*. 2018, ISBN: 978-3-319-75243-3 978-3-030-09180-4.

[3] P. Gullo, B. Elmegaard and G. Cortella, 'Energy and environmental performance assessment of R744 booster supermarket refrigeration systems operating in warm climates,' *International Journal of Refrigeration*, vol. 64, pp. 61–79, 1st Apr. 2016, ISSN: 0140-7007. DOI: 10.1016/j.ijrefrig.2015.12.016. [Online]. Available: https://www.sciencedirect.com/science/article/pii/S0140700715003941 (visited on 04/03/2021).

[4] *CO2OLTecEvo. Energy Savings of up to 30% compared with standard transcritical CO2 systems*, 2020. [Online]. Available: www.profroid.com.

[5] K. E. Ringstad, Y. Allouche, P. Gullo, s. Ervik, K. Banasiak and A. Hafner, 'A detailed review on CO2 two-phase ejector flow modeling,' *Thermal Science and Engineering Progress*, vol. 20, p. 100 647, 1st Dec. 2020, ISSN: 2451-9049. DOI: 10.1016/j.tsep.2020.100647. [Online]. Available: http://www.sciencedirect.com/science/article/pii/S2451904920301670 (visited on 27/01/2021).

[6] S. Elbel and P. Hrnjak, 'Experimental validation of a prototype ejector designed to reduce throttling losses encountered in transcritical R744 system operation,' *International Journal of Refrigeration*, vol. 31, no. 3, pp. 411–422, 1st May 2008, ISSN: 0140-7007. DOI: 10.1016/j.ijrefrig.2007.07.013. [Online]. Available: https://www.sciencedirect.com/science/article/pii/S0140700707001508 (visited on 08/02/2021).

[7] R. F. de Albuquerque, 'Untersuchung von Ejektor-Kälteanlagen beim Einsatz in tropischen Gebieten,' Cuvilier Verlag, Göttingen, 2011.

[8] S. Elbel and N. Lawrence, 'Review of recent developments in advanced ejector technology,' *International Journal of Refrigeration*, vol. 62, pp. 1–18, 1st Feb. 2016, ISSN: 0140-7007. DOI: 10.1016/j.ijrefrig.2015.10.031. [Online]. Available: https://www.sciencedirect.com/science/article/pii/S0140700715003266 (visited on 22/02/2021).

[9] K. Banasiak, A. Hafner, E. E. Kriezi, K. B. Madsen, M. Birkelund, K. Fredslund and R. Olsson, 'Development and performance mapping of a multi-ejector expansion work recovery pack for R744 vapour compression units,' *International Journal of Refrigeration*, vol. 57, pp. 265–276, 1st Sep. 2015, ISSN: 0140-7007. DOI: 10.1016/j.ijrefrig.2015.05.016. [Online]. Available: http://www.sciencedirect.com/science/article/pii/S0140700715001553 (visited on 03/02/2021).

[10] G. Besagni, R. Mereu and F. Inzoli, 'Ejector refrigeration: A comprehensive review,' *Renewable and Sustainable Energy Reviews*, vol. 53, pp. 373–407, 1st Jan. 2016, ISSN: 1364-0321. DOI: 10.1016/j.rser.2015.08.059. [Online]. Available: http://www.sciencedirect.com/science/article/pii/S1364032115009223 (visited on 20/01/2021).

[11] N. Lawrence and S. Elbel, 'Experimental investigation on control methods and strategies for off-design operation of the transcritical R744 two-phase ejector cycle,' *International Journal of Refrigeration*, vol. 106, pp. 570–582, 1st Oct. 2019, ISSN: 0140-7007. DOI: 10.1016/j.ijrefrig.2019.04.020. [Online]. Available: https://www.sciencedirect.com/science/article/pii/S0140700719301768 (visited on 22/02/2021).

[12] P. Gullo, A. Hafner and G. Cortella, 'Multi-ejector R744 booster refrigerating plant and air conditioning system integration – A theoretical evaluation of energy benefits for supermarket applications,' *International Journal of Refrigeration*, vol. 75, pp. 164–176, 1st Mar. 2017, ISSN: 0140-7007. DOI: 10.1016/j.ijrefrig.2016.12.009. [Online]. Available: https://www.sciencedirect.com/science/article/pii/S0140700716304212 (visited on 22/02/2021).

[13] C. Doerffel, C. Thomas and U. Hesse, 'Experimental results of various efficiency enhancing measures for CO2 refrigeration systems,' presented at the Refrigeration Science and Technology, vol. 2020-December, 2020, pp. 476–481. DOI: 10.18462/iir.gl.2020.1009.

[14] C. Lucas and J. Koehler, 'Experimental investigation of the COP improvement of a refrigeration cycle by use of an ejector,' *International Journal of Refrigeration*, vol. 35, no. 6, pp. 1595–1603, 1st Sep. 2012, ISSN: 0140-7007. DOI: 10.1016/j.ijrefrig.2012.05.010. [Online]. Available: https://www.sciencedirect.com/science/article/pii/S0140700712001247 (visited on 12/04/2021).

[15] Y. Zhu, C. Li, F. Zhang and P.-X. Jiang, 'Comprehensive experimental study on a transcritical CO2 ejector-expansion refrigeration system,' *Energy Conversion and Management*, vol. 151, pp. 98–106, 1st Nov. 2017, ISSN: 0196-8904. DOI: 10.1016/j.enconman.2017.08.061. [Online]. Available: http://www.sciencedirect.com/science/article/pii/S0196890417307811 (visited on 28/01/2021).

[16] A. Hafner, S. Försterling and K. Banasiak, 'Multi-ejector concept for R-744 supermarket refrigeration,' *International Journal of Refrigeration*, vol. 43, pp. 1–13, 1st Jul. 2014, ISSN: 0140-7007. DOI: 10.1016/j.ijrefrig.2013.10.015. [Online]. Available: https://www.sciencedirect.com/science/article/pii/S0140700714000668 (visited on 22/02/2021).

[17] C. Corazzol, W. Muvegi, L. Mattiello and L. Nalini, 'Analysis and comparison between different energy consumption performances of a CO2 trans-critical booster system with modulating ejectors and parallel compression in various configurations and different climate conditions,' presented at the Refrigeration Science and Technology, vol. 2020-December, 2020, pp. 464–469. DOI: 10.18462/iir.gl.2020.1060.

[18] M. Karampour and S. Sawalha, 'State-of-the-art integrated CO2 refrigeration system for supermarkets: A comparative analysis,' *International Journal of Refrigeration*, vol. 86, pp. 239–257, 1st Feb. 2018, ISSN: 0140-7007. DOI: `10.1016/j.ijrefrig.2017.11.006`. [Online]. Available: `https://www.sciencedirect.com/science/article/pii/S0140700717304474` (visited on 08/04/2021).

[19] S. Minetto, R. Brignoli, C. Zilio and S. Marinetti, 'Experimental analysis of a new method for overfeeding multiple evaporators in refrigeration systems,' *International Journal of Refrigeration*, vol. 38, pp. 1–9, 1st Feb. 2014, ISSN: 0140-7007. DOI: `10.1016/j.ijrefrig.2013.09.044`. [Online]. Available: `http://www.sciencedirect.com/science/article/pii/S0140700713002788` (visited on 28/01/2021).

[20] P. Gullo, A. Hafner, K. Banasiak, S. Minetto and E. E. Kriezi, 'Multi-Ejector Concept: A Comprehensive Review on its Latest Technological Developments,' *Energies*, vol. 12, no. 3, p. 406, Jan. 2019. DOI: `10.3390/en12030406`. [Online]. Available: `https://www.mdpi.com/1996-1073/12/3/406` (visited on 24/02/2021).

[21] Y. He, J. Deng, L. Zheng and Z. Zhang, 'Performance optimization of a transcritical CO2 refrigeration system using a controlled ejector,' *International Journal of Refrigeration*, vol. 75, pp. 250–261, 1st Mar. 2017, ISSN: 0140-7007. DOI: `10.1016/j.ijrefrig.2016.12.015`. [Online]. Available: `http://www.sciencedirect.com/science/article/pii/S0140700716304285` (visited on 28/01/2021).

[22] J. Smolka, M. Palacz, J. Bodys, K. Banasiak, A. Fic, Z. Bulinski, A. J. Nowak and A. Hafner, 'Performance comparison of fixed- and controllable-geometry ejectors in a CO2 refrigeration system,' *International Journal of Refrigeration*, vol. 65, pp. 172–182, 1st May 2016, ISSN: 0140-7007. DOI: `10.1016/j.ijrefrig.2016.01.025`. [Online]. Available: `http://www.sciencedirect.com/science/article/pii/S0140700716000311` (visited on 27/01/2021).

[23] J. Zhu and S. Elbel, 'A New Control Mechanism for Two-Phase Ejector in Vapor Compression Cycles for Automotive Applications Using Adjustable Motive Nozzle Inlet Swirl,' *SAE International Journal of Passenger Cars - Mechanical Systems*, vol. 9, no. 1, pp. 44–51, 5th Apr. 2016, ISSN: 1946-4002. DOI: `10.4271/2016-01-0243`. [Online]. Available: `https://www.sae.org/content/2016-01-0243/` (visited on 26/06/2021).

[24] P. Gullo, M. R. Kærn, M. Birkelund and E. E. Kriezi, 'Preliminary experimental investigation on a transcritical R744 condensing unit using the novel PWM ejector,' in *Proceedings of The14th IIR-Gustav Lorentzen Conference on Natural Refrigerants*, International Institute of Refrigeration, 2020, pp. 363–368. DOI: `10.18462/iir.gl.2020.1001`. [Online]. Available: `https://orbit.dtu.dk/en/publications/preliminary-experimental-investigation-on-a-transcritical-r744-co` (visited on 27/05/2021).

[25] P. Gullo, M. R. Kærn, M. Haida, J. Smolka and S. Elbel, 'A review on current status of capacity control techniques for two-phase ejectors,' *International Journal of Refrigeration*, vol. 119, pp. 64–79, 1st Nov. 2020, ISSN: 0140-7007. DOI: `10.1016/j.ijrefrig.2020.07.014`. [Online]. Available: `https://www.sciencedirect.com/science/article/pii/S0140700720303169` (visited on 22/02/2021).

[26] M. Haida, M. Palacz, J. Bodys, J. Smolka, P. Gullo and A. J. Nowak, 'An experimental investigation of performance and instabilities of the R744 vapour compression rack equipped with a two-phase ejector based on short-term, long-term and unsteady operations,' *Applied Thermal Engineering*, vol. 185, p. 116 353, 25th Feb. 2021, ISSN: 1359-4311. DOI: 10.1016/j.applthermaleng.2020.116353. [Online]. Available: http://www.sciencedirect.com/science/article/pii/S135943112033831X (visited on 27/01/2021).

[27] G. Besagni, N. Cristiani, L. Croci, G. R. Guédon and F. Inzoli, 'Computational fluid-dynamics modelling of supersonic ejectors: Screening of modelling approaches, comprehensive validation and assessment of ejector component efficiencies,' *Applied Thermal Engineering*, vol. 186, p. 116 431, 5th Mar. 2021, ISSN: 1359-4311. DOI: 10.1016/j.applthermaleng.2020.116431. [Online]. Available: http://www.sciencedirect.com/science/article/pii/S1359431120339090 (visited on 28/01/2021).

[28] K. Banasiak and A. Hafner, 'Experimentelle Untersuchung verschiedener R744-Ejektorgeometrien,' in *Proceedings of the DKV-Tagung, Magdeburg, Germany*, 2010.

[29] L. Zheng and J. Deng, 'Research on CO2 ejector component efficiencies by experiment measurement and distributed-parameter modeling,' *Energy Conversion and Management*, vol. 142, pp. 244–256, 15th Jun. 2017, ISSN: 0196-8904. DOI: 10.1016/j.enconman.2017.03.017. [Online]. Available: http://www.sciencedirect.com/science/article/pii/S0196890417302200 (visited on 27/01/2021).

[30] M. Haida, J. Smolka, A. Hafner, M. Mastrowski, M. Palacz, K. B. Madsen, A. J. Nowak and K. Banasiak, 'Numerical investigation of heat transfer in a CO2 two-phase ejector,' *Energy*, vol. 163, pp. 682–698, 15th Nov. 2018, ISSN: 0360-5442. DOI: 10.1016/j.energy.2018.08.175. [Online]. Available: http://www.sciencedirect.com/science/article/pii/S0360544218317110 (visited on 28/01/2021).

[31] Y. Biner, 'Modellierung und experimentelle Untersuchung eines CO2-Kältekreislaufs mit Multi-Ejektor-Block,' 2020. DOI: 10.21256/ZHAW-2531. [Online]. Available: https://digitalcollection.zhaw.ch/handle/11475/20521 (visited on 12/04/2021).

[32] M. Palacz, J. Smolka, A. Fic, Z. Bulinski, A. J. Nowak, K. Banasiak and A. Hafner, 'Application range of the HEM approach for CO2 expansion inside two-phase ejectors for supermarket refrigeration systems,' *International Journal of Refrigeration*, vol. 59, pp. 251–258, 1st Nov. 2015, ISSN: 0140-7007. DOI: 10.1016/j.ijrefrig.2015.07.006. [Online]. Available: http://www.sciencedirect.com/science/article/pii/S0140700715002030 (visited on 28/01/2021).

[33] M. Haida, K. Banasiak, J. Smolka, A. Hafner and T. M. Eikevik, 'Experimental analysis of the R744 vapour compression rack equipped with the multi-ejector expansion work recovery module,' *International Journal of Refrigeration*, vol. 64, pp. 93–107, 1st Apr. 2016, ISSN: 0140-7007. DOI: 10.1016/j.ijrefrig.2016.01.017. [Online]. Available: http://www.sciencedirect.com/science/article/pii/S0140700716000232 (visited on 03/02/2021).

[34] N. Purohit, V. Sharma, S. Sawalha, B. Fricke, R. Llopis and M. S. Dasgupta, 'Integrated supermarket refrigeration for very high ambient temperature,' *Energy*, vol. 165, pp. 572–590, 15th Dec. 2018, ISSN: 0360-5442. DOI: 10.1016/j.energy.2018.09.097. [Online]. Available: https://www.sciencedirect.com/science/article/pii/S0360544218318619 (visited on 22/02/2021).

[35] P. Gullo, K. M. Tsamos, A. Hafner, K. Banasiak, Y. T. Ge and S. A. Tassou, 'Crossing CO2 equator with the aid of multi-ejector concept: A comprehensive energy and environmental comparative study,' *Energy*, vol. 164, pp. 236–263, 1st Dec. 2018, ISSN: 0360-5442. DOI: 10.1016/j.energy.2018.08.205. [Online]. Available: http://www.sciencedirect.com/science/article/pii/S0360544218317419 (visited on 28/01/2021).

[36] I. H. Bell, J. Wronski, S. Quoilin and V. Lemort, 'Pure and pseudo-pure fluid thermophysical property evaluation and the open-source thermophysical property library CoolProp,' *Industrial & Engineering Chemistry Research*, vol. 53, no. 6, pp. 2498–2508, 2014. DOI: 10.1021/ie4033999. [Online]. Available: http://pubs.acs.org/doi/abs/10.1021/ie4033999.

[37] E. Granryd, I. Ekroth, P. Lundqvist, k. Melinder, B. Palm and P. Rohlin, *Refrigerating Engineering*. Stockholm: Royal Institute of Technology, KTH, Department of Energy Technology, Division of Applied Thermodynamics and Refrigeration, 2009, ISBN: 978-91-7415-415-3.

[38] S. Sawalha, 'Carbon dioxide in supermarket refrigeration,' Energiteknik, Energy Technology, Kungliga Tekniska högskolan, Stockholm, 2008, ISBN: 9789171789655.

[39] T. Månsson, Y. Ostermeyer and A. S. Kalagasidis, 'Exploratory investigation of return air temperature sensor measurement errors in refrigerated display cabinets,' *Energy Efficiency*, vol. 14, no. 1, p. 11, Jan. 2021, ISSN: 1570-646X, 1570-6478. DOI: 10.1007/s12053-020-09912-1. [Online]. Available: http://link.springer.com/10.1007/s12053-020-09912-1 (visited on 12/05/2021).

TRITA TRITA-ITM-EX 2021:444